FINAL REPORT

Manufacturing Advanced Engineered Components Using Lost Foam Casting Technology

By

HARRY E. LITTLETON

And

JOHN GRIFFIN (PI)

TO

THE DEPARTMENT OF ENERGY,

THE AMERICAN FOUNDRY SOCIETY,

and

AFS-DOE-LFC FOAM CASTING CONSORTIUM MEMBERS

DOE CONTRACT N0. DE-FC36-04GO14230

Project Final Report

July 2011

Manufacturing Advanced Engineered Components Using Lost Foam Casting Technology

Acknowledgment, Disclaimer and Proprietary Notice

This report is based upon work supported by the U. S Department of Energy under award No. DE-FC36-04GO14230

Any findings, opinions, and conclusions or recommendations expressed in this report are those of the authors and do not necessarily reflect the views of the Department of Energy

There is no proprietary data or patentable material in this report

Reports are available free via the U.S. Department of Energy (DOE) Information Bridge Website: http://www.osti.gov/bridge

Reports are available to DOE employees, DOE contractors, Energy Technology Data Exchange (ETDE) representatives, and Informational Nuclear Information System (INIS) representatives from the following source:

Office of Scientific and Technical Information
P.O. Box 62
Oak Ridge, TN 37831
Tel: (865) 576-8401
FAX: (865) 576-5728
E-mail: reports@osti.gov
Website: http://www.osti.gov/contract.html

Manufacturing Advanced Engineered Components Using Lost Foam Casting Technology PHASE VI

Table of Contents

List of Acronyms

PS	polystyrene
PMMA	methylmethacrylate
UAB	University of Alabama at Birmingham
MCT	Materials Casting Technology
GM	General Motors
LFC	Lost Foam Casting
AFS	American Foundry Society
pcf	pound per cubic feet
EPS	Expanded Polystyrene
mm.	millimeters
perm	permeability
psig	pound per square inch gage
in.	inches
kPa	kilo pascals
SEM	scanning electron microscope
EDS	energy dispersive spectrometer
I4	inline four cylinder block
I6	inline six cylinder block
ksi	kilograms per square inch
MPa	megapascals
DAS	dendrite arm spacing
SiC	silicon carbide
ppm	parts per million
ppi	pores per square inch
LF	Lost Foam
Wc	with chill
SuP	solidified under pressure
cm	centimeter
HCF	high cycle fatigue
CGI	compacted graphite iron
CG	compacted graphite
GPa	gigapascals
Nc	no chill
MHz	megahertz
Sr	strontium

List of Figures

List of Tables

Advanced Engineered Components Using Lost Foam Casting Technology Manufacturing

EXECUTIVE SUMMARY

Previous research, conducted under DOE Contracts #DE-FC07-89ID12869, DE-FCO7-93ID12230, DE-FC07-95ID113358 and DE-FC07-99ID13840 made significant advances in understanding the Lost Foam Casting (LFC) Process and clearly identified areas where additional developments were needed to improve the process and make it more functional in industrial environments. This project was a subtask of Energy Saving Melting and Revert Reduction Technology ("Energy SMARRT") Program. Through this project, technologies, such as computer modeling, pattern quality control, casting quality control and marketing tools, were developed to advance the Lost Foam Casting process application and provide greater energy savings. These technologies have improved (1) production efficiency, (2) mechanical properties, and (3) marketability of lost foam castings. All three reduce energy consumption in the metals casting industry.

This report summarizes the work done on all tasks in the period of January 1, 2004 through June 30, 2011. This project was originally scheduled for January 1, 2004 through December 30, 2006; however, scheduled funding was delayed. The project continued at a reduced research effort that reflected funding through June 30, 2011. The results obtained in each task are summarized in this Executive Summary and details are provided in subsequent sections of the report.

Task 1. Pattern Replacement and Solidification Modeling

The objectives of this task were: 1) the development of an accurate physical model of the metal/pattern replacement process, 2) development of a data base of pattern degradation properties and 3) to provide assistance to commercial software suppliers to develop commercial computational codes for modeling the Lost Foam Casting Process.

Subtask 1.1 Physical Model

A physical model has been developed over the course of the Lost Foam research to provide guidance for research efforts and for the development of a computational code for modeling the Lost Foam Process. This physical model was recently updated to include the effects of pattern permeability. Pattern permeability provides another escape path for the gases generated during the metal/pattern replacement process. This additional escape path produces an uneven metal front shape (fingers) as local areas of metal follow the areas of varying pattern permeability. Casting defects such as folds and lustrous carbon can form between these fingers of metal. This

phenomenon was discovered using the Real Time X-Ray where views of metal filling indicated varying degrees of fingering that correlated with varying levels of pattern fusion (permeability). The updated physical model directed research efforts toward the root cause of varying levels of local permeability in patterns.

Subtask 1.2 Data Base

A database of pattern degradation properties has been completed using the Pattern Pyrolysis Apparatus. The properties recorded are temperature, recession velocity, pattern density, gas fraction, liquid fraction, energy consumption, and pressure. This data was developed to improve the commercial computational codes used for modeling the Lost Foam process. Two important discoveries were made in this data base research. First, patterns with a bromide additive exhibited a significantly larger decrease in molecular weight (lower viscosity of liquid pyrolysis products) than patterns with no additive. This explains why aluminum castings, poured using patterns with bromide, have significantly less metal folds. Second, patterns with higher fusion levels generate higher resistant metal to pattern pressures due to the decrease in permeability. The percent of bromide additive to the pattern material was maximized using the Pattern Pyrolysis Apparatus.

Subtask 1.3 Commercial Codes

Three major commercial software companies, Flow 3D, Magma and ProCast have participated in the Lost Foam Consortium as cost sharing sponsors. The database compiled in Subtask 1.2 has been provided to these companies and two of these codes have incorporated some of the data. General Motors, A major automotive company, developed a proprietary code, using the data base and other data developed during the course of the entire Lost Foam Consortium, to substantially reduce casting scrap and processing costs. This code has the ability to predict the formation of casting defects during filling of aluminum engine blocks and heads. Plans to commercialize this code were not successful due to the cost of implementation compared to the limited marketability.

Flow 3D has been used extensively at UAB throughout this program due to their willingness to provide technical assistance and to implement suggested improvements in their code. Since metal fill in Lost Foam castings is a relatively slow event compared to open cavity molds, the prediction of accurate temperatures during and after filling are important for solidification predictions of metal shrinkage. Considerable effort was directed toward improving the accuracy of Flow 3D temperature predictions. Replacing inaccurate published enthalpy data with corrected enthalpy data provided predicted temperatures that agreed with measured values.

Shrinkage predictions in engine blocks and cylinder heads, using Flow3D with more accurate enthalpy and metal density input data, have been

performed and validated using cut sections of castings. Elimination of shrinkage was achieved through predictive changes in gating. This has been a breakthrough technology that provides designers with a predictive tool to produce new products with a minimum of shrinkage for first production castings.

Task 2.Improve Pattern Quality and Consistency

Past research has shown that pattern permeability is a major source of control for metal filling and defect formation in Lost Foam Castings. A commercially available Pattern Permeability Apparatus was developed and validated to assist pattern producers to maintain consistent quality. The objective of this task was to improve pattern quality and consistency through 1.) determination of the root causes of pattern permeability variations within patterns and 2.)implementation of procedures to control these variations.

Subtask 2.1 Pattern Properties

Determination of pattern fusion (permeability) has historically been achieved through visual examination of the pattern surface after molding. Following the development of the Pattern Permeability Apparatus locations of high and low areas of permeability were quantified by the rate of air flowing through the pattern surface at a specified pressure differential. Using Real Time X-Ray, areas of variable permeability were observed to have variable metal velocities and metal front shapes. Areas with high permeability had high metal velocities and areas with low permeability had lower metal velocities. Metal front shapes, with fingers and high velocities, were clearly identified as areas containing folds and porosity.

Threshold values of permeability were studied in the laboratory and production foundries. This study revealed that pattern, coating and sand permeabilities form a system permeability and is the control that foundries use to minimize casting scrap due to casting defects. Unfortunately, changes in pattern permeability from batch to batch dictate changes in coating permeability. Since previous research has provided coating manufacturers with the technology to consistently control coating properties the next breakthrough in improved casting quality will be through uniform control of pattern permeability.

The root cause of variable permeability within a pattern was traced to the inability to uniformly pack the beads in the pattern tool during bead filling. Two transparent polycarbonate tools were used to visually inspect beads during the blowing process. Variables examined were vented and ventless tooling, fill gun pressure, fill gun location, variable fill gun on/off timing, antistatic beads, and mechanical vibration of the tool during and after bead fill. Mechanical vibration applied to the vented tool after bead filling produced a 12% decrease in bead volume. Mechanical vibration of the tool provided the necessary energy to pack the beads

uniformly while the other variables provided little improvement. Due to tool geometry and vent location, areas where beads compete for position were clearly visible. This competition for position is a major cause of high and low permeability areas within a pattern. Tools with complex geometry are more prone to exhibit these variable permeability areas. Implementation of mechanical vibration into production tooling is a recommended solution.

Task 3. New Pattern and Coating Materials

The objective of this task was to develop new pattern and coating materials that produces less casting scrap due to folds and metal porosity.

Subtask 3.1 Alternate Pattern Materials

Developing new pattern materials is a lengthy process and the cost may outweigh the benefits. Based on these facts UAB has concentrated on enhancing existing pattern materials through the use of additives and innovated processing. Previous research has shown that the addition of bromide to polystyrene beads accelerates the decomposition during exposure to molten metal, providing a more timely exit for the decomposition products. The amount of bromide additive has been optimized through a comprehensive study. Several aluminum foundries have placed these beads into production and experienced a significant decrease in the incidence of casting defects.

Subtask 3.2 Pattern and Coating Additives

Working with cost sharing sponsors Styrochem and GM, a project was launched to optimize the level of additive in polystyrene beads. The Pattern Pyrolysis Apparatus was used to measure gas fraction, liquid fraction, degradation energy and resistance pressure on sample patterns. Results indicated that increases in additive level created increases in gas fraction resulting in increases in resistance pressure. An optimum level of additive was determined based on predictions of metal velocity using the GM Foam Fill code and the incidence of casting defects.

Another study was performed to determine if the bromide addition could be added to the coating used for iron castings. Five levels of additive were used. Results indicated a significant decrease in lustrous carbon defects for increasing levels of additive.

Task 4. Pressure Solidification of Aluminum Lost Foam Castings

The objective of this task was to study the effects of gating on aluminum castings solidified under pressure in an effort to reduce unfed metal shrinkage. Gating of Lost Foam Castings has historically been designed to make the cluster rigid in order to survive the coating and compaction steps in the process. Studies in this task have shown that location of the gates

required to prevent metal shrinkage must be placed in the central location of complex castings to provide the shortest possible path for metal feeding. Several complex castings were modeled using conventional gating and indicated metal shrinkage in specific areas. These areas were validated with sectioned castings. New gating systems were designed, modeled and used to make castings. In all cases the new gating systems eliminated metal shrinkage.

Task 5. Design Data and Marketing Plan
The objective of this task was to provide designers with data from various aluminum alloys and casting processes that result in improved mechanical properties. Three processes were studied in this program. Pressure solidification and vacuum assisted pouring were studied for aluminum castings. The Lost Foam process was used to produce compacted graphite (CGI) engine blocks.

Subtask 5.1. Mechanical Properties

Subtask 5.1.1 Pressure Solidification
Tensile properties of aluminum alloys A319, A356 and A206 were evaluated on specimens extracted from a wedge casting poured using Lost Foam and bonded sand molds, with and without pressure solidification. Pressure solidification significantly decreased metal density by suppressing the growth of gas pores and increased the elongation.

Subtask 5.1.2 Vacuum Assisted Pouring of Aluminum
A vacuum assisted pouring process was developed and used to study the effects on tensile properties of A319 and A356. Results indicated a significant decrease in porosity and an increase in elongation.

Subtask 5.1.3 Pouring Compacted Graphite Iron
Compacted graphite iron engine blocks were cast using Lost Foam with no gray iron skin that is present in green sand and bonded sand molds. This is a breakthrough technology that justifies additional research.

Subtask 5.2 Design Package
An attempt to develop an ASTM standard for Lost Foam properties was abandoned due to number of variables that control properties. A summary of tensile properties was developed that includes three aluminum alloys solidified with pressure and without pressure, with and without a chill and using Lost Foam and sand molds.

Subtask 5.3 Marketing Plan
Two design conferences were held to showcase the advantages of the Lost Foam Casting Process and present technical improvements achieved through the Lost Foam Consortium to existing and prospective Lost Foam suppliers. These conferences were successful in providing valuable insight for the designers and producers. In addition two designer workshops were held. Presentations and panel discussions were conducted at AFS-sponsored

Metalcasting Congresses / CastExpos. Another significant accomplishment of this program was the publication of a book titled “Lost Foam Casting Made Simple”, which included the most recent advancements in Lost Foam Casting technology and practices.

Task 6. Technology Transfer
Technology developed in this program was transferred to the production floor through scheduled meetings with sponsors, plant trials and tutorials and presentations at AFS conferences. This interaction with sponsors has served to transfer technology and provide direction for this program based on their particular needs.

Benefits Assessment

This new technology was predicted to result in an average energy savings of 7.77 trillion BTU’s/year over a 10 year period. Current (2011) annual energy saving estimates based on commercial introduction in 2011 and a market penetration of 97% by 2020 is 5.02 trillion BTU’s/year and 6.46 trillion BTU’s/year with 100% market penetration by 2023.

Along with these energy savings, reduction of scrap and improvement in casting yield will result in a reduction of the environmental emissions associated with the melting and pouring of the metal which will be saved as a result of this technology. The average annual estimate of CO_2 reduction per year through 2020 is 0.03 Million Metric Tons of Carbon Equivalent (MM TCE).

INTRODUCTION

Process Description - The lost foam process is the most energy efficient casting process available. “Foundry Management and Technology” magazine analyzed the lost foam process and reported 27% energy savings, a 46% improvement in labor productivity and 7 weight percent fewer materials compared to other molding processes.

The Lost Foam Casting Process produces high value parts by combining cast components into single castings, improving energy efficiency by achieving better metal yields, reducing materials consumption by eliminating cores, and improving casting dimensional accuracy. All of these process features reduce the energy consumption during manufacturing. For example, energy savings of 7.7×10^{12} BTU/Year were achieved by converting Cast Iron, Ductile Iron and Aluminum castings produced by the green sand and shell molding processes to Lost Foam.

Lost foam casting production has grown in value from about $5,000,000 per year in 1988 to $800,000,000 in 2002. This is the result of persistent investment by the industry with financial assistance from the DOE Office of Industrial Technology. During this time period many technical issues have been resolved and the technology has been transferred to the production floor, resulting in scrap reductions from 25% to less than 3%. This program has decreased casting scrap and matured the technology through expanding the Lost Foam marketplace. With the economic downturn in 2006 and the decision of a major automotive supplier to change to another casting process the LFCP has decreased significantly. The process continues to grow slowly through existing Lost Foam Casting suppliers as new products are introduced using the attractive features of the process.

Focus - Previous research, conducted under DOE Contracts #DE-FC07-89ID12869, DE-FCO7-93ID12230, DE-FC07-95ID113358 and DE-FC07-99ID13840 made significant advances in understanding the Lost Foam Casting (LFC) Process and clearly identified areas where additional developments were needed to improve the process and make it more functional in industrial environments. This research was performed by a consortium consisting of the University of Alabama at Birmingham (UAB), the American Foundry Society (AFS), the AFS Lost Foam Casting (Division 11) and companies in the cast metals industry increased productivity, reduced lead time, and reduced energy consumption. This project addressed these issues and was a subtask of Energy Saving Melting and Revert Reduction Technology (“Energy SMARRT”) Program. Through this project, technologies, such as computer modeling, pattern quality control, casting quality control and marketing tools, were developed to advance the Lost Foam Casting process application and provide greater energy savings. These technologies have improved (1) production efficiency, (2) mechanical properties, and (3) marketability of lost foam castings. All three reduced energy consumption in the metals casting industry.

Potential Applications - The lost foam process is accepted as the process of choice for complex high volume components such as automotive and marine blocks and heads; compressors for the heating and air conditioning industry; electric motor housings; counterweights for heavy equipment; hydraulic valves, hydrants, and pipe fittings for the water distribution industry; heat exchangers for various industries. The value added features such cast-in holes, threaded fasteners and internal fluid passages have made the LFCP attractive to many casting buyers.

Commercialization – Throughout this research a major effort was expended in transferring the developed technologies to the industrial sponsors through scheduled technical exchange meetings, plant trials and tutorials. In addition the developed technology was transferred to industry through publications and presentations at meetings of the AFS Casting Congress, European Lost Foam Council, and casting industry magazines. Several technologies have been made commercially available such as the Coating Permeability Apparatus and the Pattern Permeability Apparatus. The Real Time X-Ray equipment at UAB has been used by many Lost Foam Casting suppliers to resolve casting quality issues.

BACKGROUND

State of the Art – The Lost Foam Casting Process continues to be an emerging process although most of the technical issues that previously restricted the process growth have been resolved. These issues have been resolved through the persistent support by AFS, DOE and the many industrial sponsors. Through the previous research efforts, technical issues have been identified by the industrial sponsors, root causes identified using casting laboratory experiments, solutions developed and validated in plant trials. The major achievements of previous research were:

- Pattern dimensional measurement equipment (commercialized)
- Pattern filling and compaction – developed methods and equipment to measure the filling and compaction of patterns to minimize distortion and fill related casting defects (fill gauges commercialized)
- Coating quality control – developed procedures (Coating Quality control Manual) and equipment to measure coating permeability
- Pattern density – developed procedures and equipment to measure local pattern density
- Laps and folds in Aluminum castings – identified root cause as oxide on merging metal front, aggravated by pattern pyrolysis products – bromide addition to pattern eliminated these defects
- Casting dimensions – Identified sand expansion as root cause, low expansion sands such as Olivine and synthetic Mullite eliminated this defect
- Metal/Pattern replacement – Developed a Pattern Pyrolysis Apparatus to measure gas fraction, heat transfer and forces generated during metal/pattern replacement – basis of improved computational modeling
- Real Time X-Ray – Using this equipment the influence of pattern permeability on metal filling and defect formation was discovered – used to examine casting defect formation

Prior to the start of the current research program a survey was performed to identify the most significant technical issues of the industrial sponsors. The industrial sponsors identified six areas of research to be addressed in the current program. The tasks to resolve these issues were:

1. Increased understanding of the metal/pattern replacement process to reduce casting defects and improve computational models.
   Approach – Identify the mechanism of gas and liquid pyrolysis removal from the casting cavity using the Pattern Pyrolysis Apparatus and the Real Time X-Ray equipment. This mechanism is essential to improve the current computational models and direct further research that would result in improved casting quality. Data will be added to the existing data base.

2. Improve pattern quality and consistency to reduce casting defects.
   Approach - Long time Lost Foam Casting suppliers have believed that 80% of casting defects are a direct result of poor pattern quality. The approach for this task is to identify the specific properties of patterns that control metal filling and subsequent casting defects and develop equipment to measure these properties.
3. Develop innovative techniques to expedite pattern pyrolysis product removal to reduce casting defects and improve casting quality.
   Approach – Since the addition of bromide to the pattern material has been successful a study to optimize the level of bromide. In addition, studies to determine the effects of bromide addition to the coating are planned. Additional studies on other additives are planned.
4. Develop techniques and procedures for improving casting mechanical properties using solidification under pressure and vacuum assisted metal filling.
   Approach – Data from the literature are varied in their opinion of the effects of solidification under pressure for aluminum castings. A study is planned to determine the mechanical properties of 319, A356 and 206 aluminum alloys solidified under pressure. A wedge casting will be used to separate the effects of cooling rate from the pressure solidification.
5. Develop a design package including mechanical properties for casting designers and implement a marketing plan to increase Lost Foam casting applications.
   Approach – Develop a design package that indicates the current state of the art for mechanical properties of aluminum alloys. The data will compare properties open cavity, bonded sand and Lost Foam processes using pressure solidification and atmospheric pressure. Most of the data will be extracted from Task 5; however, additional data will be from another process (vacuum assisted pouring). Additional data will be developed for Compacted Graphite Iron (CGI).
6. Transfer the developed technologies to production management and the production floor.
   Approach – Technical exchange meetings will be held every four months, alternating between UAB, AFS and a sponsoring Lost Foam facility. Approved technical papers will be presented at casting conferences worldwide.

Personnel – Dr. Charles Bates was the principal investigator (PI) until his retirement in 2006. John A. Griffin assumed the PI responsibilities from 2006 until the present. Dr. Bates directed the Lost Foam Consortium since the inception and has been instrumental in solicitation of funding for equipment such as the Real Time X-Ray equipment, pressure solidification chamber and other foundry equipment.

Harry E. Littleton directed the technical approaches and equipment development surrounding the program as he has since the program inception.

John A. Griffin supervised the laboratory procedures and experiments

throughout the entire program.
Dr. Robin Foley provided all metallographic inspections through the entire consortium.

RESULTS AND DISCUSSION

Task 1. Pattern Replacement and Solidification Modeling

The ultimate goal of this task is to provide the Lost Foam industry with computational models that can be used to minimize start up times for new product introduction into production and to provide designers a predictive tool to assist in this process. Existing product production issues would also benefit from this predictive tool. Several computational models currently exist and vary in the level of physics used, based on current understanding of metal/pattern replacement. This task extends the current level of understanding of the metal/pattern exchange with the intent of improving computational codes.

Subtask 1.1 Physical Model

An accurate physical model of the metal/pattern exchange is vital to the success of a computational model. Previous research indicated the metal replaced the pattern by melting and gasifying with the gases escaping into the coating and surrounding sand through a gap between the metal front and the receding pattern. Calculations prove this is not possible since the gap size required to allow gas escape is too large to provide sufficient heat transfer to sustain known metal velocities. Later research provided an answer to this dilemma, indicating that gases can escape through the pattern permeability ahead of the metal front. Unfortunately modeling of two phase flow is complex and currently no commercial codes perform with this level of complexity. Research at Metal Casting Technology[1] (MCT) increased the understanding of the physical events occurring as the metal replaced the pattern. The results of their research proposed the physical model illustrated in Figure 1.1.1. Liquid pyrolysis products are deposited onto the coating behind the metal front in the form of globules where they are heated and vaporized by the metal and subsequently escape through the coating as gases. The features of this model have been incorporated into the model illustrated in Figure 1.1.2. It is important to understand that the pattern permeability can exceed the coating permeability, allowing the metal to finger which causes multiple merging fronts which cause folds and porosity. This condition exists when the pattern surface is not properly fused. This condition is discussed later in this report.

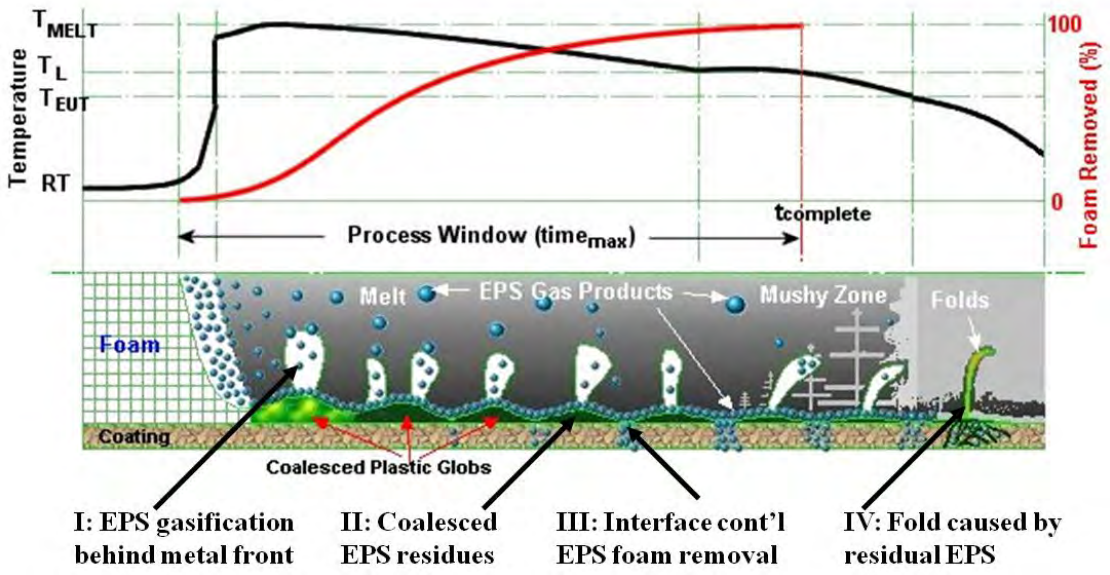

Figure 1.1.1 – MCT Physical Model of Metal/Pattern Replacement

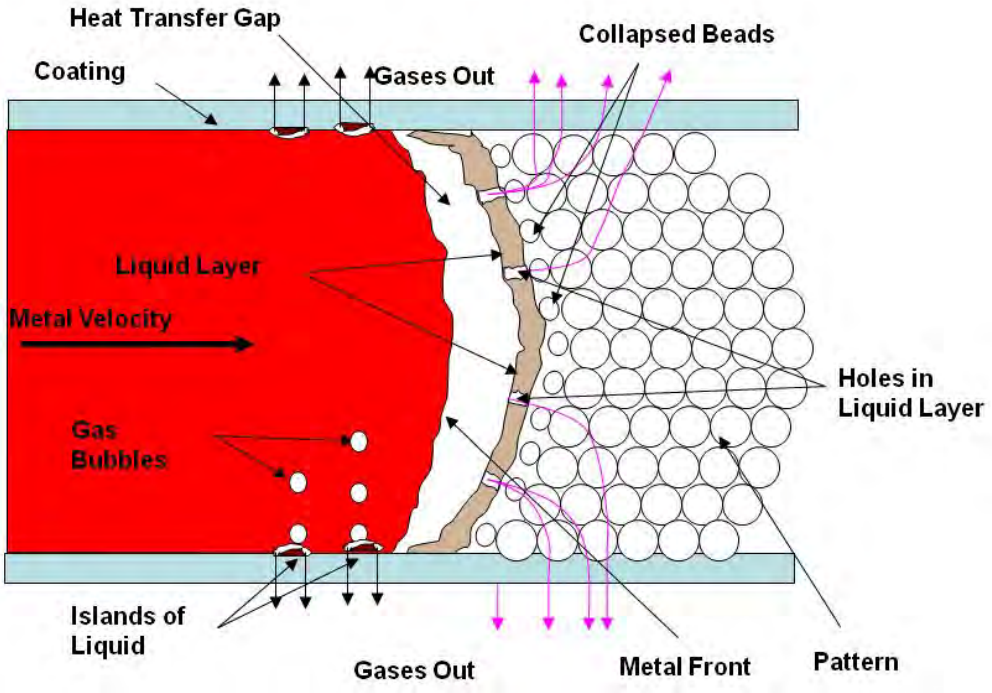

Figure 1.1.2 – Physical Model of the Lost Foam Metal/Pattern Replacement

One of the cost share partners, General Motors, Inc, released their research[2,3] achievements on the development of the physical and computational model of the lost foam casting process. Using data generated in previous research in the Lost Foam Consortium along with early research by various authors, many conflicting results were explained by allowing patterns to decompose in four distinct modes: contact mode, gap mode, collapse mode, engulf mode.

Different modes create a wide variety of observed behaviors. *Contact mode* (Figure 1.1.3) is desired and uses the formation of an undercut in the pattern during heating by the metal to resolve the heat flux/gap size dilemma mentioned above. *Gap mode* (Figure 1.1.4) is caused by excess polymer liquid (coating route is saturated by this escape mechanism) vaporizing behind the metal front. It occurs more frequently in patterns with thick sections which when they decompose in contact mode create more liquid than that pattern is able to absorb. This liquid vaporizes behind the metal front, forming bubbles that rise through the liquid metal to form a finite gap along another flow front higher up in the pattern. Along that front, the foam decomposes by melting and the coating does not absorb polymer liquid. *Collapse mode* (Figure 1.1.5) is caused by foam "fissures" connecting inter-bead pattern porosity to the coated surface. Beads collapse inside a fissure with air exhausted through coating with liquid metal filling the fissure to form a "finger". *Engulf mode* is caused by liquid foam viscosity affecting the shape of the metal flow front. It is characterized by unsteady, pulsating foam encirclement in which the metal appears to "chew" its way through the foam. This creates large bubbles filled with air, polymer liquid, and vapor.

An experimental apparatus was developed to validate the undercut feature in contact mode. With this apparatus, a coated foam pattern surrounded with bonded sand, which simulates the condition of the lost foam casting process, was dipped into liquid melt and then quenched in a tank of water right after the immersion. The quenching was expected to preserve the evidence left on the metal/pattern interface. The foam metal interface was investigated under stereo microscope. A coating undercut was observed using this method. At the metal foam interface, an undercut gap was formed between the coating and pattern to provide more coating area to remove the gaseous pyrolysis products generated during the metal/pattern replacement. The coating undercut profile such as width and length was measured. The predicted value from the model is in general agreement with the measured value.

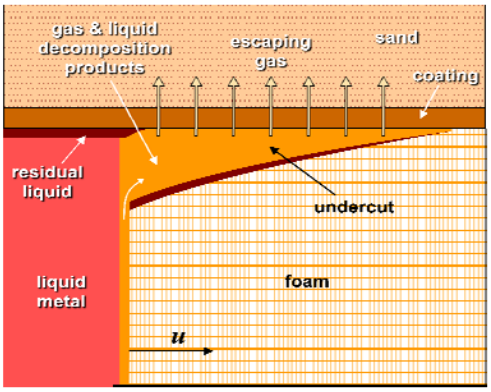

Figure 1.1.3 – Contact Mode

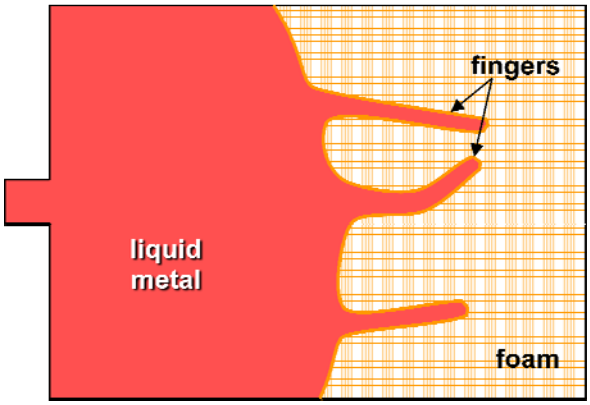

Figure 1.1.4 – Collapse Mode

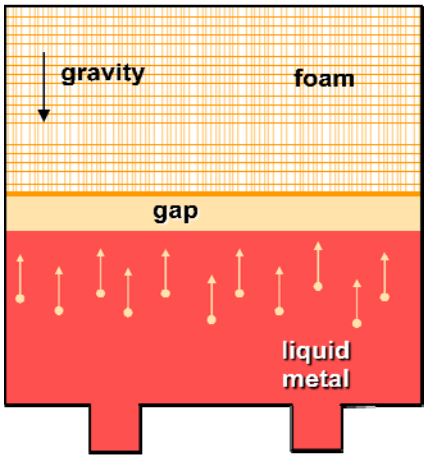

Figure 1.1.5 – Gap Mode

Subtask 1.2 Data Base

The data base of pattern pyrolysis properties was developed using the Pattern Pyrolysis Apparatus (Figure 1.2.1). The data base for currently used pattern materials is covered in detail in REPORT NO. 527985-2004 - Project Final Report submitted under DOE CONTRACT N0. DE-FC07-99ID13840. These data include gas fraction, liquid fraction, energy consumption, and pressure for various velocities, foam densities and temperatures. This data base was considered to be complete; however, additional evaluations on patterns with various levels of three types of additives were performed in the current program. This focus of this effort was intended to maximize the effect of various amounts of additives on the molecular weight reduction of patterns. The data was intended to provide properties that the GM code could use.

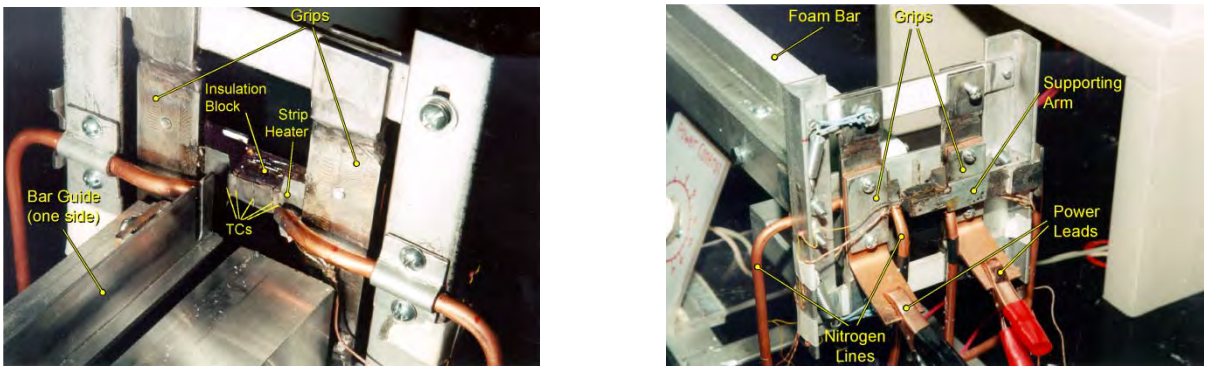

Rear View Front View

Figure 1.2.1 – Front and rear views of the Pattern Pyrolysis Apparatus

Since the Pattern Pyrolysis Apparatus had been idle for an entended time (2001 to 2005)the apparatus was inspected and recalibrated. Experiments were conducted on Expanded Polystyrene (EPS) bars 0.75 in. wide, 1.5 in. tall, and 20 to 24 in. long with an approximate density of 1.4 pcf. These bars were molded using three types of additives developed by GM R&D (GM Research and Development Center) (see Table 1.2.1) and two levels of molecular weight. The bromide additive used in production beads functions to reduce the molecular weight more rapidly during heating, hence the viscosity of the liquid pyrolysis products are moved to the coating more rapidly. Foundry experience has shown that a bromide additive in the amount of 0.36 % significantly reduced fold and porosity casting defects in aluminum.

Table 1.2.1 – Bead Descriptions

Bead A.	T175 - 0.5 wt. % BC-48; Mw 240,000 (typical)
Bead B.	T175 – 0.2 wt. % BC-48; Mw 240,000
Bead C.	T175 - 0.7 wt. % BE-51; Mw 240,000

Bead D. T175 - 0.7 wt. % BE-51; Mw 190,000
Bead E. GM1 (Proprietary)
Bead F. GM1 (Proprietary)

The test matrix for these materials is illustrated in Table 1.2.2. Prior to evaluations on the bars listed in Table 1.2.1 bars made with production T170 and T175 (bromide) beads were evaluated to establish the repeatability of the Pattern Pyrolysis Apparatus. This was considered necessary due to the reconstruction of the apparatus after usage in 2001.

Table 1.2.2 - Experimental Matrix for Foam Pyrolysis Experiments

	600 °C	670°C	730 °C	800 °C
Feeding velocity: 1.5cm/s	T170, T175, X1 - X6; Three duplicates and two liquid samples for each.	T170, T175, X1-X6; Three duplicates	T170, T175, X1-X6; Three duplicates	T170, T175, X1-X6; Three duplicates and two liquid samples for each.
Feeding velocity: 3.0cm/s	T170, T175, X1-X6; Three duplicates and two liquid samples for each.	T170, T175, X1-X6; Three duplicates	T170, T175, X1-X6; Three duplicates	T170, T175, X1-X6; Three duplicates and two liquid samples for each.
Feeding velocity: 4.5cm/s	T170, T175, X1-X6; Three duplicates and two liquid samples for each.	T170, T175, X1-X6; Three duplicates	T170, T175, X1-X6; Three duplicates	T170, T175, X1-X6; Three duplicates and two liquid samples for each.

Data recorded were gas fraction, molecular weight of liquid residue, heat flux and pressure to maintain the feeding velocities. The low feeding velocity of 1.0 cm./sec. used in 2001 was increased to 1.5 cm./sec. to increase the accuracy of the pressure measurement. This was necessary due to the noise level created by bar friction in the guides as the bars are driven into the heater (see Figure 1.2.1).

Results from these evaluations indicated acceptable repeatability of the gas fraction (Figure 1.2.2 and Figure 1.2.3)at the same velocities for bars molded with T170 and T175 beads (0.36 %bromide). The resistance pressure for these materials is illustrated in Figure 1.2.4 and indicates that the pressure values for the T170 bars were consistant between the years 2001 and 2005 ; however, the pressures for the T175 bars evaluated in 2005 were significantly higher than the 2001 data. Since the T170 pressure values

were consistent the repeatability of the apparatus was not the cause, rather a suspicion arose that the bars molded in 2005 were fused to a higher level. The pattern samples used in the previous studies were produced during a batch cycle under controlled conditions while the second batch was produced about four years later. Experience has shown that patterns from separate batches can have considerable different values of permeability. This suspicion was not confirmed with pattern permeability evaluations.

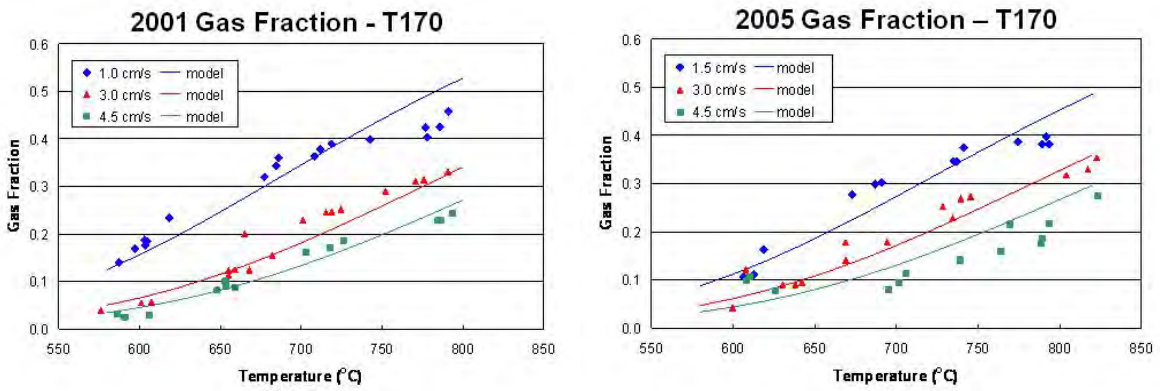

Figure 1.2.2 – Repeatability of Gas Fraction Results for T170

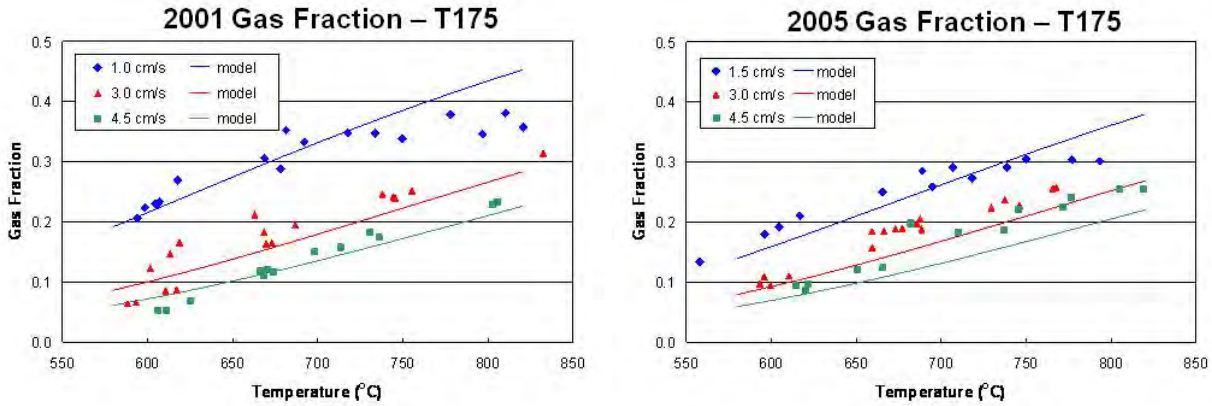

Figure 1.2.3 - Repeatability of Gas Fraction Results for T175

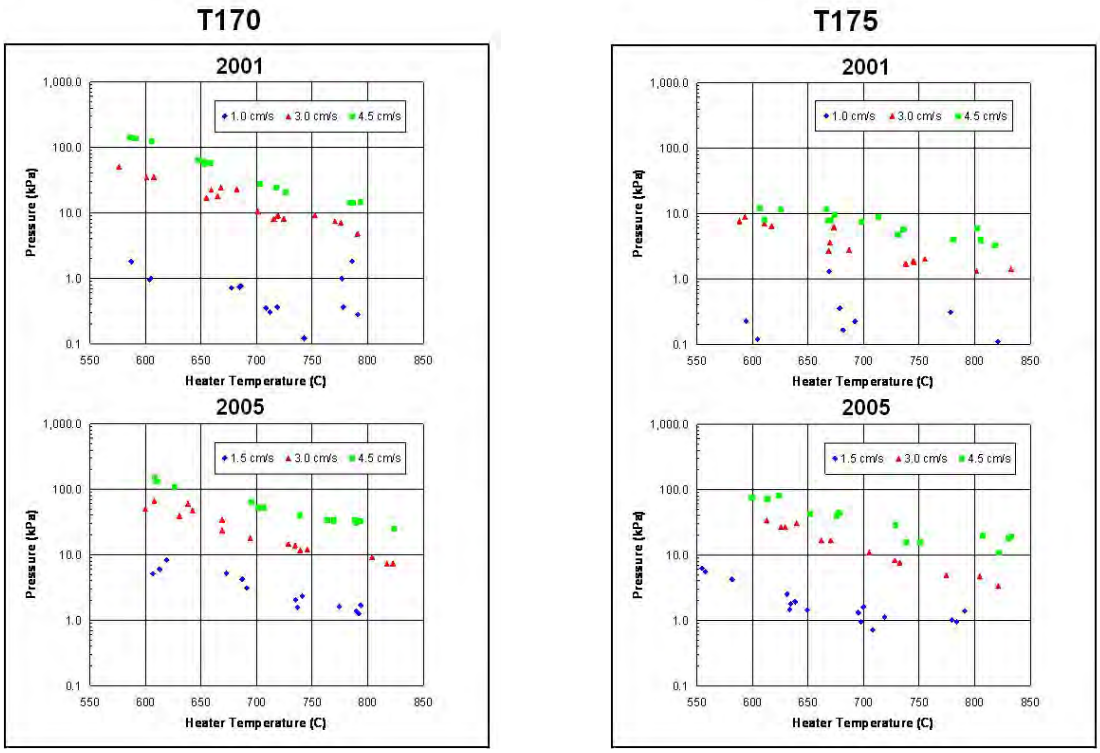

Figure 1.2.4 – Repeatability of Resistance Pressure for T170 and T175

The results for the molecular weight of the residual liquid products for all test bars are illustrated in Figure 1.2.5. Clearly the production beads with 0.5 % BC48 additive and a initial molecular weight of 240,000 (BeadA)demonstrated the largest reduction in molecular weight for the bars made for this study; however, the molecular weight reduction for production T175 (typical 0.36 wt. % of bromide) was slightly more. In general, none of the other beads (B,C,D,E,F) had molecular weight reductions comparable to bead A or T175.

Note the reduction in molecular weight for T170 (no additive) compared to T175 (0.36 % bromide). This comparison explains why aluminum castings made from patterns produced with bromide have significantly less fold and porosity defects.

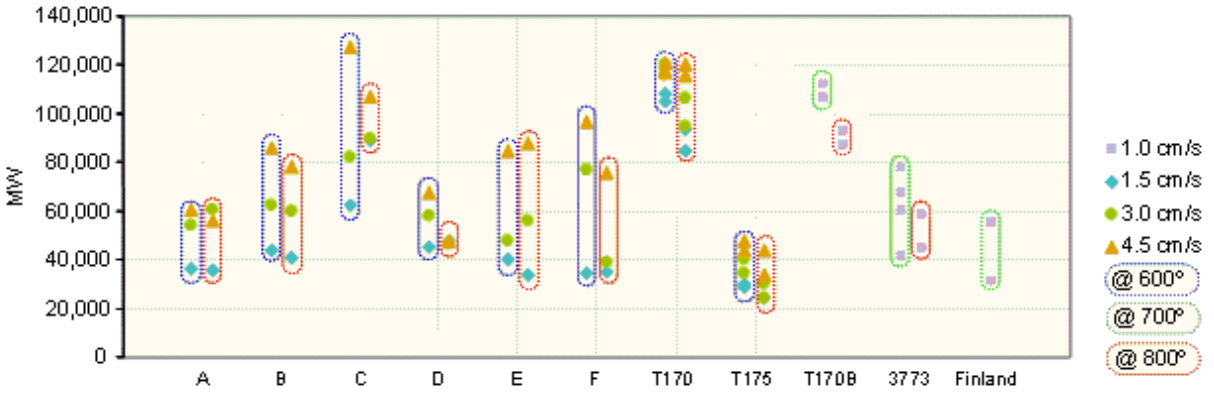

Figure 1.2.5 – Molecular Weight of Residual Liquid for Test Bars

Assuming the second batch of patterns was indeed fused at a higher level (lower permeability) the higher pressures were a result of the inability of the pyrolysis gases to escape freely. This phenomenon was previously described in Subtask 1.1. The gas escape paths in the Pattern Pyrolysis Apparatus are the gap between the heater and receding pattern along with the permeable path through the pattern, hence, if the path through the pattern is more restrictive higher pressures will result.

Subtask 1.3 Commercial Codes

Over the course of previous and current research computational modeling of fill and solidification for Lost Foam castings has matured. The improvements described in this section and later in Subtask 4.1 have provided the necessary technology for this maturity.

Three major commercial software companies, Flow Science (Flow3D), ESI North America and Magma Soft were cost share sponsors of this program. All three companies demonstrated strong interests in improving their codes using experimental data developed at UAB. Flow3D has historically expressed the most interest with assistance in resolving processing issues and willingness to incorporate changes to their code. General Motors also developed their own code, “Foam Fill”, for the lost foam process. Development of this code is the best utilization of research achievements made by UAB. This code was submitted to the commercial software companies; however, none of the companies were willing to spend the necessary funds to integrate the code into theirs due to the lack of return on investment. General Motors has used this code extensively to identify casting defect issues on existing castings and to identify production parameters for new castings.

A trial simulation using the ESI Procast software matrix was processed. Input parameters such as pattern properties, coating thickness, coating permeability, gas fraction, and heat transfer coefficients were selected

from the ESI and UAB data bases. Data from the two sources have different values. Results from the simulation predict the metal filling velocity using UAB data was half of that using ESI data. The metal filling velocity using UAB data agrees with the measured data using real time X-Ray. Effects of coating permeability on metal velocity were observed but at a higher than measured permeability value. The effect was not as significant as observed in Real Time X-Ray. Effects of glue joints on metal filling were predicted. The metal response was generated by simply pausing the metal filling for one second when the metal reached the glue joint. Based on these results a decision was made that using the ESI software for further simulations was not efficient for the program.

Shrinkage Predictions – Practically all commercial codes used for foundry applications possess the ability to predict metal shrinkage. Experience has shown that most of the commercially available code perform satisfactorily when predicting shrinkage in empty cavity molds such as green sand, bonded sand and die casting. These molds fill rapidly which results in small temperature differences throughout the casting. Modeling shrinkage in castings from these casting processes is straightforward and for practical purposes instantaneous fill (at uniform temperatures) can be used except in complex casting with thin wall sections. Lost Foam presents a challenge to the modeler through a relatively slow fill rate which produces non-uniform temperatures throughout the casting. Hence the solidification process must consider these temperature variations for correctly predicting shrinkage during solidification.

Initial attempts to predict shrinkage in complex Lost Foam castings were unsuccessful. Using published values for enthalpy and metal density simulation results were compared to sectioned castings, the predicted location and size of the shrinkage did not agree with the casting results. In addition the temperatures measured with thermocouples in castings did not agree with predicted temperatures[4]. Figure 1.3.1 illustrates the difference in predicted and measured temperatures in a four cylinder head casting using published enthalpy. These predicted temperatures did not accurately predict metal shrinkage or other defect location and size.

Reasons for the discrepancies were traced to inaccurate published values of enthalpy in the mushy zone (liquidus to solidus temperatures) where energy is released. Significant efforts were devoted to develop accurate enthalpy values for commonly used aluminum - silicon casting alloys. Figure 1.3.2 illustrates the published values for enthalpy for an aluminum - silicon alloy compared to calculated values. The technique used for calculations is the Silicon Equivalence Method described in the literature. This method incorporates the effect of silicon which contains four times the enthalpy compared to aluminum. Using the calculated values of enthalpy the predicted values of temperatures agreed satisfactorily (Figure 1.3.3).

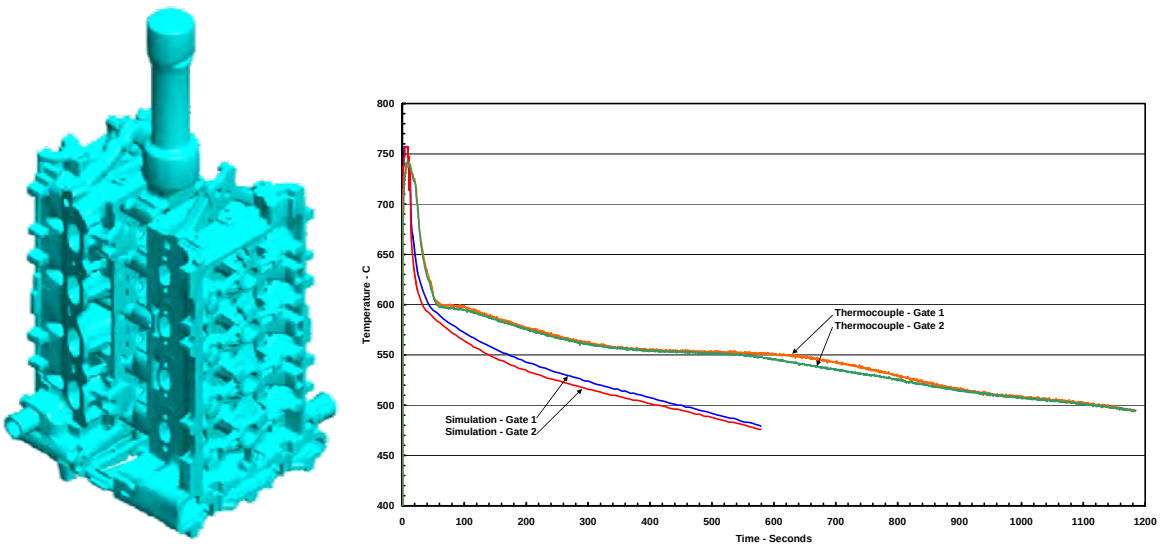

Figure 1.3.1 – Temperature Comparisons in a Four Cylinder Head Casting

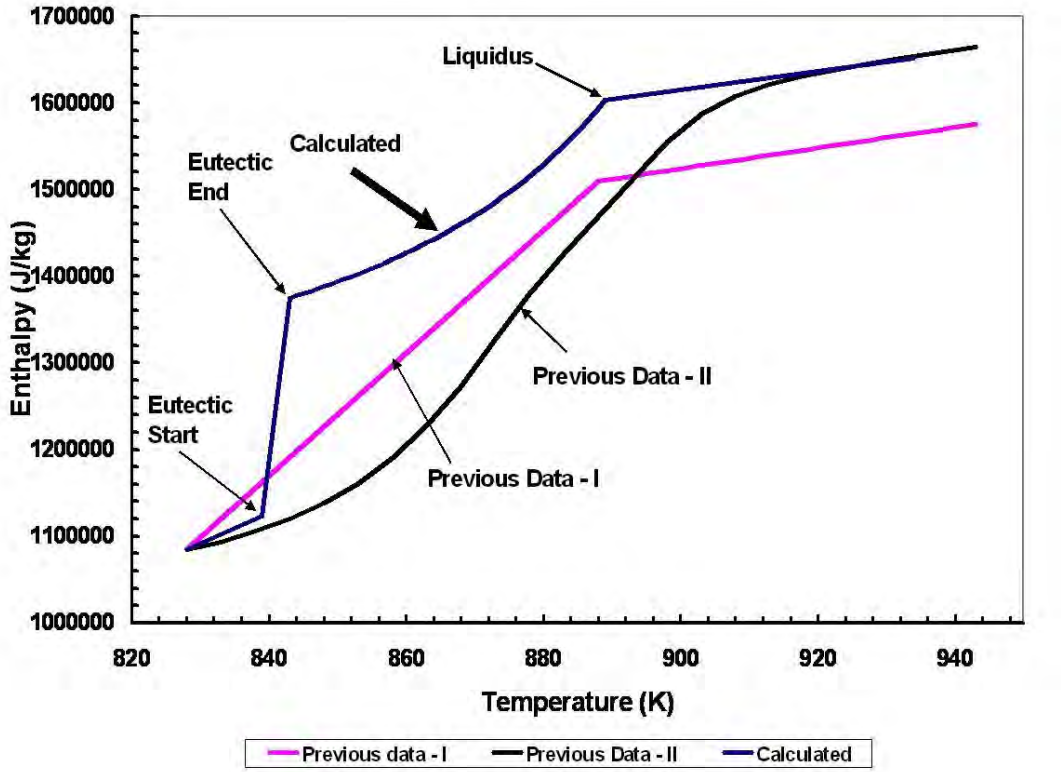

Figure 1.3.2 – Comparison of Published and Calculated Enthalpy Values

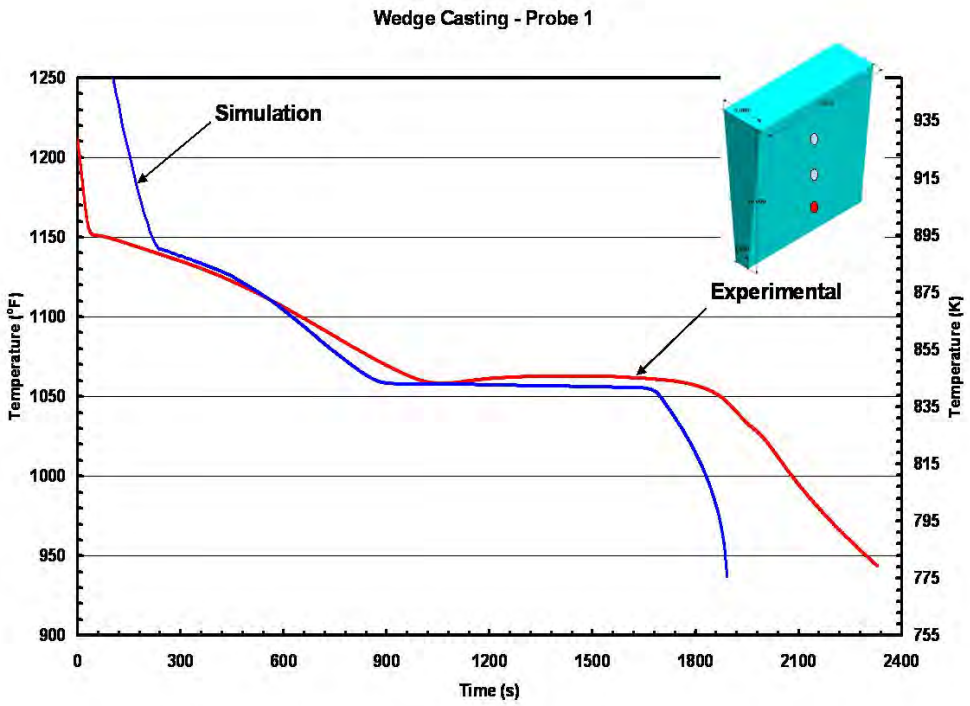

Figure 1.3.3 – Comparison of Simulated and Measured Temperatures Using Calculated Enthalpy Values

Another important discovery concerned the metal density values used in predicting shrinkage. When typical measured density values of finished castings were used in shrinkage prediction simulations the shrinkage predicted were accurate for large areas but did not predict smaller areas. When theoretical values of density were used the smaller areas of shrinkage were predicted and confirmed with sectioned castings.

Modeling of complex castings using Flow 3D has been evaluated using a cluster of 16 processors to decrease computation time. The results indicate that computation time can be reduced by factors of 10 to 20 depending on the number of processors used. Shrinkage predictions for V6 engine blocks, L6 engine blocks, 25 mm plates and wedge castings have been completed. These predictions were compared to cut sections of castings and X-Ray results of the plates and wedge. Results indicate that the predicted location and size of shrinkage matched the location and size in the castings. The simulation results from the V6 engine block studies are illustrated in Figure 1.3.4. Note that the size and location of the shrinkage in the cut sections of these castings match the simulations. These simulations were performed using the calculated metal enthalpy and theoretical metal density. Similar predictions and confirmations of shrinkage were performed on in-line four and six cylinder blocks. This shrinkage was eliminated by changing the gating arrangement and will be presented in Subtask 4.1 (Gating)

of this report. This breakthrough technology can aid designers in eliminating shrinkage in castings prior to production.

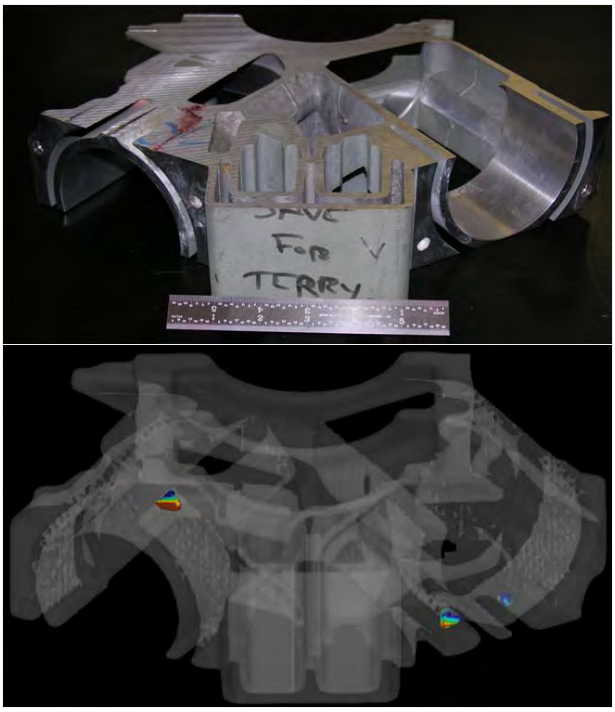

Shrinkage in a Cut SectionPredicted Shrinkage

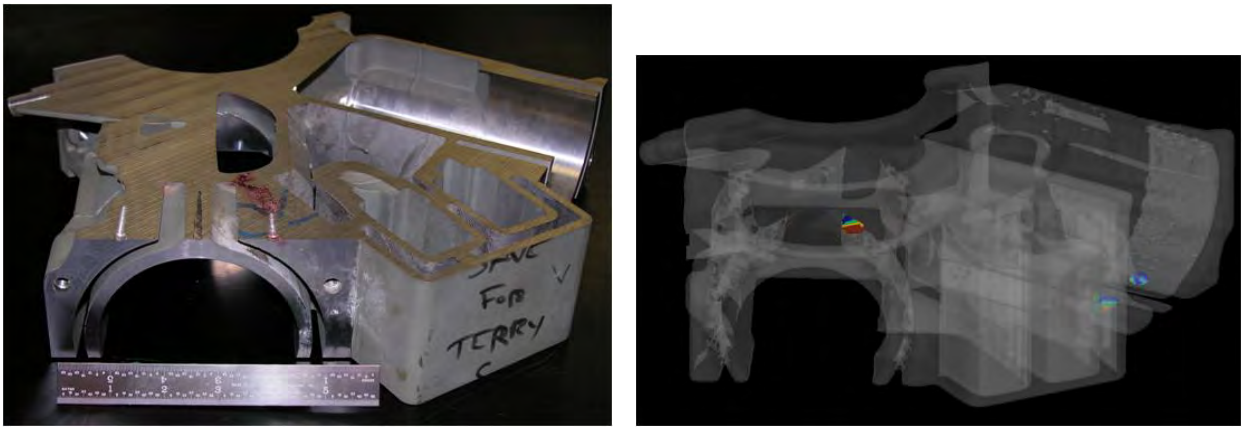

Shrinkage in a Cut SectionPredicted Shrinkage

Figure 1.3.4 – Shrinkage Predictions and Validation for a V6 Engine Block

Task 2 – Improve Pattern Quality and Consistency

Subtask 2.1 – Pattern Properties

Past research[5,7] has shown that pattern permeability is a major source of

control for metal filling and defect formation in Lost Foam Castings. This was discovered using Real Time X-Ray to view metal replacement of plate patterns and is discussed in detail in REPORT NO. 527985-2004 - Project Final Report submitted under DOE CONTRACT N0. DE-FC07-99ID13840.

The objective of this task was to improve pattern quality and consistency through 1.) identification of the root causes of pattern permeability variations within patterns and 2.)implementation of procedures to control these variations. Prior to any laboratory evaluations to identify the root causes of pattern permeability variations a large design of experiment (DOE) was performed to confirm that indeed pattern permeability was a major control in metal filling and defect formation in aluminum Lost Foam castings.

This DOE consisted of 12 patterns each with 4, 12 and 24 mm. thicknesses, high and low fusion (controlled by steaming time) and low and high coating permeability. All patterns were coated with the same coating (high or low perm) using the same batch of coating. Permeability maps were generated using the prototype pattern permeability apparatus shown in Figure 2.1.1. Coated patterns were poured using de-gassed 356 aluminum and metal filling viewed by the Real Time X-Ray. The pattern and gating arrangement is shown in Figure 2.1.2. Metal velocities and metal front shapes were determined from the X-Ray videos. Castings were visually inspected and defects were recorded.

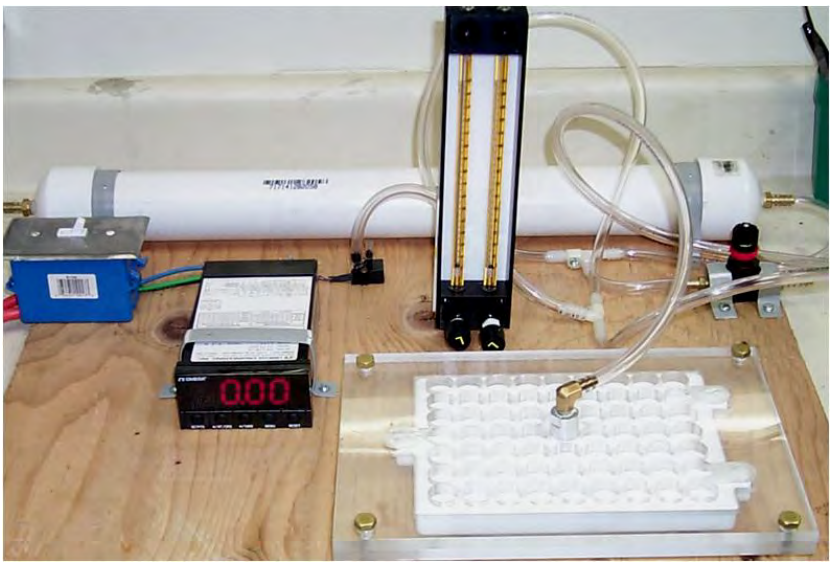

Figure 2.1.1 – Prototype Pattern Permeability Apparatus and Fixtures

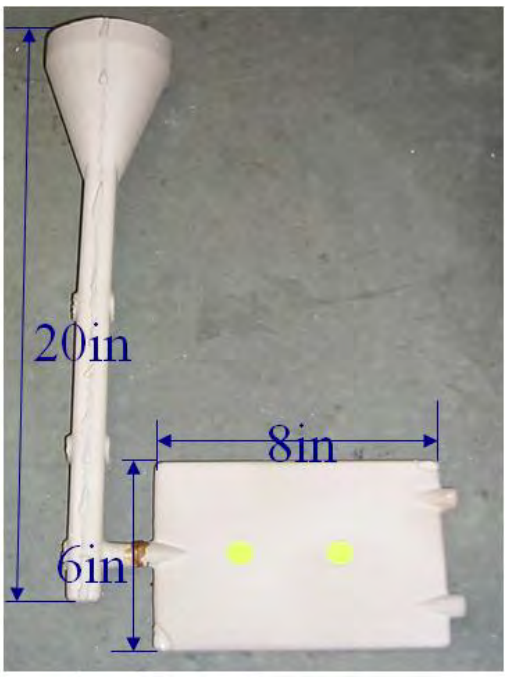

Figure 2.1.2 – Coated Pattern, Sprue and Gating

A summary of the results is shown in Table 2.1.1. Pattern thicknesses are listed in mm., pattern fusion (permeability) and coating perm levels are shown as Low (L) and High (H), filling velocities are listed in in./sec., filling behavior describes the number of converging metal fronts, number of fold defects observed on castings and progressing angle describes the overall velocity vector of the metal filling.

Table 2.1.1 – Results of Casting Trials

Part Number	Thickness	Pattern Fusion	Coating Perm	Filling Velocity	Filling Behavior	Fold Defect	Progressing angle
6111	24	L	L	0.568	3	7	10
6112	24	L	L	0.525		2	
6113	24	L	L	0.571	2	5	10
6121	24	L	H	0.597	2	4	20
6122	24	L	H	0.625		1	
6123	24	L	H	0.726	1	11	20
6221	24	H	L	0.658	3	2	0
6222	24	H	L	0.612	1	4	0
6223	24	H	L	0.685	2	2	0
6211	24	H	H	0.624	1	3	10
6212	24	H	H	0.490	0	3	7
6213	24	H	H	0.596	2	2	3
1111	4	L	L	1.221	5	0	90
1112	4	L	L	1.287	5	0	90
1113	4	L	L	0.981	5	0	90
1121	4	L	H	1.279	8	0	90
1122	4	L	H	1.227	7	0	90
1123	4	L	H	1.203		1	90
1211	4	H	L	0.394	3	2	90
1212	4	H	L	0.362	2	3	90
1213	4	H	L	0.378	4	2	90
1221	4	H	H	0.470	3	1	90
1222	4	H	H	0.443	3	3	90
1223	4	H	H	0.467		2	90
3111	12	L	L	0.871		8	
3112	12	L	L	0.778	7	7	90
3113	12	L	L	0.817	8	6	90
3121	12	L	H	0.716	9	5	90
3122	12	L	H	0.712	9	3	90
3123	12	L	H	0.707		3	
3211	12	H	L	0.495	0	0	10
3212	12	H	L	0.474		0	
3213	12	H	L	0.460	2	0	10
3221	12	H	H	0.475		0	
3222	12	H	H	0.440	3	0	10
3223	12	H	H	0.497	2	0	10

ANOVA analyses of the results are illustrated in Figures 2.1.3, 2.1.4 and 2.1.5. Pattern thickness and pattern fusion had the most significant effect on the metal filling velocity (Figure 2.1.3). Note that the coating perm had the least effect on metal filling velocity. Historically foundries attempted to control metal filling with coating perm changes when, in fact,

the pattern fusion and thickness were controlling by their interactions. For aluminum castings the pattern and coating permeabilities form a system permeability with the pattern perm dominating. When the driving force for metal filling is decreased because of the highly fused patterns, the surface tension of the molten aluminum dominates the metal filling.

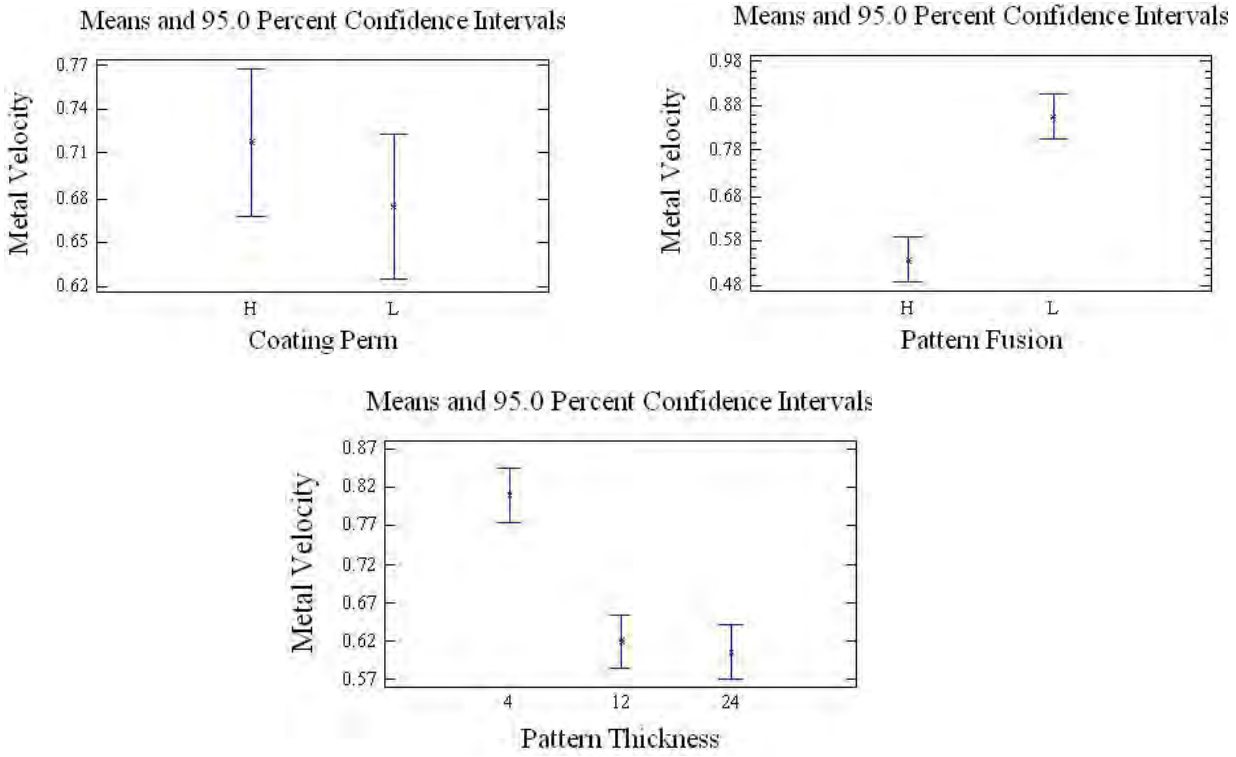

Figure 2.1.3 – Effect of Coating Perm, Pattern Fusion and Pattern Thickness on Metal Velocity

Figure 2.1.4 indicates that pattern perm and pattern thickness exercise the most control of the filling behavior (number of converging metal fronts) while coating had the least effect and largest spread in the data. This indicates a reasonably strong interaction between coating perm with pattern perm and thickness.

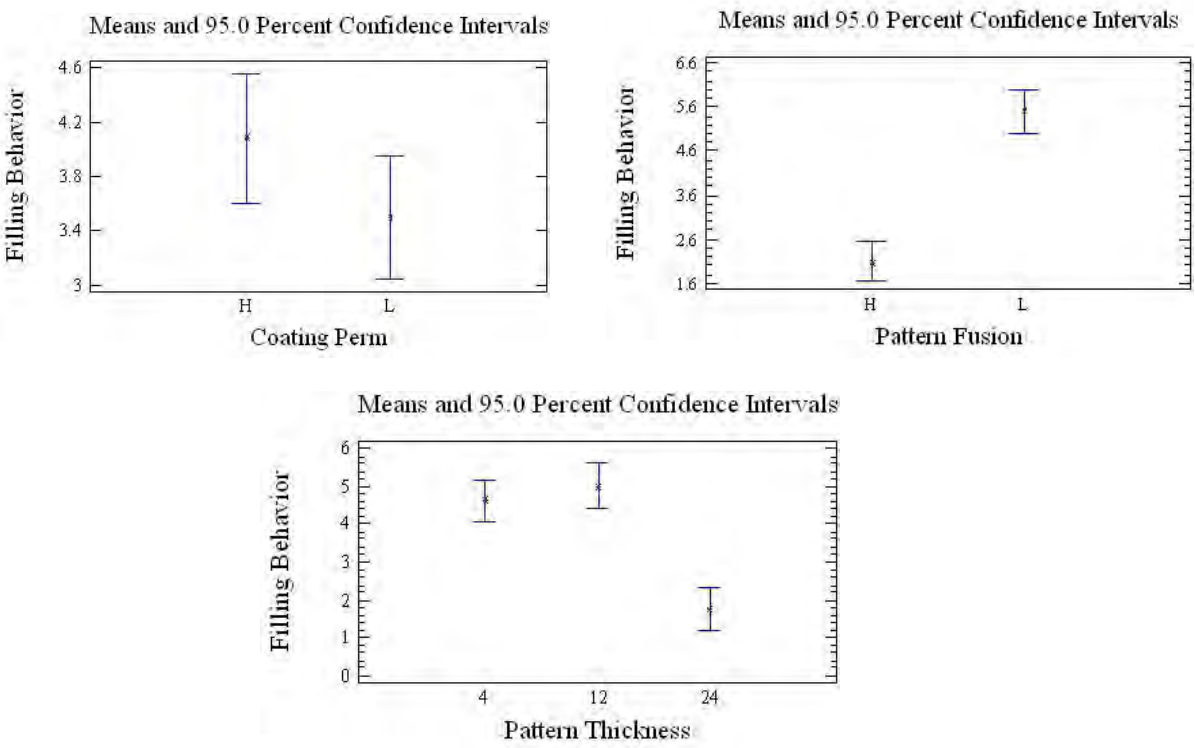

Figure 2.1.4 – Effect of Coating Perm, Pattern Fusion and Pattern Thickness on Filling Behavior (Number of Converging Metal Fronts)

Figure 2.1.5 illustrates the effect of coating perm, pattern fusion (perm) and pattern thickness on the incidence of fold defects. Clearly the pattern fusion (perm) and pattern thickness are dominating the incidence of fold defect while coating perm has a smaller effect. However, remember that the interaction between the three factors is significant.

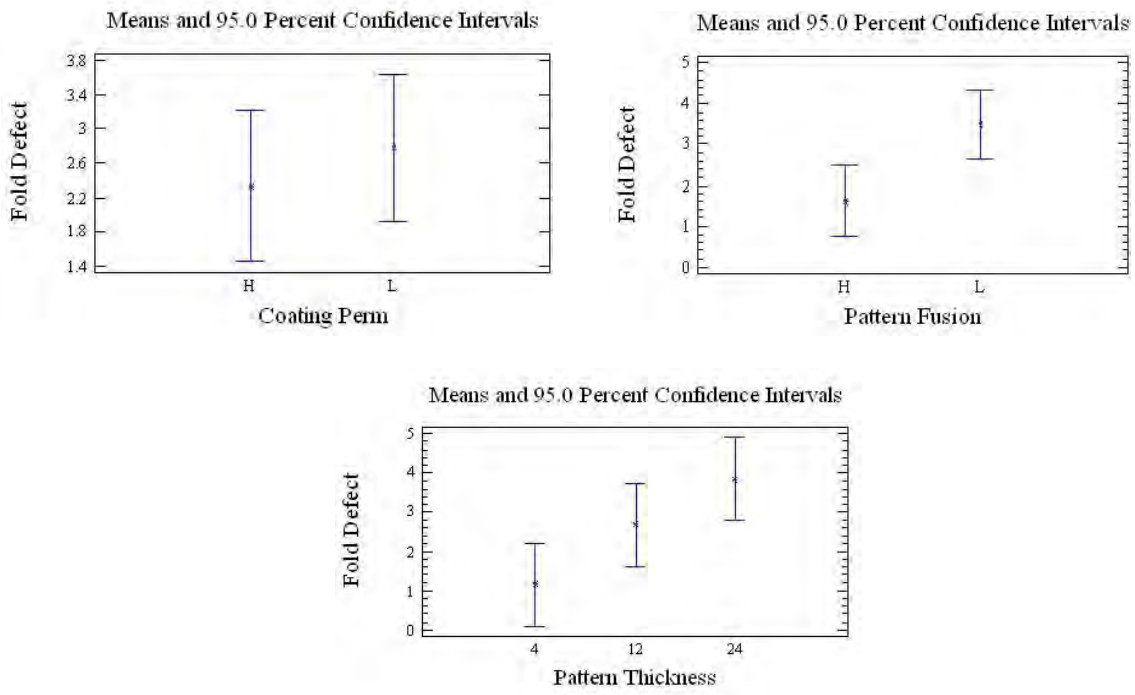

Figure 2.1.5 - Effect of Coating Perm, Pattern Fusion and Pattern Thickness on Number of Fold Defects on Castings

A clearer understanding of the effects of pattern fusion, coating perm and pattern thickness can be observed in Figure 2.1.6. In this figure LL indicates low pattern fusion (high perm) and low coating perm, LH indicates low pattern fusion and high coating perm, HL indicates high pattern fusion (low perm) and low coating perm and HH indicates high pattern fusion and high coating perm. Note that the low fusion patterns have the highest number of merging metal fronts and folds and that the coating perm has little effect. Likewise the high fusion patterns have the least number of merging metal fronts and folds and that the coating perm has little effect.

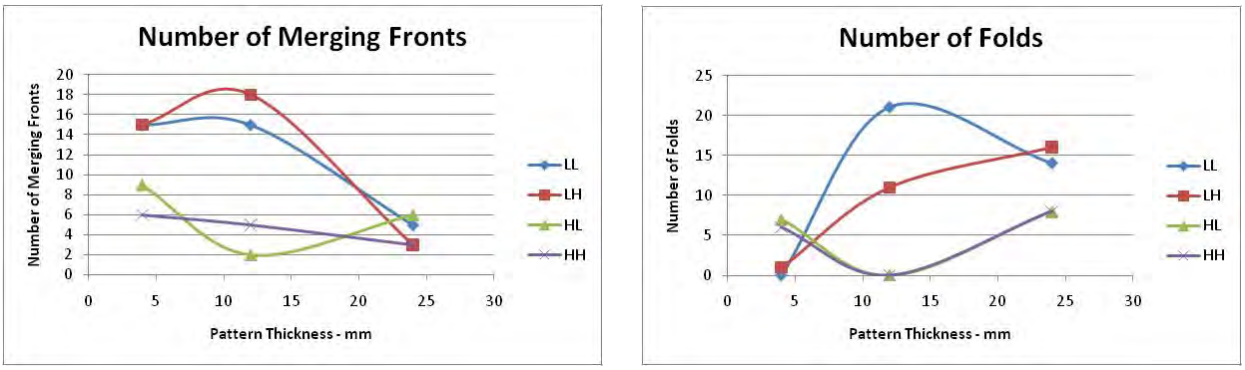

Figure 2.1.6 – Effect of Pattern Fusion, Coating Permeability and Pattern Thickness on the Number Merging Metal Fronts and Fold Defects

This study clearly revealed the role of pattern permeability in the formation of fold defects in aluminum Lost Foam castings and warranted further study to identify the pattern properties that control permeability.

Characteristics of Pattern Permeability – With an in kind contribution from one of the sponsors in this program, the effect of pattern molding parameters on pattern quality was investigated. A series of foam pattern molded by different parameters, such as steam time, steam pressure, cross steaming direction, cooling time and format, were studied using pattern permeability (air flow rates – $cm^3/sec.\text{-}cm^2$) and density as the measured parameters. Patterns were 10 mm. thick and molded using vented and ventless tooling. These measurements were made using the prototype pattern permeability apparatus (Figure 2.1.1) and a fixture that provides measurements at specific locations. Throughout this discussion the term permeability will be used to describe the air flow rate measured by the pattern permeability apparatus. Hence high permeability infers high air flow rates. Preliminary analysis of these data showed that there is a strong relationship between molding parameters and pattern permeability.

When cross steaming was used, the pattern surface facing the direction of the steaming was much better fused (lower permeability) than the opposite surface. This is illustrated in Figures 2.1.7 and 2.1.8 for the fill gun side and non fill gun side of a cross steamed pattern. As the steam travels through the pattern, the steam energy was consumed and cannot fuse the beads on the opposite surface as well as the first exposed surface. Additionally, as the cross steaming direction is reversed steam cannot penetrate the pattern thickness due to the decreased permeability from the initial steaming. Hence the pattern surfaces are fused differently. Note the non fill gun side (Figure 2.1.8) of the pattern has larger areas of lower permeability than the fill gun side (Figure 2.1.7). This is the result of cross steaming as explained above.

The average pattern permeability and permeability gradient within the pattern also varied from cycle-to-cycle or pattern-to-pattern due to unidentified causes; however later evidence indicated the variation was caused by inconsistent bead filling. The values of average permeability are plotted in sequence of molding from left to right. This is illustrated in Figure 2.1.9.

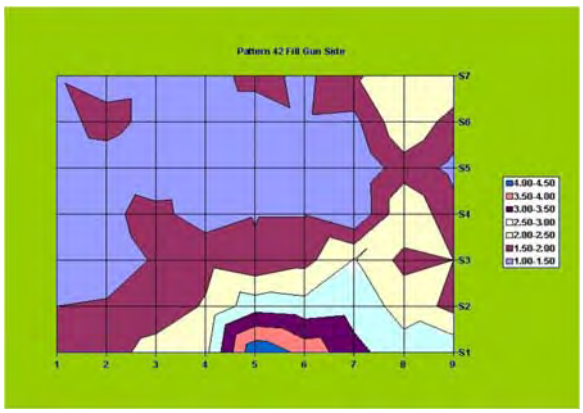

Figure 2.1.7 – Permeability Map for Plate 42 – Fill Gun Side

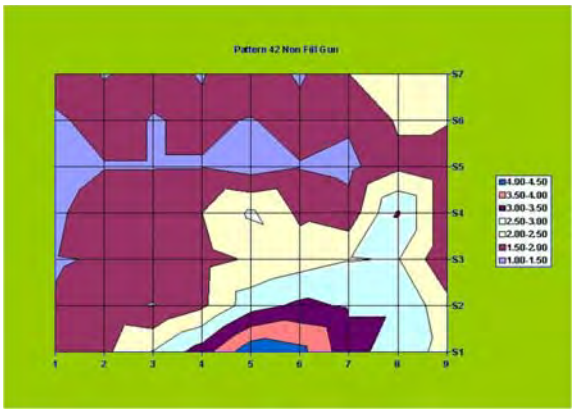

Figure 2.1.8 – Permeability Map for Plate 42 – Non Fill Gun Side

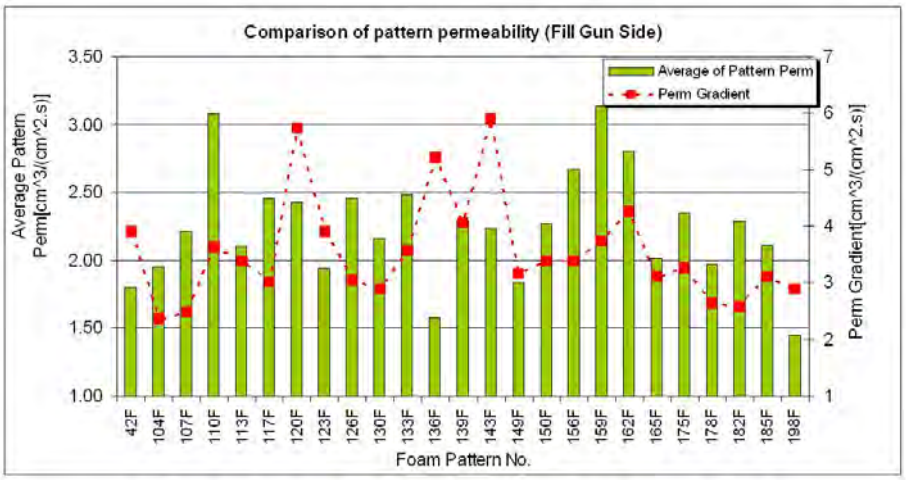

Figure 2.1.9 – Average Pattern Permeability and Permeability Gradient as a Function of Molding Sequence – Left to Right.

This variability was troubling and prompted a study to determine the threshold of permeability that affects the metal front shape which is known to affect casting defects. Permeability measurements for patterns were compared to metal front shapes using the Real Time X-Ray for the same pattern indicate that local pattern air flow rates above 0.5 $cm^3/sec.\text{-}cm^2$ appears to cause local perturbations in metal front shapes that could generate casting defects from merging metal fronts. Uniformity in pattern air flow rates may be more important than the absolute value. Producing uniform local bead density during pattern filling may require improvement to make the lost foam casting more robust.

On the other hand, the moving steam can move beads in a loosely packed area (generated during bead filling) to achieve a better packing arrangement. This phenomenon has been observed using high speed videos by GM personnel[7].

Measurements of air flow at specific locations on a batch of plate patterns prepared by a sponsor are generally repeatable. To some extent, pattern density profiles are similar to pattern permeability; however, there is no physical or theoretical relationship that defines permeability in a fixed geometry filled with deformable beads.

Bead size and number of non-uniformly packed bead locations in high perm and low perm areas in the same foam pattern were compared. The number of non uniformly packed locations is slightly higher in the high permeability areas of both high and low fusion patterns, compared to the low permeability areas, the bead size of both high and low perm area is very close, indicating that these areas got similar steaming. Therefore, in both low and high fusion patterns, bead packing (the bead size and number of non-uniformly packed bead locations) determines pattern permeability and consistency.

Pattern permeability was determined to be repeatable at all thicknesses within a batch of patterns. For low fusion patterns, the thinner the plates are, the higher the permeability. However, for high fusion patterns the thinner the plates, the lower the permeability. This indicates that pattern steaming can reduce the effects of non uniform bead packing and pattern geometry. Uniformity in pattern air flow rates appears to be more important than the absolute value. Producing uniform local bead density during pattern filling may require improvements to make the lost foam casting more robust.

Arena-flow-EPS software tool was validated on test patterns to predict the final fill behavior as well as the transient filling. In addition, calculations of final pattern density variations were validated by Arena-flow-EPS computation fluid dynamics. This engineering software tool is being used for production process design development of lost foam patterns to identify deficiencies and improvements.

Pattern Permeability Apparatus – The importance of uniform pattern permeability has been established. The need for a commercial apparatus to measure pattern permeability prompted the development of a Pattern Permeability Apparatus that could be used at the pattern molding equipment or other locations within a Lost Foam facility. This apparatus is illustrated in Figure 2.1.10. The apparatus is portable and requires only electrical power and compressed air for operation. The contact probe is fitted with a soft plastic insert that contacts the pattern. These units were calibrated at UAB using traceable sources for pressure and flow rates. The apparatus provides a vacuum of -3.0 psig to the probe. Vacuum was chosen to allow operation at the molding equipment where molded patterns, containing condensed steam, are extracted. An internal filter removes the water to prevent damage to the mass flowmeter that measures the air flow rates. Approximately twenty of the Pattern Permeability Apparatus devices have been delivered to Lost Foam foundries and Pattern blowing companies. A Pattern Permeability Apparatus Manual has been assembled and is supplied with each apparatus. In addition UAB personnel have demonstrated the

utility of the apparatus in Lost Foam companies through tutorials and applications where improvements to pattern quality were required.

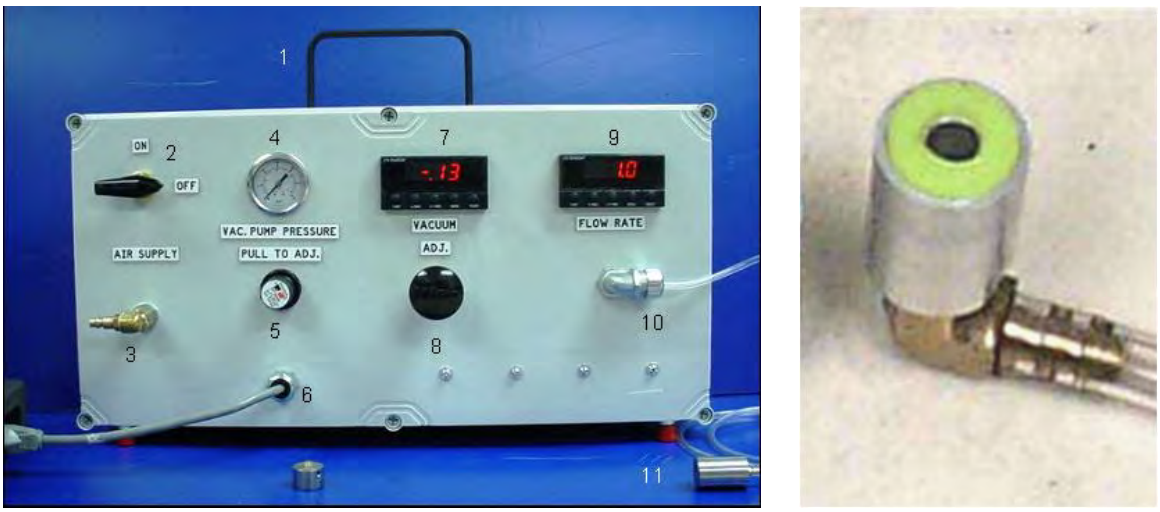

Figure 2.1.10 – Pattern Permeability Apparatus and Probe

Bead Filling of Patterns – Non uniform packing of beads during pattern mold filling has been identified as necessary to provide uniform pattern permeability. Beads packing arrangements during filling have been observed to include cubic, tetrahedral and bridged. The literature reveals that a cubic packing of spheres (beads) has a density of 25 % less than the tetrahedral packing and a permeability that is an order of magnitude higher. Bridged packing has an even lower density with an unknown higher permeability. As previously mentioned steaming of these packing arrangements can reduce the permeability by deforming the spheres into shapes to close the void space between beads. When pattern molds contain combinations of beads packed in the three packing arrangements mentioned above prior to steaming the result is varying permeability throughout the molded pattern. The goal of this study was to determine the causes of inconsistent bead packing and develop techniques to reduce the variability.

A study to identify the controlling parameters of bead filling was completed. The experimental equipment is illustrated in Figure 2.1.11 and consists of a commercial fill gun, a repeat timer with independent on/off times and a high volume, fast acting, four way air valve. A canister of pre-expanded beads (not shown) was placed below the equipment to provide a supply of beads.

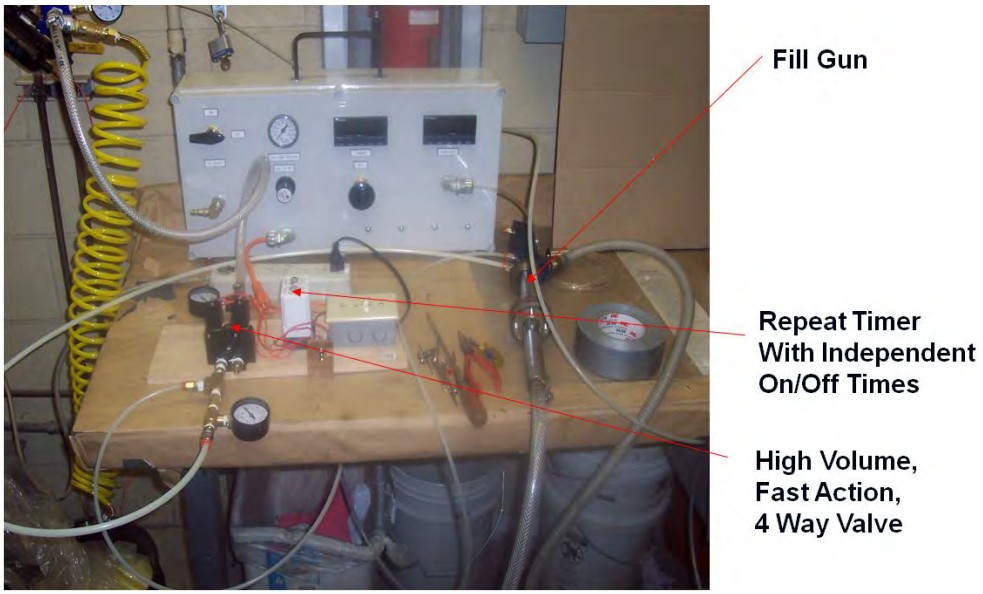

Figure 2.1.11 – Experimental Equipment for Bead Filling

The test matrix for the bead blowing experiments is shown in Table 2.1.2. This matrix provided evaluations of fill gun pressures, the effect of pulsing the air flow to the fill gun, the effect of pulsing the bead flow while maintaining air flow to the fill gun, mechanical vibration to the pattern tool and the effect of anti-static beads.

Table 2.1.2 – Bead Filling Test Matrix

Fill Gun Pressure	20 – 80 psig
Pulsed Air to Fill Gun	1 – 5 seconds
Pulsed Beads – Constant Air	1 – 5 seconds
Vibration During Filling	Normal and Pulsed Air
Antistatic Beads	
Horizontal Vertical Orientation	
Fill Gun Location	

Both vented and ventless tools were used for these evaluations and are shown in Figure 2.1.12 and 2.1.13. The vented tool was constructed using polycarbonate sheets with .375 dia. vents spaced at 2 inch intervals. The ventless tool was similarly constructed without discrete vents and venting was provided by spacing the plates apart a specified amount with shims. Inside dimensions of these tools are 10.31 in. wide x 17.62 in. long x 0.5 in. thick. Each tool has the capability of changes in thickness, fill gun location, vent function and internal features.

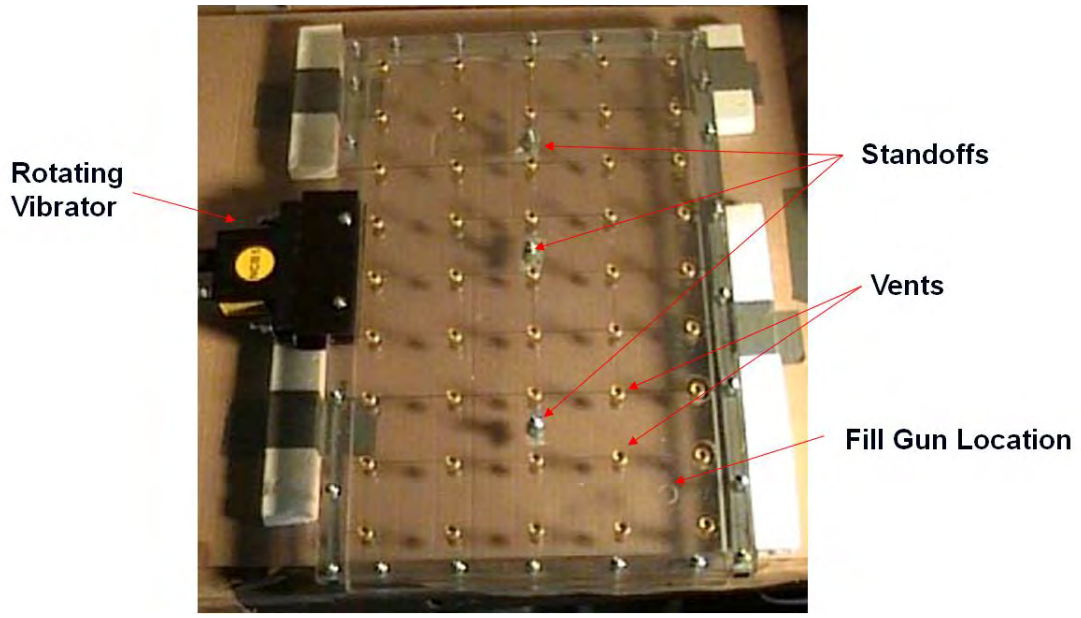

Figure 2.1.12 – Polycarbonate Pattern Tool with Discrete Vents

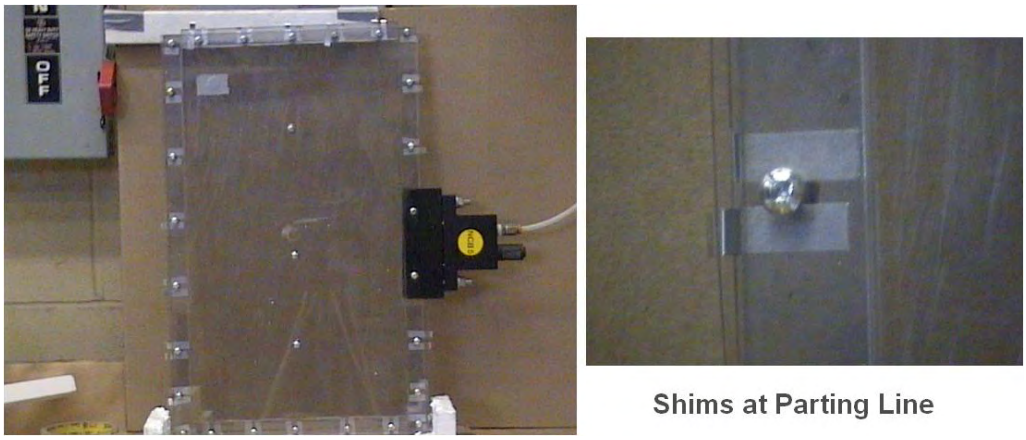

Figure 2.1.13 – Polycarbonate Pattern Tool with Parting Line Venting

The test procedures followed in this study were:

1. Fill the tool according to the test matrix.
2. Activate the mechanical vibrator.
3. Observe and record the amount of bead settling in the tool. Bead settling after filling was an indication of incomplete bead packing during filling. Patterns steamed with incomplete bead packing would have permeability gradients as described previously. This technique is similar to the mechanical vibration applied to a flask to fill and densify the sand in and around a Lost Foam pattern cluster. Figure 2.1.14 illustrates the bead settling in a discrete vented tool after applying mechanical vibration.

4. Video recording of fill and results of vibration.
5. Inspection of bead packing using back lighted X-Ray viewer.

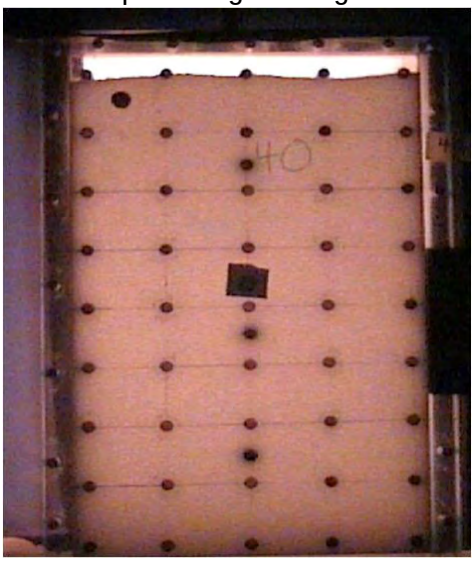

Figure 2.1.14 – Bead Packing Enhanced by Mechanical Vibration

Results using discrete vented tool:

Fill gun pressure – As expected, tool fill times were significantly reduced for higher fill gun pressures and bead packing efficiency increased; however, at a typical production pressure of 80 psig (552 kPa), the volume occupied by the beads decreased by 10% - 12% when vibration was applied.
Pulsed air to the fill gun –The results indicated some improvement in bead packing at the surface of the tool; however, the volume decrease during vibration was about 10% – 12 %.
Pulsed beads with constant air flow – These fills yielded improved bead packing (over the pulsed air) but fell short of maximum packing as revealed by settling during vibration.
Anti–static beads – These fills used beads coated with an anti-static agent. Although bead handling improved significantly, the bead packing efficiency experienced little improvement.
Horizontal and vertical tool orientations – Bead packing efficiency was practically the same for both orientations although the horizontal orientation tended to improve the surface packing.
Vibration during fill – These fills indicated that bead packing efficiency was significantly improved. No visible settling was observed when vibration was applied after fill.
Visual Observations – Figure 2.1.15 illustrates the formation of high density lines and high density areas around each vent. These observations were made prior to any mechanical vibration.

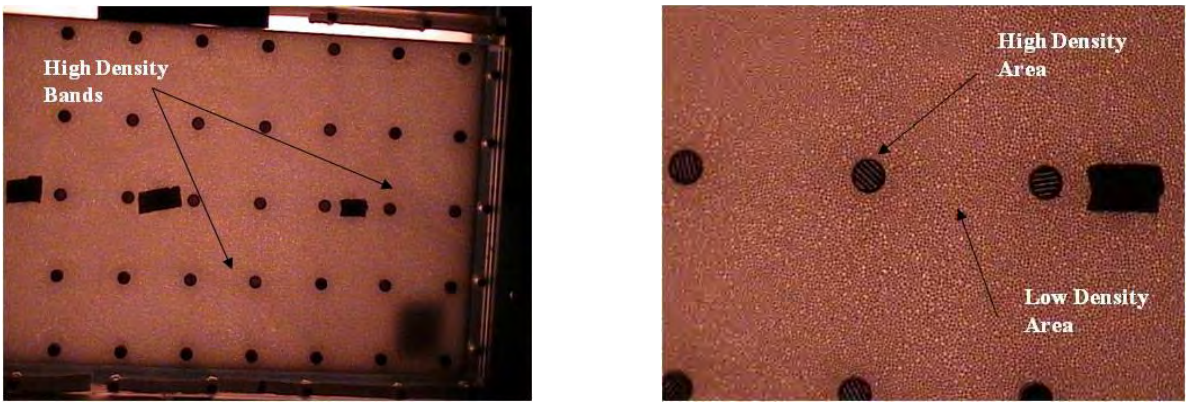

Figure 2.1.15 – Observations of Bead Packing Efficiency Using Back Lighting

Results using parting line vented tool:

Since the test conditions of pulsed air, pulsed beads and anti static beads indicated little or no influence on the bead packing efficiency with the discrete vented tool, these conditions were omitted from the test matrix used in the centerline vented tool evaluations. Fill gun pressure was fixed at 80 psig (552 kPa). Variables studied were the effect of tool orientation, fill gun location and vibration during filling.

Horizontal and Vertical Tool Orientations – Bead packing efficiency was practically the same for both orientations although the horizontal orientation tended to improve the surface packing. No visible bead settling was observed when vibration was applied.
Fill Gun Location – Multiple fill gun locations changed the filling pattern; however, the bead packing efficiency remained unchanged – no visible settling when vibration was applied.
Visual Observations - Figure 2.1.16 illustrates the formation of high density lines. These observations were made prior to any mechanical vibration.

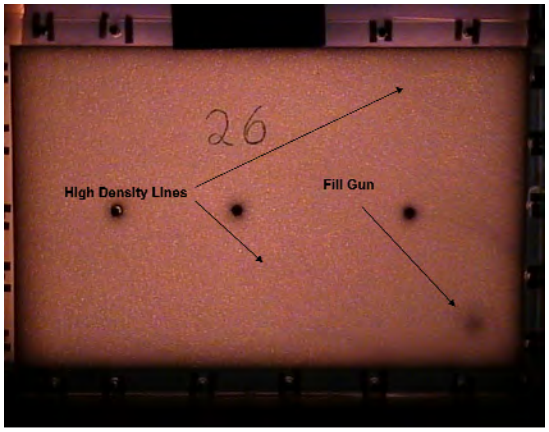

Figure 2.1.16 - Observations of Bead Packing Efficiency Using Back Lighting

Conclusions -Generally both tool types have similar bulk bead movement during filling. As beads enter the tools they travel to the tool boundaries farthest from the fill gun where they begin packing. This packing continues and the bead front moves toward the fill gun. Packing efficiently was significantly improved using the centerline vented tool with a 0.005 inch gap. Increasing this centerline gap to 0.010 inch caused inefficient bead packing similar to the discrete vented tool. Calculations indicate the discrete vented tool has over 5 times the vent area of the centerline vented tool. Subsequent bead blowing studies, using a series of pressure probes, indicate that the centerline vented tool has internal pressures more than 10 times the pressures in the discrete vented tool. Fill time for the discrete vented tool was 5.4 seconds compared to 7.0 for the centerline vented tool. This could be caused by increased bead packing efficiency requiring a larger quantity of beads and/or lower backpressure in the discrete vented tool.

Inefficient bead packing during filling of pattern tools has been identified as the cause of permeability gradients in steamed patterns. Ultimately these gradients cause merging metal fronts leading to folds in castings.
Foundry experience indicates that this applies to both aluminum and iron Lost Foam castings. Both discrete vented and parting line vented tools are currently used in production with a large majority of these tools being of the discrete vented type. A study was initiated to implement the mechanical vibration to production pattern molding equipment; however, the complexity of this implementation was outside the scope of this program. Implementation of this vibration would be a major breakthrough and advance the Lost Foam Casting industry to the next level.

Task 3 – New Pattern and Coating Materials

Subtask 3.1 Alternate Pattern Materials

Developing new pattern materials is a lengthy process, and the cost may outweigh the return on investment for most polymer companies. Also the price of the new pattern materials could be too high to be marketed. Based on these factors, UAB has concentrated on enhancing existing pattern polymers and coating additives for improving casting quality. Working with cost share partners, a study was launched to optimize the additive level in T185 beads, and evaluate effects of other additives in the foam pattern. The results of this study were presented earlier in Subtask 1.2.

Subtask 3.2 – Pattern and Coating Additives

The addition of bromide to polystyrene beads has proven to significantly reduce casting defects such as folds and porosity in both aluminum and iron Lost Foam castings. A study to further reduce casting defects through even more efficient removal of liquid pyrolysis products from the casting cavity was completed. This study included the addition of bromide in the form of

SAYTEX BC-48 flame retardant - Tetrabromocyclo-octane to the coating in various amounts. The mechanism of liquid pyrolysis removal is described in Figure 3.2.1. As the metal front degrades the pattern liquid pyrolysis products collect in globules behind the metal front between the liquid metal and coating. The liquid is subsequently heated and vaporized where the gases pass through the coating. The hypothesis for adding the bromide to the coating is to provide further molecular weight and viscosity reduction to expedite the degradation process. This could be beneficial for aluminum castings since 70% of pattern weight is converted to liquid as the metal replaces the pattern.

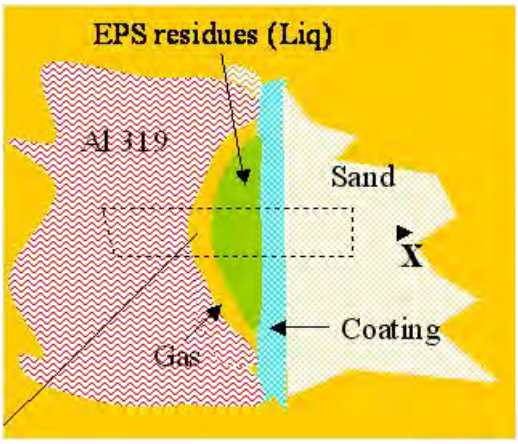

Figure 3.2.1 – Mechanism of Liquid Pyrolysis Removal

Coating Additives - Two levels of BC-48 (3% and 6%) were added to the coating prior to coating each pattern. Castings were poured using 356 aluminum alloy. The cluster arrangement is shown in Figure 3.2.2 and has two plates attached to a common sprue and runner. One plate was coated with a coating without additives while the other plate was coated with the same coating with additives. The patterns used in this study were T170 and contained no bromide.

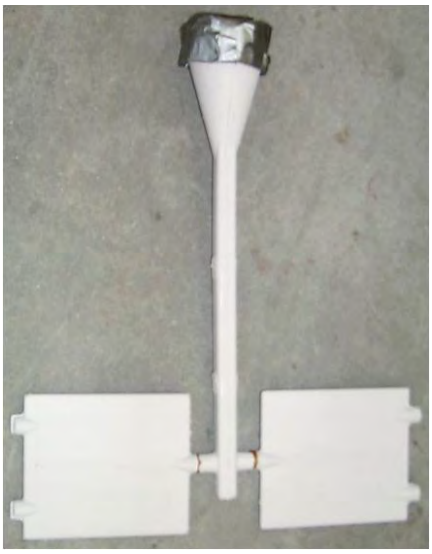

Figure 3.2.2 – Cluster Arrangement for Coating Additives Casting

Castings were cleaned and inspected for defects. Figure 3.2.3 illustrates the surface appearance of typical castings. The dark lines on the castings

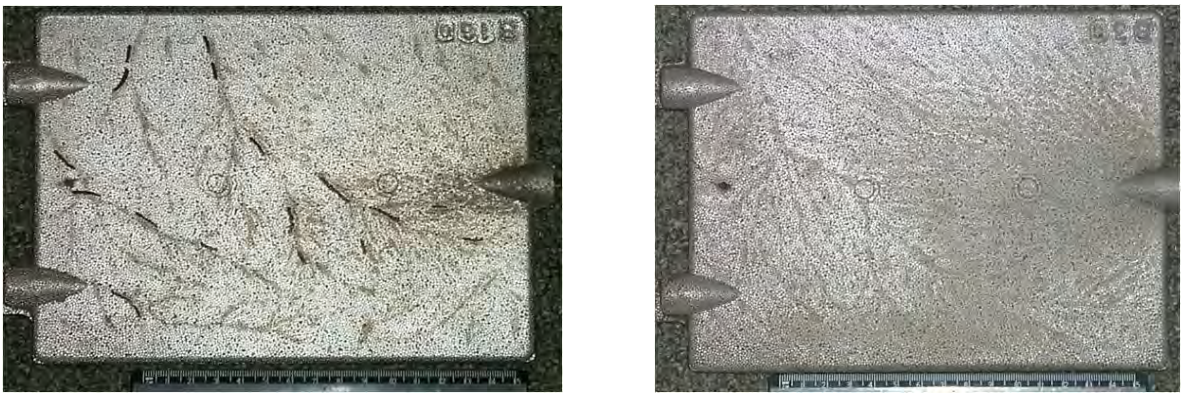

Without Additives With Additives

Figure 3.2.3 – Comparison of Casting Surfaces of Plate Castings

are locations of folds. The number of folds for each type of casting is shown graphically in Figure 3.2.4. Clearly the additives reduced the number and length of folds. Although not validated the addition of BC-48 to currently used coatings along with T175 beads (with bromide) could significantly reduce the incidence and severity of folds in aluminum Lost Foam castings.

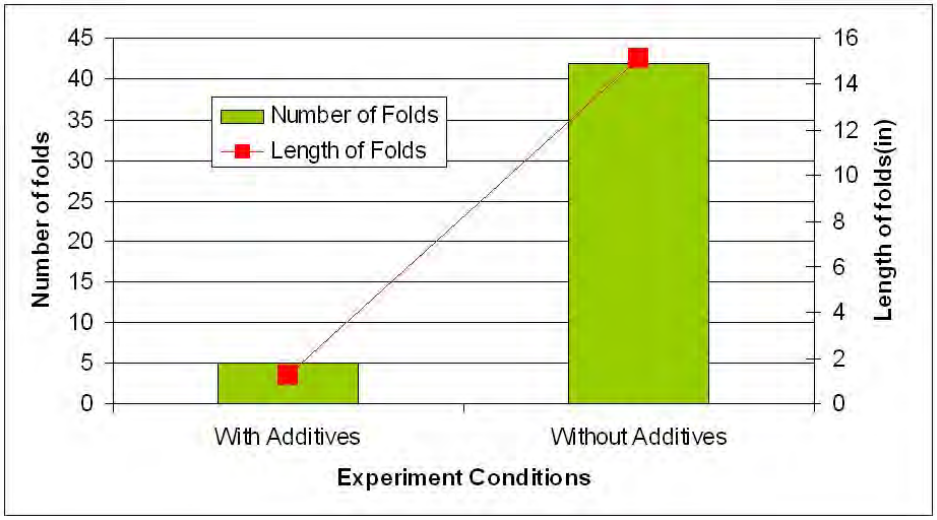

Figure 3.2.4 – Effect of Coating Additive BC-48 on Casting Defects

Subsurface Ductile Iron Defects – A sponsor in an iron Lost Foam foundry was experiencing significant subsurface defects in several castings and appeared almost entirely on the cope surface. The defects occurred on castings made using both EPS and CoPolymer patterns. The subsurface defects do not occur when the casting is made with cast iron. These defects were detectable only after machining which is unacceptable on sealing surfaces. Figure 3.2.5 illustrates the subsurface defects on a transmission clutch housing.

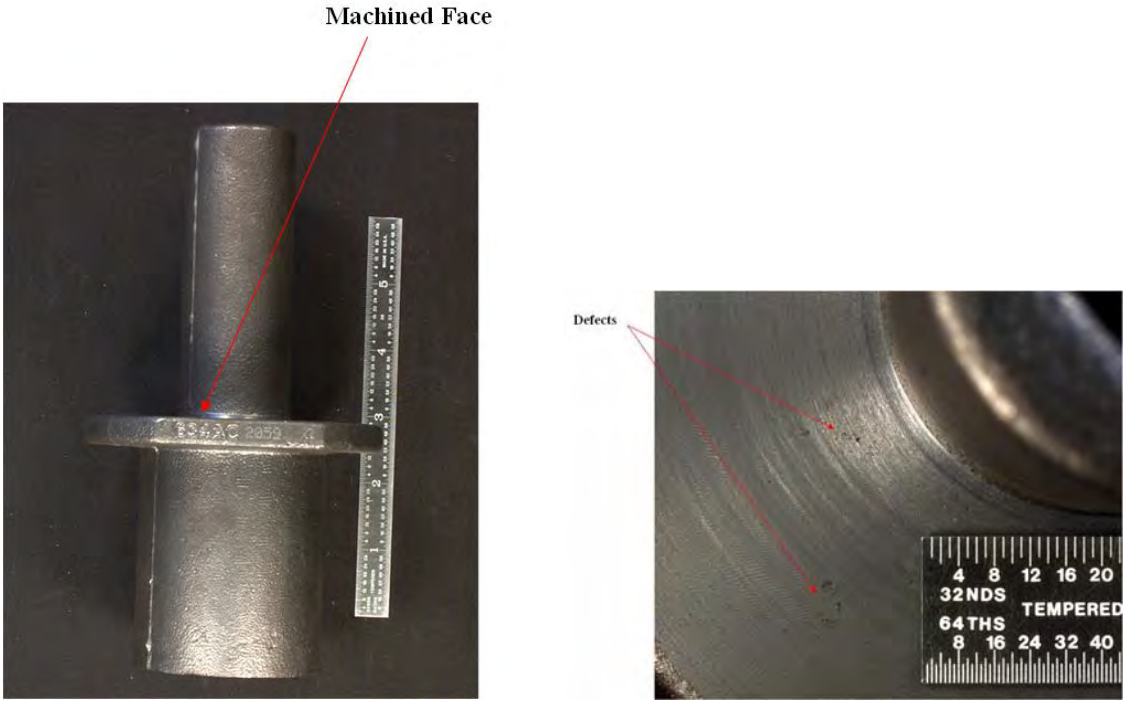

Figure 3.2.5 – Subsurface Defects in a Ductile Iron Clutch Housing

Defects were examined using SEM with EDS equipment and revealed they contained oxides of Magnesium (Figure 3.2.6). The coating was suspected as being the root cause. Coatings were examined using SEM with EDS. Results revealed that oxides of Magnesium were not present in the coating.

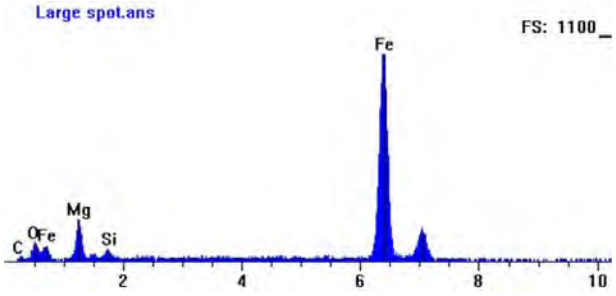

Figure 3.2.6 – EDS of Ductile Iron Defect

A series of castings were poured in the UAB laboratory to identify the root cause of the subsurface defects. Partial clusters of a bearing support were used for this study (Figure 3.2.7). The test matrix for these casting trials is shown in Table 3.2.1. Trial 1 used as received clusters to serve as a base line. Trial 2 was performed using clusters that were dried for 24 hours

at 150^0 F (76^0 C) to assure that all water was removed. Water could be a source of oxygen that would react with the magnesium in the metal. Trial 3 was performed using a ceramic filter at the bottom of the fiber sprue. The function of this filter/plug was to remove oxidation products introduced into the metal during transfer from tapping ladle to the pouring ladle and also to assist the metal pouring personnel in maintaining a full sprue. This was considered necessary after observing production pouring of clusters and noting that the metal pourer had considerable difficulty in maintaining a full sprue throughout the pour. Trial 4 was performed at the sponsor's foundry with full clusters and a ceramic filter/plug to validate the laboratory results in a production foundry.

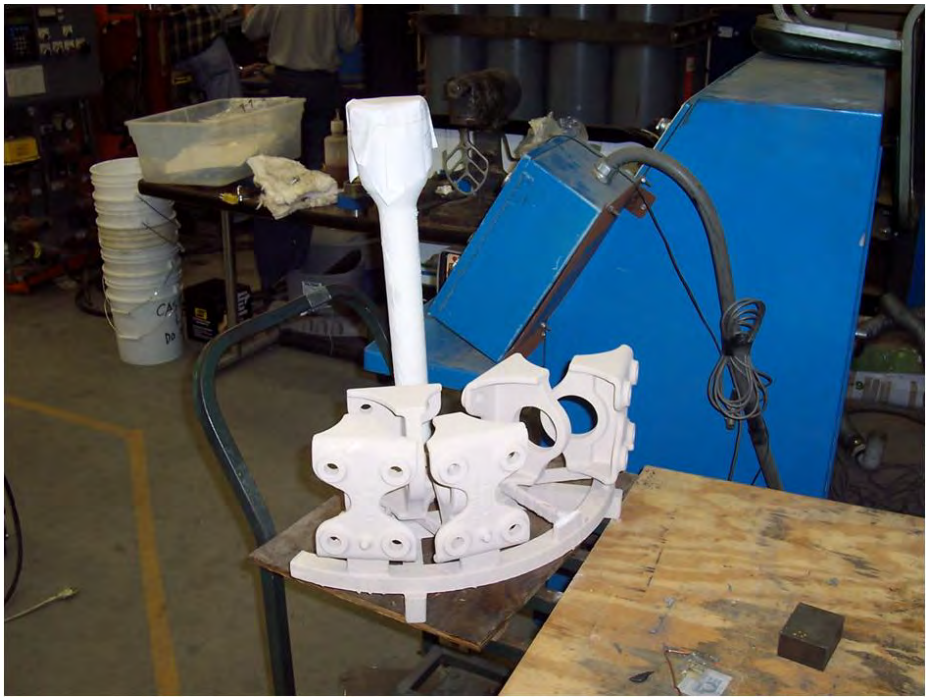

Figure 3.2.7 – Partial Cluster of Bearing Support Patterns

Table 3.2.1 – Test Matrix for Ductile Iron Defect Studies

Trial 1	As Received Cluster
Trial 2	Cluster Dried 24 Hours
Trial 3	Filter/Plug in Sprue
Trial 4	Filter/Plug in Sprue (Confirmation)

Selected castings from each trial were machined on the cope surface at 0.010 inch intervals and inspected for defects.

Based on the number and severity of subsurface defects observed after machining in castings made in the UAB laboratory the root cause of the defects was identified as re-oxidation products. This conclusion was based on the casting results which clearly illustrated that the subsurface defects were significantly reduced on castings poured with the filter/plug in place. This conclusion was validated in a production foundry.

Task 4 – Solidification Under Pressure

The objective of this task was to develop the capability to solidify aluminum castings under adequate pressures to 1.) decrease the metal porosity levels generated when hydrogen is expelled from the melt and gases from the pyrolysis of patterns are generated during metal pattern replacement (Figure 1.1.1) and 2.) study the effects of gating on unfed metal shrinkage. Accomplishing the first of these objectives was used to illustrate an improvement in mechanical properties, discussed later in this report in Subtask 5.1 - Mechanical Properties. The study of the effects of gating on unfed metal shrinkage evolved into a major breakthrough in predicting areas of metal shrinkage using improved computational modeling.

Subtask 4.1 Gating

Pressure Vessel Modifications - The pressure vessel illustrated in Figure 4.1.1 was donated by Mercury Marine. This vessel was used by Mercury Marine to study the effects of pressure on the mechanical properties of samples removed from a marine engine block. This study led to the installation of three pressure vessels in 2001 to their Lost Foam production.

Figure 4.1.1 – Pressure Vessel

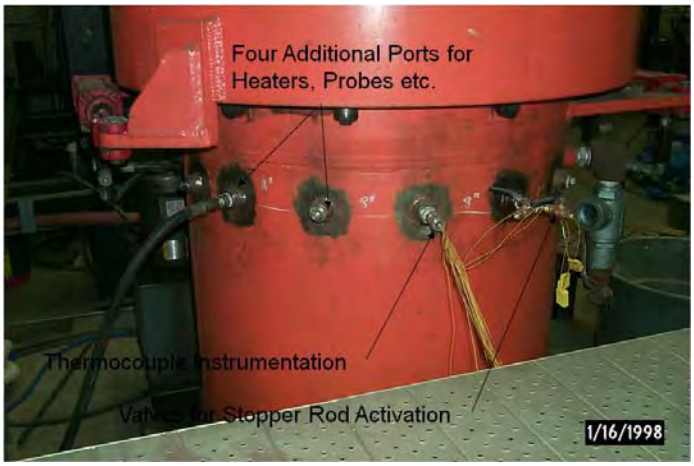

Figure 4.1.2 – Additional Ports

The pressure vessel was modified at UAB by licensed personnel to provide addition access ports for instrumentation such as thermocouples, electrical power and pressure transducers (see Figure 4.1.2).

Requalification was required by the ASTM Un-Fired Pressure Vessel Code. The vessel was hydrostatically pressurized to 10 times operating pressure and certified.

Metal pouring into the open pressure vessel was accomplished by an operator standing on an elevated platform. After metal pouring was complete the vessel was closed and pressurized. Pressurization was initially accomplished with nitrogen from a 12-pack cradle with manifold. Using this technique the time to full pressure (10 atmospheres) was excessively long. This pressurization time was shortened to an acceptable value (60 seconds) by supplementing the nitrogen flow rate with compressed air.

There was concern that the above described pouring procedure, followed by lid closure and pressurization, would be too lengthy and cause premature solidification of the metal before full pressure could be attained. A second method of metal pouring was designed and constructed to shorten the time from pouring to full pressurization. This method consisted of a pouring basin placed on top of the compacted sand with a stopper rod to activate metal flow. Figure 4.1.3 illustrates the flask, pouring basin, stopper rod and lever arrangement that was designed and constructed to fit inside the pressure vessel and provide clearance for instrumentation wiring and plumbing. The stopper rod was remotely activated by an air cylinder/lever arm arrangement. This pouring process could be used with the vessel closed and pressurized. In reality, with experience, the open vessel metal pouring followed by pressurization was deemed adequate for the studies.

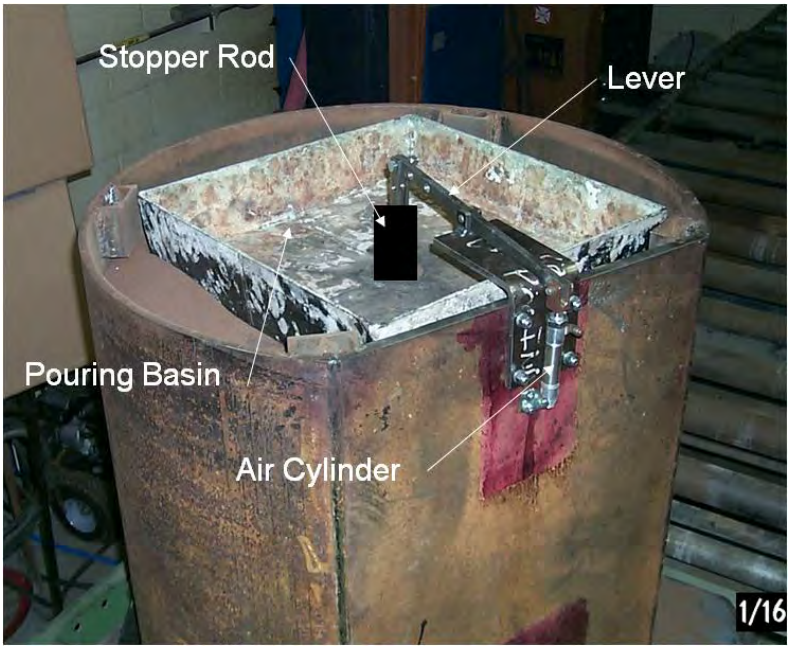

Figure 4.1.3 – Flask, Pouring Basin and Stopper Rod Assembly

Gating Studies - Preliminary evaluations using 6 inch x 8 inch x 1 inch plates, poured at atmospheric pressure and under 10 atmospheres, indicated that the shrinkage location (center of plate) for both conditions was identical. The magnitude of the shrinkage was significantly reduced, but not eliminated, using pressure solidification. Predictions of shrinkage, using the modeling tool discussed in Subtask 1.3, revealed that simple changes to the peripheral gating and runner systems would not eliminate this shrinkage. This was the first indication that the commonly used gating rules for Lost Foam castings were incorrect. Historically, design of gating geometries of Lost Foam castings focused on rigidity of the cluster in order to survive the coating and sand fill/compaction steps in the process. The following discussion will establish new gating rules for complex castings to eliminate or significantly reduce metal shrinkage.

Commercial castings with complex geometries were identified to be used for investigation of effect of gating and casting design on soundness of castings solidified under pressure. Shrinkage porosity was observed in the castings using the current designs. The results for a V6 engine block were presented in Subtask 1.3.

Inline four cylinder (I4) and six cylinder (I6) four stroke blocks were selected for study. Since the results for these two blocks are similar only the I6 block results will be presented. The predicted shrinkage in the I6 block is illustrated in Figure 4.1.4. Visible in the side view there are 14 gates attached to the main bearing surfaces, producing a rigid cluster.

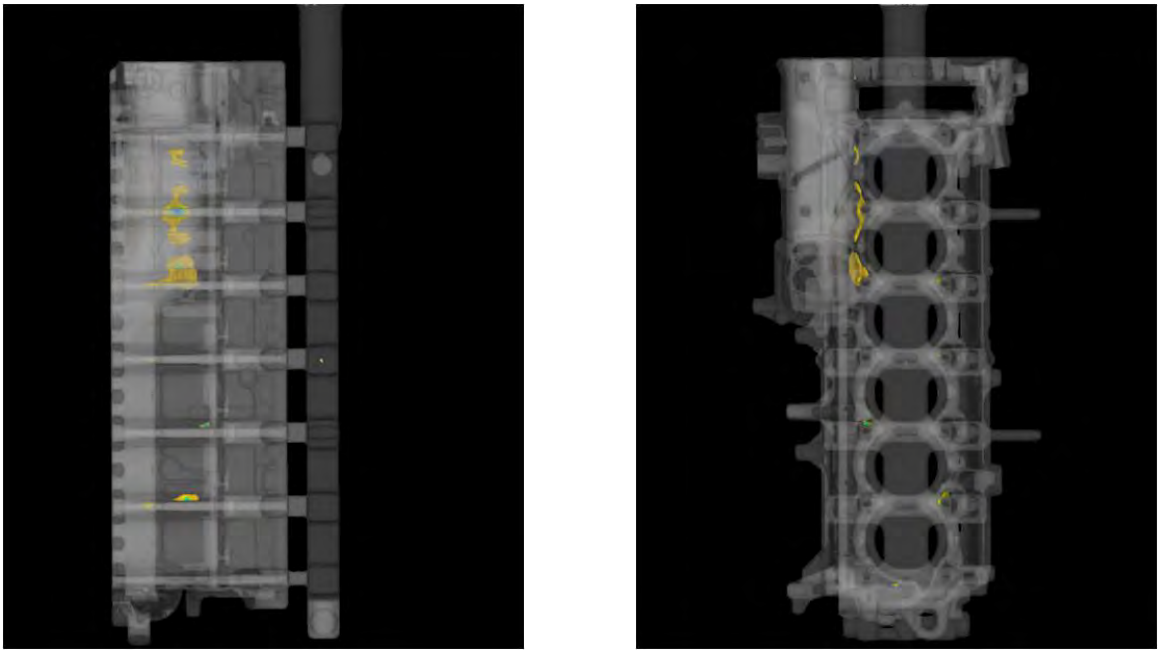

Side View Deck Face View

Figure 4.1.4 – Predicted Areas of Unfed Shrinkage in a I6 Block

Production blocks were sectioned and inspected using dye penetrant and a black light. Shrinkage defects were commonly present in the areas indicated by circles in Figure 4.1.5. Circles indicate sponge porosity in Bores #2, #5 and #6. Large porosity is present adjacent to bolt hole in Bore #6. These areas of shrinkage match the predicted areas in size and location.

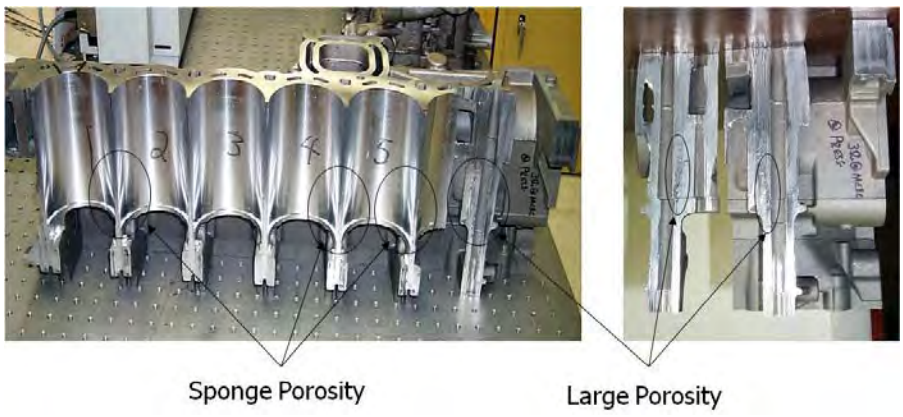

Figure 4.1.5 – Inspection of sectioned Block

Modeling of I4 and I6 blocks has revealed another cause of isolated macro – shrinkage. Since Lost Foam offers design freedoms not available in other casting processes designers have positioned water passages and other geometric features that are intended to enhance product performance. Some of these features position islands of sand in areas that block heat flow, resulting in late cooling of adjacent areas (note the islands of sand surrounding the large porosity in Figure 4.1.5). Macro – shrinkage occurs in the surrounding metal areas. These production defects can now be prevented using the predictive tool of modeling in the future. This modeling tool will provide designers of castings the opportunity to resolve these issues prior to production.

The modeling results of the I4 and I6 blocks were further analyzed by using the metal velocity vectors and gate areas to calculate metal flow rates and volumes through each gate. This analysis indicated that the lower gates are supplying up to 90 % of the metal required to fill the pattern cavity after all gates are open to the casting. This generates an undesirable inverse temperature gradient from top to bottom of the casting. Figure 4.1.6 illustrates the flow rates through each gate for the I6 block. Note that after all gates have opened into the casting the flow rates through the lower gates increases while the upper gates allow metal to flow out of the casting. This means the principles of fluid mechanics are active after all gates are open to the casting. This is a breakthrough understanding in metal filling of Lost Foam castings. Another illustration of the volume of metal

volume flowing into the casting from each gate is illustrated in Figure 4.1.7.

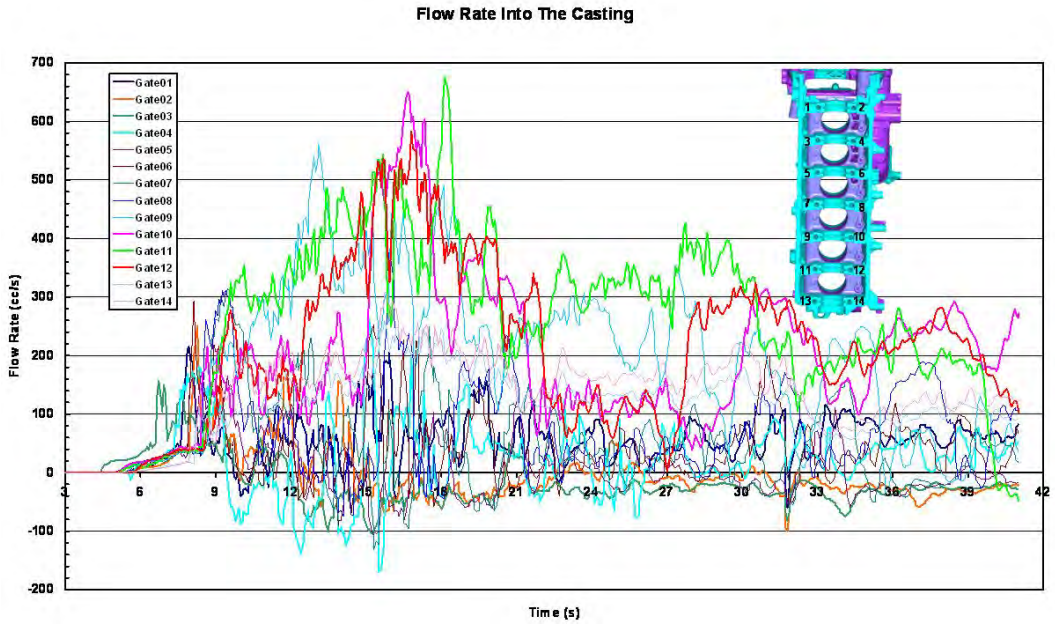

Figure 4.1.6 – Metal Flow Rates in Gates for an I6 Engine Block

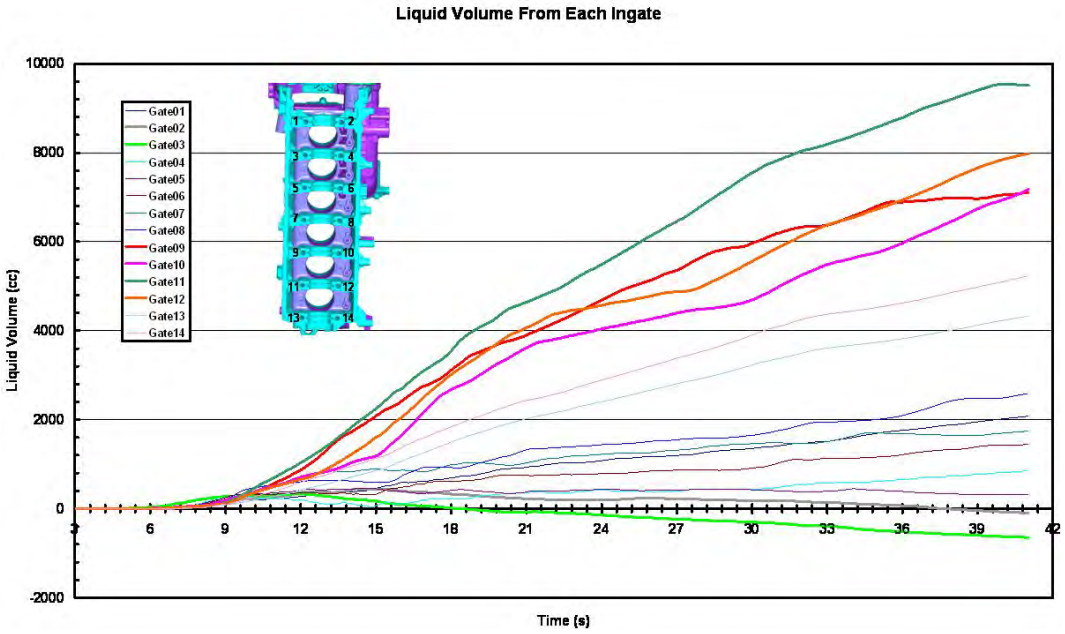

Figure 4.1.7 – Metal Volumes through Each Gate for an I6 Engine Block

The percentage of metal volume from each gate is illustrated in Figure 4.1.8. Based on this analysis it is clear that the side gating arrangement is incorrect and inverse temperature gradients are established in the casting, creating the opportunity for metal shrinkage to form. Furthermore, since the upper gates contribute very little to filling the cavity they should be eliminated. A better gating solution would be a total gating change that would maintain the required rigidity while creating a more desirable temperature gradient that eliminates the tendency for shrinkage to form.

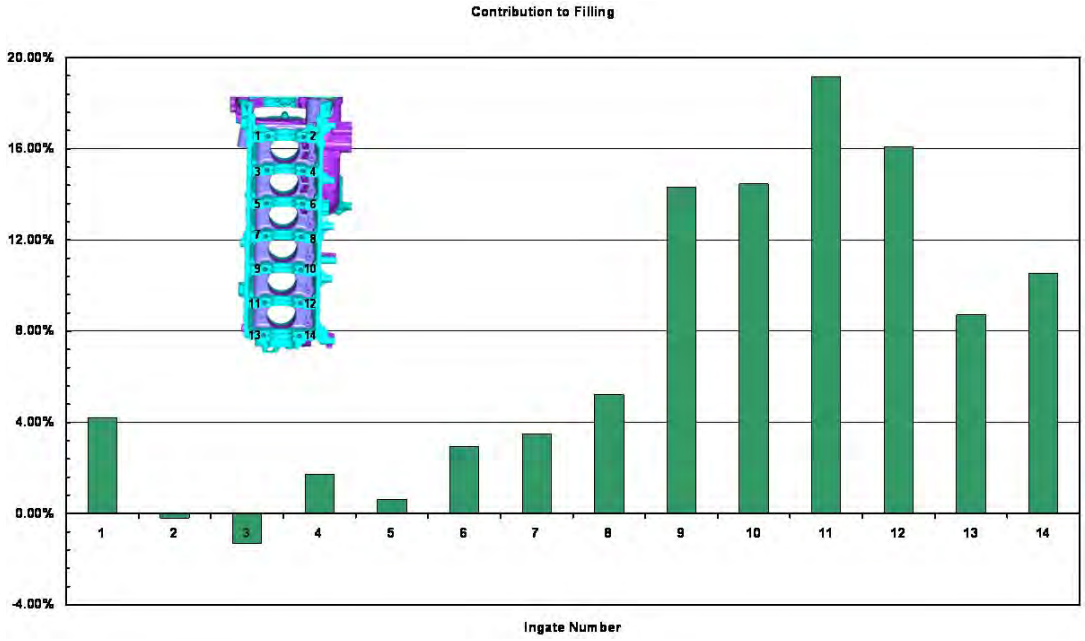

Figure 4.1.8 – Percentage of Total Metal Volume for Each Gate

The areas of shrinkage in the I4 and I6 blocks have been eliminated experimentally by gating into the cylinder bores for the I4 block. The I4 block was selected for this experimental trial due to the ease of re-gating. This gating arrangement is shown in Figure 4.1.9. Modeling of the effect of these gating changes revealed no shrinkage throughout the casting; however considerable differences in metal flow rates continued to favor the lower gates. This illustrated in Figure 4.1.10. These results have caused the normal rules of gating to be revisited. Current data suggests that gates should be positioned to feed metal into areas where shrinkage is experienced and to provide the minimum metal fill distances.

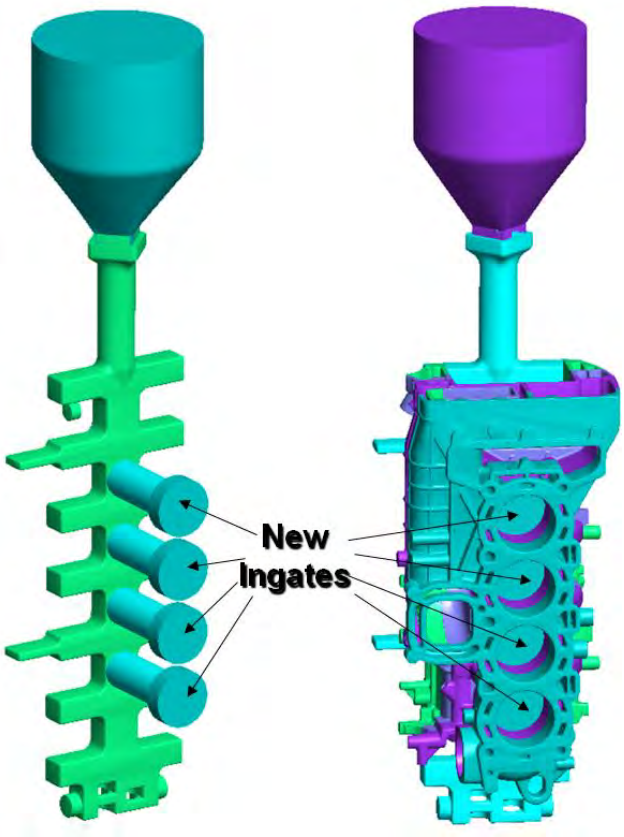

Figure 4.1.9 – Proposed Bore Gating for the I4

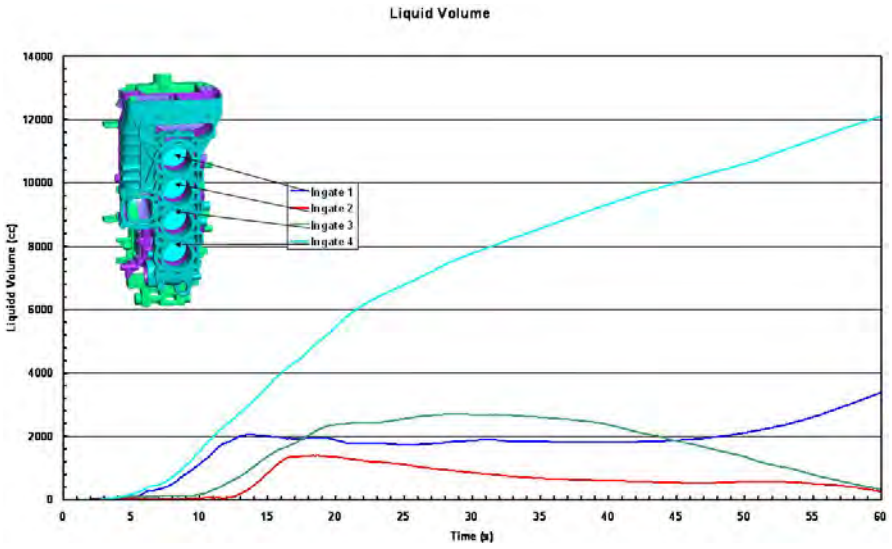

Figure 4.1.10 – Metal Volume through Each Gate for the I4 Block

Laboratory experiments were performed for the I4 and I6 blocks in an effort to validate the predicted unfed shrinkage in the bores and bolt holes. The new gating arrangements were validated by multiple pours. The areas of shrinkage in the L4 and L6 blocks have been eliminated experimentally by gating into the cylinder bores. These laboratory evaluations indicated that gating rules of Lost Foam Castings should be reconsidered. Current results indicate that gates should be located in the most central portion of the casting, providing the shortest possible path for metal filling. This gating arrangement provides the minimum temperature gradients after filling and shortest possible path lengths for feeding.

This technology has also been applied to a V6 engine block. Modeling efforts have validated the gating rules established for the I4 and I6 blocks. Gates placed at central locations in the block predicted complete removal of the unfed shrinkage. Laboratory castings validated the predicted results.

Task 5 – Design Data and Marketing Plan

Subtask 5.1 – Mechanical Properties

5.1.1 - Pressure Solidification

The objective of this task was to study the effects of solidification under pressure for aluminum castings in an effort to improve the mechanical properties. Past literature[8] has indicated mixed results on property improvements. A comprehensive literature review was made to showcase the effect of solidification under pressure on casting soundness, mechanical and fatigue properties. Researches in the last 70 years could be divided into two categories: one is before 1980s, the other is after 1980s. Before 1980s, it was reported that porosity in the casting was significantly reduced, but no improvements on mechanical properties were observed unless gassy metal was used. It was suggested that solidification under pressure did not appear to be feasible for production of high quality castings, because it is difficult to obtain directional solidification in complex castings, and concentrated gross porosity will appear if the thermal gradient is inadequate. This issue was addressed in Subtask 4.1 where gating changes for complex castings can result in improved thermal gradients which prevent metal shrinkage. In research after 1980s, it was reported that commercial application of solidification under pressure for complex lost foam castings was successful. With clean metal, porosity levels were reduced significantly and mechanical and fatigue properties were improved.

In 2005 Dr. Ray Donahue, Mercury Marine, in a presentation to the sponsors of the Lost Foam Consortium, reported that ductility and high cycle fatigue strength (HCFS) are porosity sensitive properties. A comparison of values for metal porosity and HCFS of aluminum castings produced by various casting process were reported. Typical metal porosity, elongation and HCFS values for the sand cast process are 1.0 %, 3.0 % and 8 ksi (55.2 MPa), for the permanent mold process the values are 0.1 %, 5 % and 12 ksi (82.7 MPa),

and for Lost Foam with pressure the values are 0.01 %, 8 % and 16 ksi (110.3 MPa). The reported values for Lost Foam with pressure were measured on samples of A356 aluminum castings produced in Mercury Marine's production facility. The porosity values were measured from polished sections. These values clearly indicate the strong relationship between elongation and HCFS.

Procedures - The studies in this program were designed to confirm the effect of porosity on ultimate tensile strength, yield strength and elongation and to develop non-destructive measurement techniques to provide quality control of the castings. The root cause of porosity in Lost Foam aluminum casting can be traced to pores formed when hydrogen gas in the melt is expelled, gases generated as the pattern is decomposed (see Subtask 1.1) and unfed shrinkage (discussed in subtask 4.1). The aluminum alloys selected were A319, A356 and A206. The casting geometry selected for this study was based on earlier work by Ford Motor Company[9] and consist of a wedge which provides varying thicknesses along the height to provide different cooling rates. The cooling rate of aluminum castings generally controls dendrite arm spacing (DAS) and can affect porosity when cooling rates are elevated. The wedge pattern shown in Figure 5.1.1.1 was designed to provide open cavity and Lost Foam castings. Thermocouples were placed in discrete locations to validate temperature predictions through modeling. A steel chill with dimensions 24 cm x 4 cm x 2.5 cm was placed at the narrow section of each casting. Each casting was sectioned as shown in Figure 5.1.1 to form a slice 1.000 inch thick x 9.270 inches long x 10.000 inches wide. The slices were heat treated (A319–T7, A356-T6, A206-T4) followed by machining into 1.000 inch x 1.000 inch x 9.270 inches long blanks. These blanks were X-Rayed to determine porosity levels followed by density evaluation and inspection using ultrasonic techniques such as velocity and attenuation. Following these evaluations blanks were machined into tensile specimens and evaluated at Southern Research Institute.

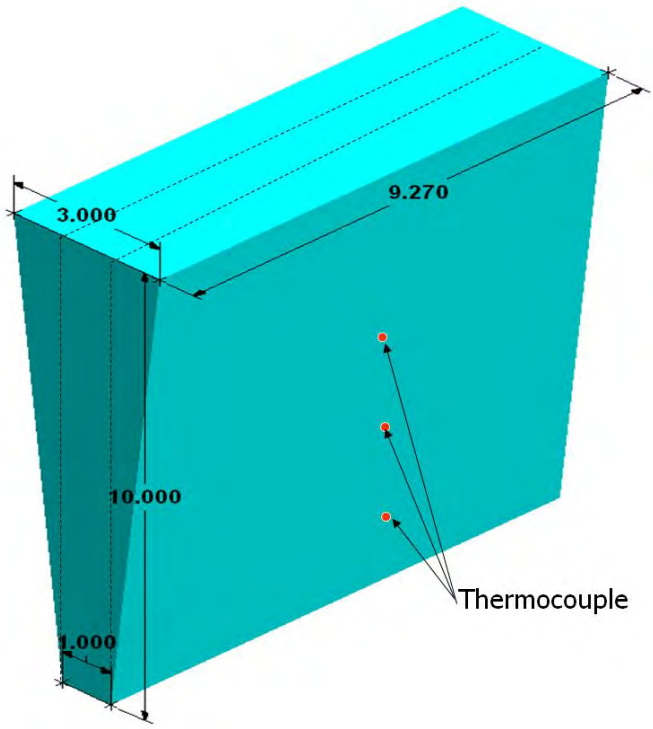

Figure 5.1.1.1 – Wedge Casting Used for Open Cavity and Lost Foam Castings

All castings were made from aluminum alloys in the form of ingots. The melting procedure detailed here is the same for both the lost foam and open cavity castings. Nearly 14 kg of aluminum alloy was cut and was melted in a SiC crucible in a resistance-heated pit furnace under normal atmosphere. Depending on the alloy, the castings were poured between 732 °C to 760 °C.

Molten metal was degassed using a mixture of argon and 2% chlorine. Degassing was performed using a rotary degasser, which consisted of a hollow rotating graphite tube with “teeth” at the bottom. These “teeth” break the large bubbles of the gas mixture into fine bubbles of higher surface area, which increase the efficiency of degassing. The graphite tube was immersed in the liquid metal and the gas mixture was made to flow through the graphite tube. After degassing, the metal was heated to the required pouring temperature. A reduced pressure test was performed to confirm low levels of dissolved hydrogen in the melt. Prior to pouring, the metal was treated with 200 ppm TiBor (5 Ti + 1B) for grain refinement. Al-Si alloys were treated with an Al-10% Sr master alloy to achieve 0.003 wt% Sr.

Castings were made in both open cavity and lost foam processes. Polyurethane bonded sand molds were used for the open cavity castings. The parting line of the molds divided the casting symmetrically along the length. Prior to joining the two halves of the mold, the mold was brushed and air blown to remove loose sand. The pouring basin was fitted with a stopper and was placed

on top of the open cavity mold. The pouring basin was filled with the required melt and the stopper was removed to allow metal flow. This technique reduced turbulence during metal fill and also the oxide entrapment in the liquid metal. In addition, a ceramic filter with 15 pores per inch (ppi) was placed in the path of the liquid metal to remove any entrapped oxides.

The patterns for lost foam were cut from a foam block supplied by a commercial lost foam EPS (expanded polystyrene) producer. The patterns were coated with Foam Kote, a suitable coating for aluminum lost foam castings. Care was taken to maintain the viscosity of the coating within the supplier's recommendation of 1100 – 1300 centipoise. Patterns were coated by manually dipping them in the coating and were allowed to air dry prior to drying in a convection oven at ~ 50 °C. The castings were filled through a sprue (7.6 cm x 7.6 cm x 7.6 cm) placed on the top of the thick section.

A steel chill of dimensions 24 cm x 4 cm x 2.5 cm was placed at the bottom of the thin section of both the lost foam and open cavity castings. To study the effectiveness of pressure at different solid fractions, additional A356 castings were made using the lost foam process including castings without the chill and castings with section thickness reduced to 0.3 cm at the thin section without a chill.

Results - Typical X-Ray exposures of the blanks extracted from a casting poured at one atmosphere and ten atmospheres are shown in Figure 5.1.1.2. Blanks at the bottom of this figure were extracted from the narrow portion of the wedge where cooling rates were the highest due to the chill and thin section size. The lower blanks extracted from the wedge cast at one atmosphere (C, O, and 1) exhibit very little porosity and the highest density. Blanks (2-6) exhibit increasing levels of porosity and lower density values due to the lower cooling rates generated by the increased section size. Blanks (C-5), extracted from the wedge cast at ten atmospheres, exhibit considerably less porosity than the blanks from the one atmosphere wedge. Large shrinkage voids occasionally occurred in blank 6 due to inadequate metal feeding (top gated). Clearly the application of pressure improved the metal soundness by suppressing the growth of gases.

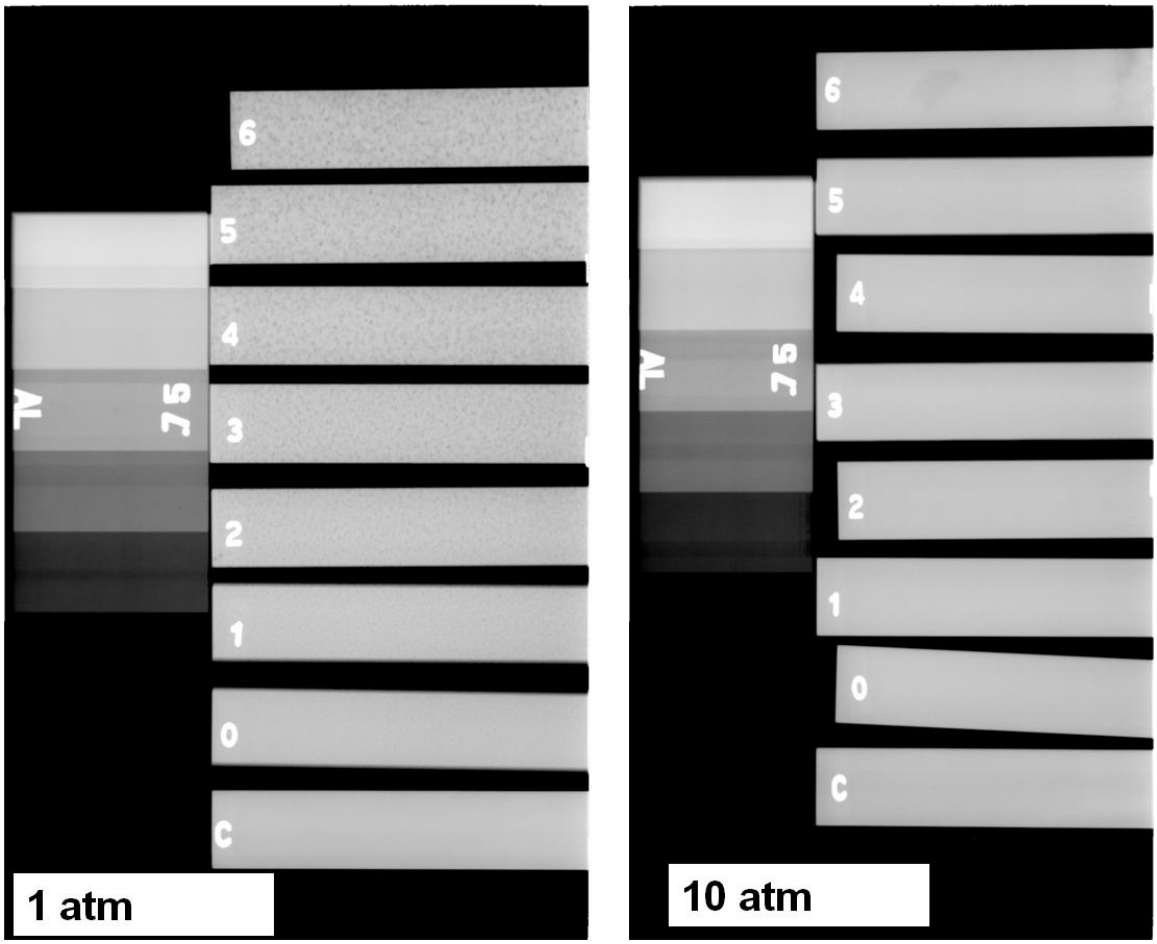

Figure 5.1.1.2 – Typical X-Ray Exposures for Specimen Blanks

A clearer understanding of the effects of solidification of castings under pressure can be viewed in Figures 5.1.1.3 and 5.1.1.4. These figures illustrate the porosity from polished samples of A319 alloy at various distances from the chill for castings poured with one and ten atmospheres of pressure. Clearly the application of pressure to the solidifying metal decreases the size and frequency of pores in A319 aluminum alloy. In addition the size of the pores increases with increasing distance from the chill for the one atmosphere casting while this phenomenon is not as pronounced in the casting poured with ten atmospheres pressure. The irregular pore shapes in the samples greater distances from the chill indicates unfed metal shrinkage.

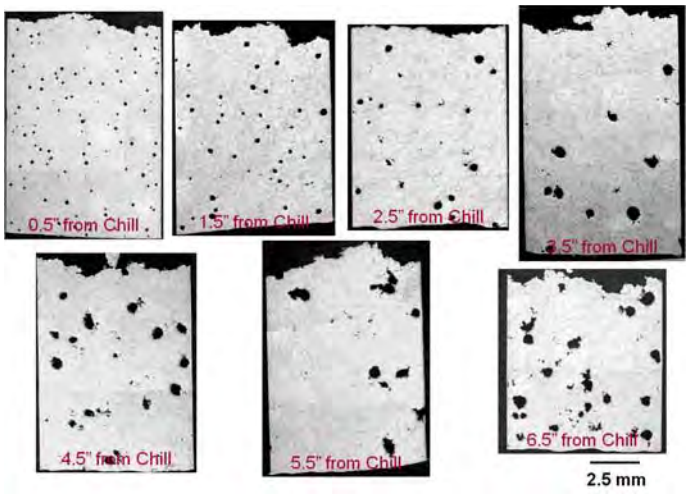

Figure 5.1.1.3 - Porosity of A319 Cast at 1 Atmosphere Pressure

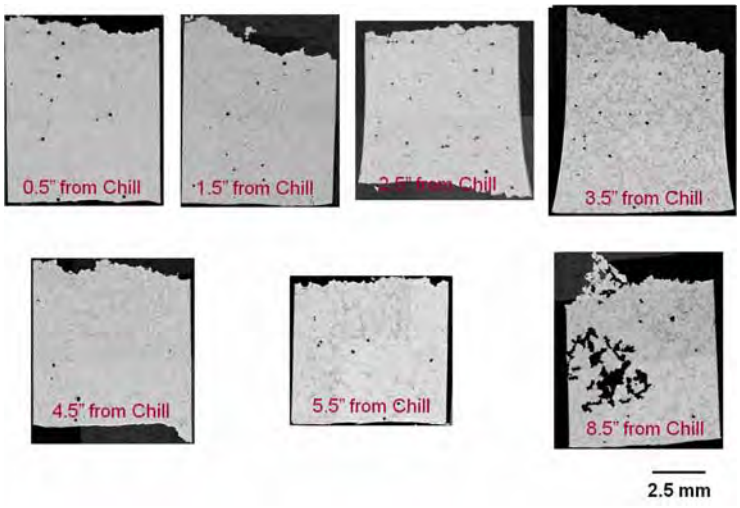

Figure 5.1.1.4 - Porosity of A319 Cast at 10 Atmospheres Pressure

The same porosity trends for A356 aluminum alloy can be observed in Figures 5.1.1.5 and 5.1.1.6.

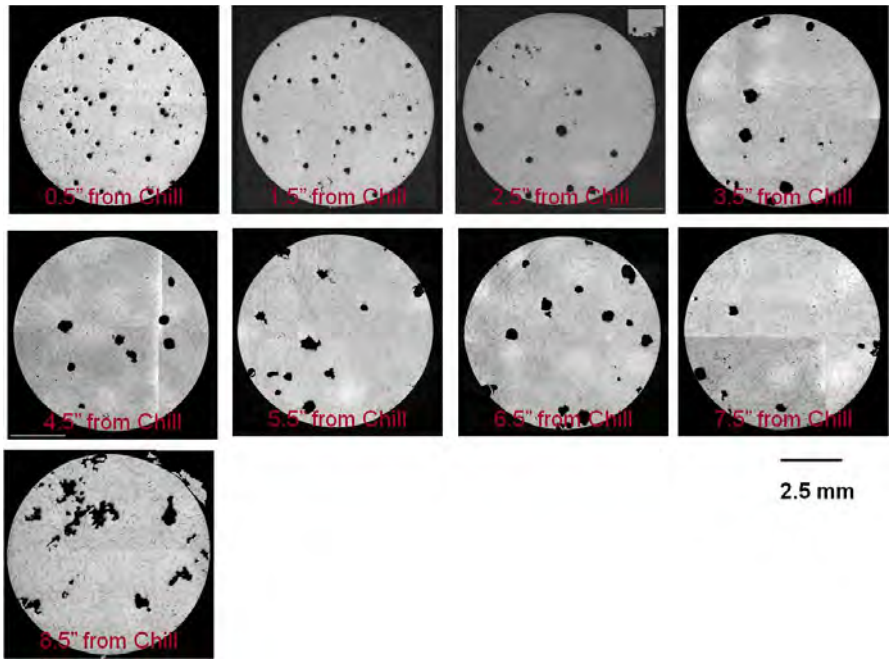

Figure 5.1.1.5 - Porosity of A356 Cast at 1 Atmosphere Pressure

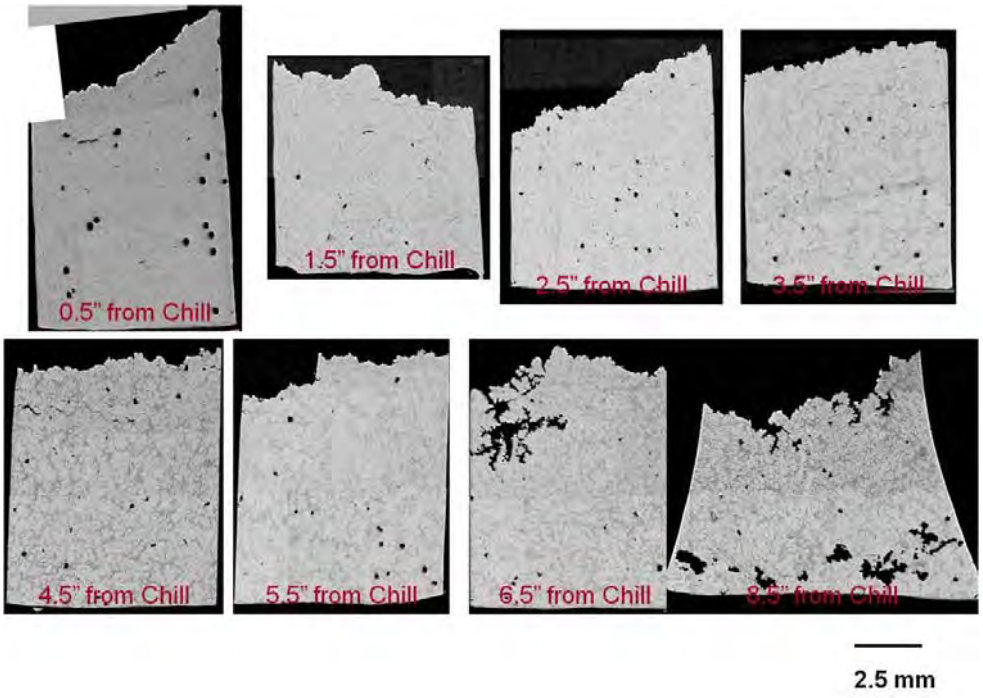

Figure 5.1.1.6 - Porosity of A356 Cast at 10 Atmospheres Pressure

Table 5.1.1.1 describes the nomenclature used to identify each casting and will aid the reader in understanding the following discussions.

Table 5.1.1.1 – Casting Identification.

Alloy/ Method	Chill	Pressure	Pouring temperature (°C)	Number of castings made	Thickness at thin section (cm)	Code
A356/LF	Yes	No	785	1	1.9	WC
A356/LF	Yes	Yes	785	1	1.9	LF-WC-SuP
A356/LF	No	No	785	2	1.9	NC
A356/LF	No	Yes	785	2	1.9	LF-NC-SuP
A356/LF	No	No	785	2	0.3	RTh
A356/LF	No	Yes	785	2	0.3	LF-RTh-SuP
A319/LF	Yes	No	775	1	1.9	WC
A319/LF	Yes	Yes	775	1	1.9	LF-WC-SuP
A206/LF	Yes	No	775	1	1.9	WC
A206/LF	Yes	Yes	775	1	1.9	LF-WC-SuP
A206/OC	Yes	No	745	1	1.9	OC-WC
A206/OC	Yes	Yes	745	1	1.9	OC-WC-SuP

Density - The effect of pressure solidification on density for A319 can be viewed in Figure 5.1.1.7. The densities of the atmospheric casting samples decreased from 2.718 to 2.515 g/cm^3 (decreased by 7%) with increasing section thicknesses, while those of the pressurized casting remained constant (about 2.752 g/cm^3) until a section thickness of ~5 cm. Beyond 5 cm, the density of the samples decreased rapidly due to unfed metal shrinkage.

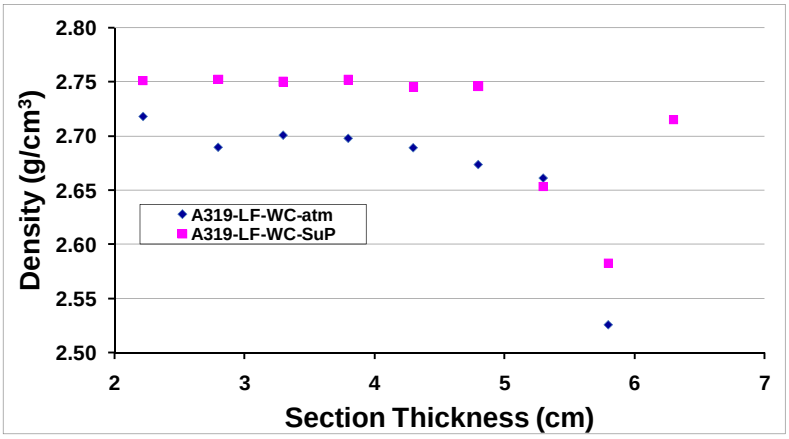

Figure 5.1.1.7 – Effect of Pressure Solidification on Density for A319

The effect of pressure solidification on A356 on density can be viewed in Figure 5.1.1.8. Similar to the A319 alloy a significant increase in density was measured for blanks extracted from section thickness of 2.0 inches and smaller. Above this section thickness metal shrinkage occurred, increasing porosity. Three A356 blanks were exposed to the Hipping process for comparison purposes. Note the density values for A356A samples cast with pressure are slightly lower than the values for the Hipped samples. This is significant and provides foundries an alternate, less expensive method of achieving sound castings.

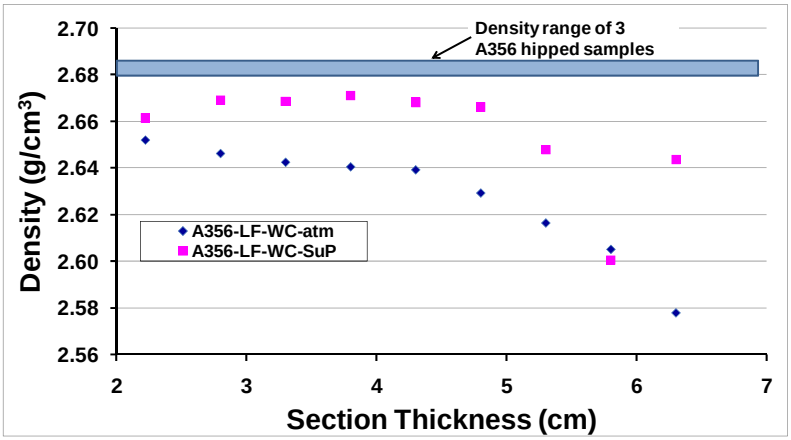

Figure 5.1.1.8 – Effect of Pressure Solidification on Density for A356

Application of pressure during solidification significantly decreased the porosity of both the lost foam and open cavity chilled A206 castings as shown in Figure 5.1.1.9. Unlike the A356 and A319 castings, the increase in density occurred even at the thickest sections. Also, in the pressurized A206 castings, there was a slight drop in density with increasing section thickness across the entire length of the wedge. The densities of the atmospheric castings also decreased more rapidly with increased section thickness compared to the densities of A356 and A319. These differences could be because of the freezing range of A206 which is about 1.5 times that of A356. Long freezing range alloys are difficult to feed shrinkage, and this coupled with the fact that A206 contains less eutectic compared to A356 makes A206 more prone to shrinkage porosity.

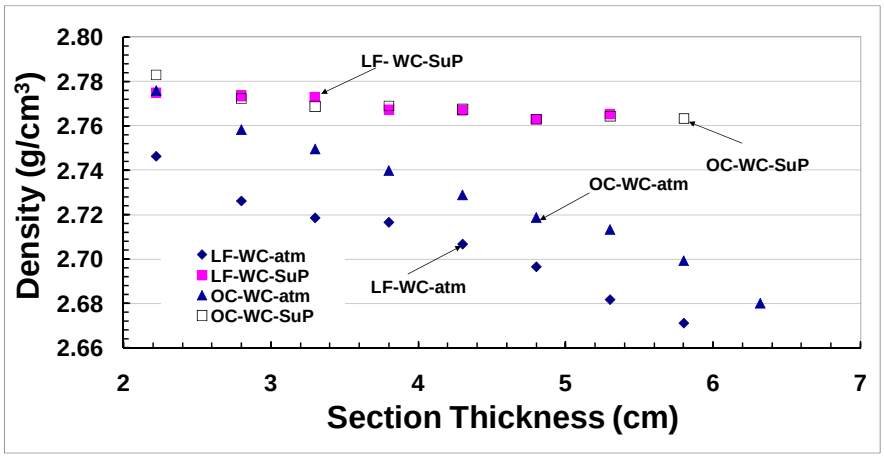

Figure 5.1.1.9 – Effect of Pressure Solidification on Density for A206

Mechanical Properties

Tensile Ultimate and Yield Strength – The variation of tensile and yield strength in the lost foam chilled A356 atmospheric and pressure solidified castings is shown in Figure 5.1.1.10. With the application of pressure, the tensile strength at different locations increased by 1.5 – 3.5 %, while no such improvement was seen in the yield strength. Other researchers have shown that the porosity concentration had to reach significant levels, 3 to 25 % depending on the ductility of the alloy before an observable effect in the ultimate tensile strength was seen. The largest density decrease seen in the wedge solidified at atmospheric pressure was 3% until 6 cm section thicknesses. No significant improvement in tensile strength was expected from the solidification under pressure.

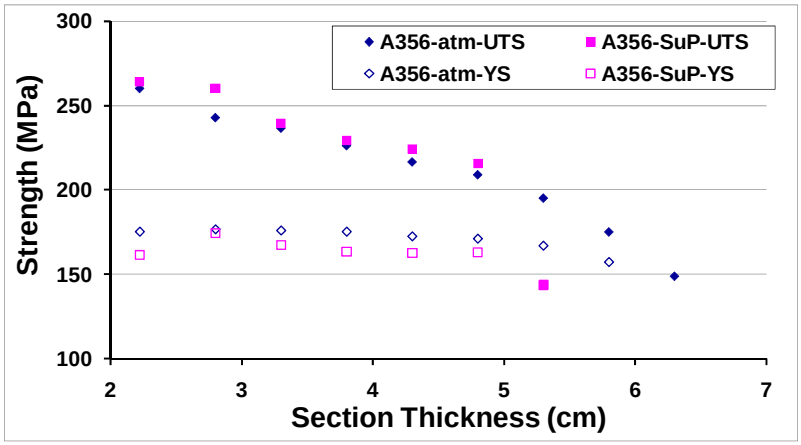

Figure 5.1.1.10 – Variation of Tensile and Yield Strengths with Section Thickness in A356 Lost Foam Chilled Castings.

The variation of tensile and yield strengths with section thickness in the lost foam, chilled A319 atmospheric and pressurized castings is shown in Figure 5.1.1.11. Both tensile and yield strength decreased with increasing section thickness and the tensile strength decreased more than the yield strength. These observations were true for both the atmospheric and pressurized castings. The tensile strengths in the castings solidified under pressure were slightly higher than those solidified at atmospheric pressure and the difference increased with increasing section thickness. There was no significant difference between the yield strength in the castings solidified at atmospheric and elevated pressure.

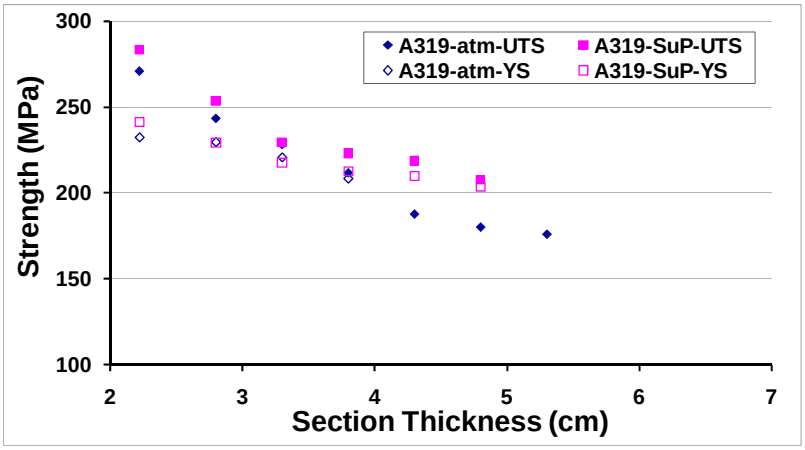

Figure 5.1.1.11 - Variation of Tensile and Yield Strengths with Section Thickness in A319 Lost Foam Castings.

The tensile strengths of the atmospheric and pressurized lost foam and open cavity A206 castings are shown as a function of section thickness in Figure 5.1.1.12. With increasing section thickness, the tensile strength of the atmospheric lost foam casting decreased from 380 to 200 MPa while that of the pressurized lost foam casting decreased from 380 to 310 MPa. In the open cavity atmospheric casting, the tensile strength decreased from 410 to 200 MPa with increasing section thickness, while a decrease from 410 to 354 MPa was observed in the open cavity pressurized casting. With the application of pressure, the tensile strength at different section thicknesses increased by 12 to 55% in both the lost foam and open cavity castings.

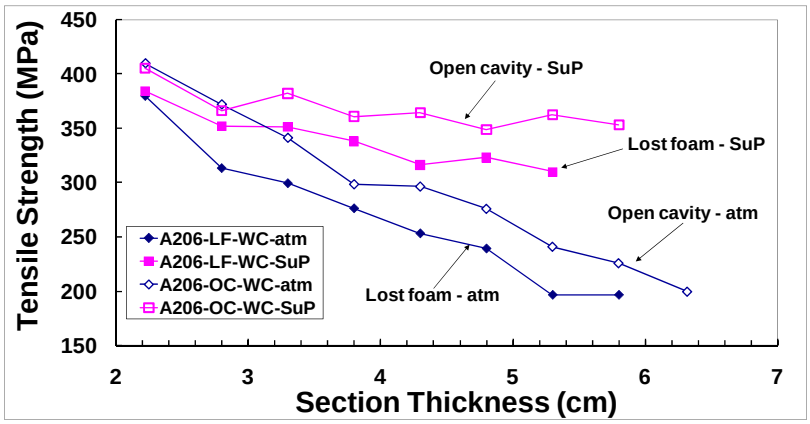

Figure 5.1.1.12 - Variation of Tensile Strenth with Section Thickness in A206 Lost Foam Castings.

The variation of yield strength for the four A206 castings under consideration is shown in Figure 5.1.1.13. Yield strength only increased slightly at most thicknesses and was even reduced in a few section thicknesses. The open cavity castings exhibited higher yield strength compared to the lost foam castings in both atmospheric and open cavity castings.

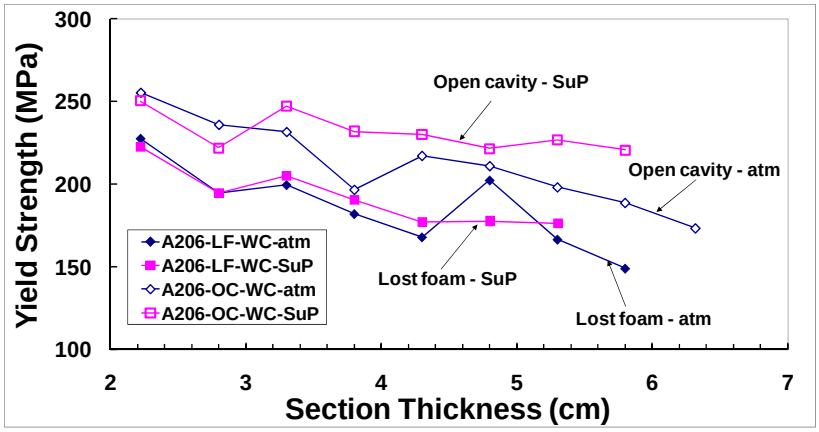

Figure 5.1.1.13 - Variation of Yield Strength with Section Thickness in A206 Lost Foam Castings.

Elongation - The percent elongation of A356 and A319 lost foam castings solidified at atmospheric and 1.034 MPa pressures are shown in Figures 5.1.1.14 and 5.1.1.15. Porosity has a detrimental effect on the elongation so it was expected that the application of pressure would increase elongation. It can be seen from Figures 5.1.1.14 and 5.1.1.15 that at the same section thickness ductility increased with the application of pressure in both the 356 and 319 alloys. Elongation increased by 50% to 130% in A356 and about 13% to 45% in A319.

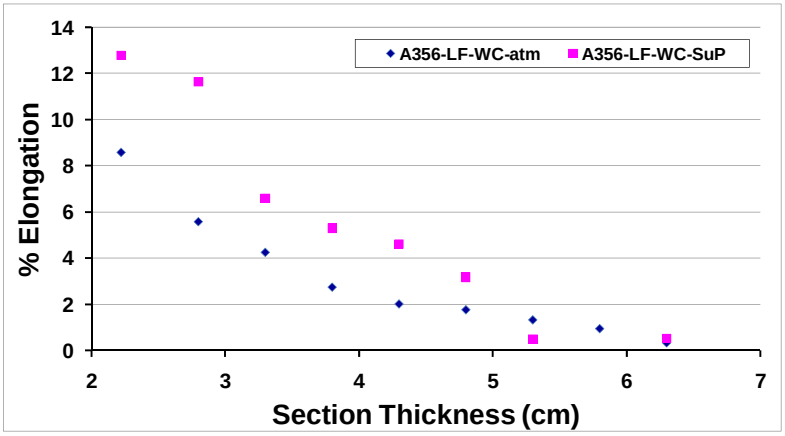

Figure 5.1.1.14 - Variation of Elongation with Section Thickness in Lost Foam Chilled A356 Atmospheric and Pressurized Castings.

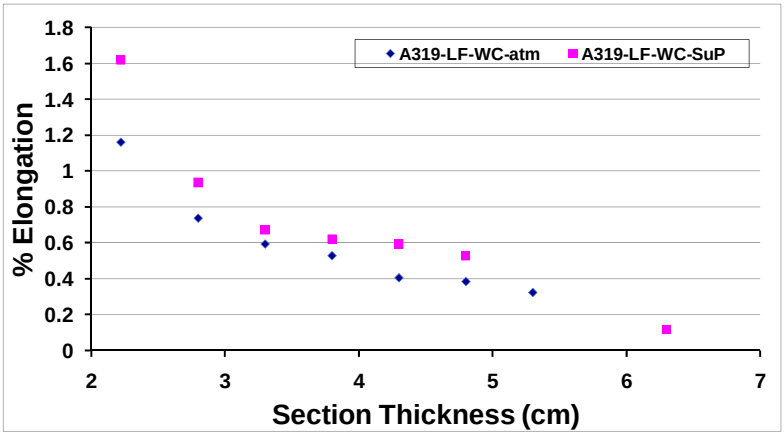

Figure 5.1.1.15 - Variation of Elongation with Section Thickness in Lost Foam Chilled A319 Atmospheric and Pressurized Castings.

The variation of elongation for the A206 alloy with section thickness for atmospheric and pressurized lost foam and open cavity castings is shown in Figure 5.1.1.16. The elongation of the atmospheric lost foam casting decreased from 17 to 1.3% with increasing section thickness, while that of the lost foam pressurized casting decreased from 17 to 11%. Similarly, the elongation of the atmospheric open cavity casting samples decreased from 18 to 1.3%, while that of pressurized open cavity casting decreased from 17 to 12%. The application of pressure resulted in an increase in elongation of 110% – 750% and 3 to 560% in lost foam and open cavity castings, respectively, at different section thicknesses, except at the sample close to the chill.

The effect of porosity on the mechanical properties is more prominent in A206 than in the Al-Si alloys due to the absence of the large volume fraction of intermetallics. The data from the lost foam and open cavity castings is separated due to the difference in pouring temperature, resulting in a difference in grain sizes. Also, the data for the atmospheric and pressurized samples is separated. A reduction of elongation correlated with increased porosity and increased grain size in the atmospheric castings in both the lost foam and open cavity castings, while the correlation in the pressurized castings was weaker.

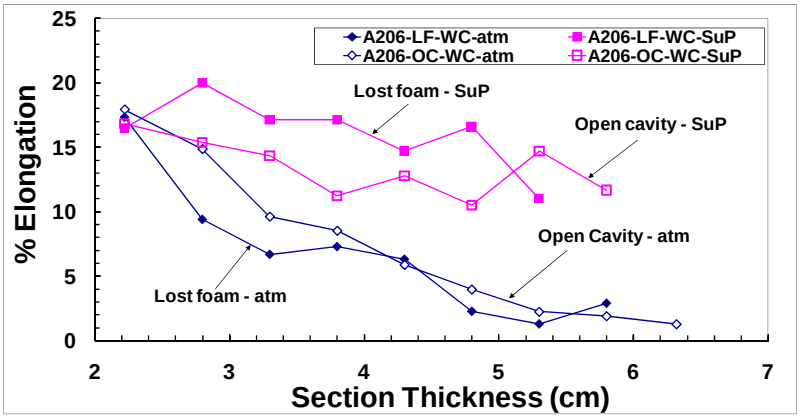

Figure 5.1.1.16 - Variation of Elongation with Section Thickness in Lost Foam Chilled A206 Atmospheric and Pressurized Castings

Ultrasonic Velocity Correlations – The results in Figure 5.1.1.17 shows that the velocity through the samples decreased with increasing porosity irrespective of the composition of the alloy. However, the data for A319 was separated from the other two alloys, showing that the velocity through these samples might be affected by other parameters, perhaps the iron needle structure of this alloy. Note that the velocity values for all alloys tends to become constant at porosity levels below 1%.Pore sizes tend to decrease at lower porosities levels which explains this behavior. For the castings solidified under pressure, the pore size was below the detectable limits of the ultrasonic wave at a frequency of 2.25 MHz, which corresponds to a wavelength of ~ 2.5 mm in aluminum alloys.

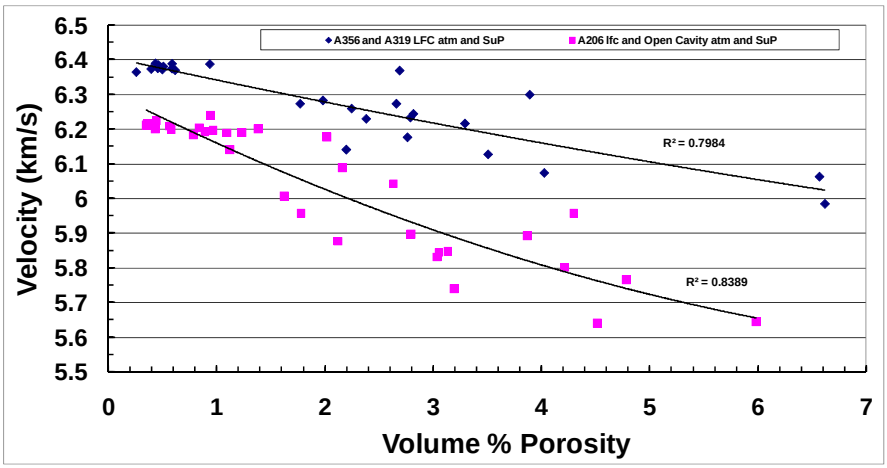

Figure 5.1.1.17 - Variation of Ultrasonic Velocity with Metallurgical Volume Percent Porosity in A356, A319 and A206 Castings under Different Conditions.

These results are further illustrated in Figure 5.1.1.18. In this figure there is a definite relationship between elongation and velocity for the castings poured at atmosphere pressure while the velocities are constant for the castings poured at pressure. Consequently ultrsonic velocity cannot be used as a quality control of pressurized castings unless a higher frequency is used. More research is needed in this area.

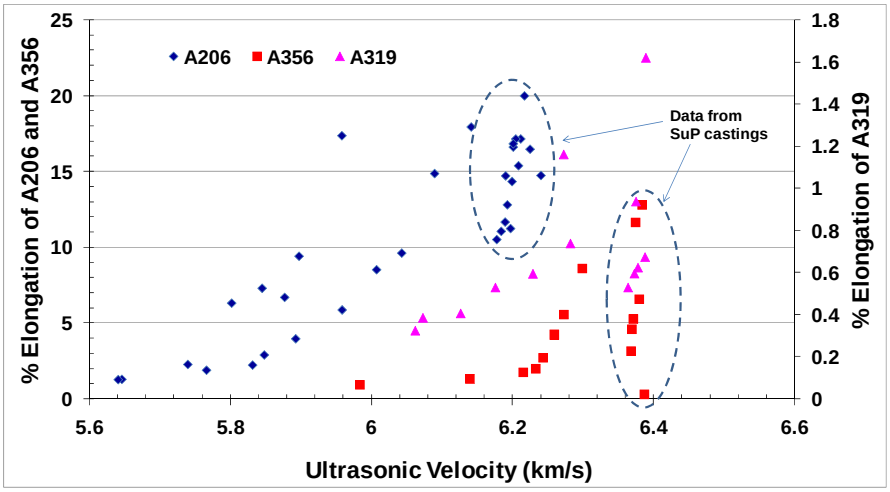

Figure 5.1.1.18 – Variation of % Elongation at Various Ultrasonic Velocities for Castings Poured at Atmospheric and Pressurized Conditions

Summary:

- Application of 1.034 MPa pressure during solidification increased the density in the castings of all the three alloys significantly. The density increase of reduced section thickness castings varied with

section thickness. No increase in density was achieved at 0.7 and 1.4 cm section thicknesses, while the rest of the casting with section thickness 2.8 cm and beyond exhibited an increase in density of 1.9 to 2.3%.

- Pore size and frequency decreased significantly for all three alloys with the application of pressure.

- Elongation in A356 and A319 increased by 50 – 130% and 13 – 45%, respectively, with the application of pressure.

- In A206 castings, application of pressure increased elongation by 110 – 750% and 3 – 560% in lost foam and open cavity processes, respectively. Similarly, the solidified under pressure castings exhibited a 12 – 55% increase in tensile strength in both lost foam and open cavity castings. Yield strength was not affected by the applied pressure.

- Tensile strength and yield strength were affected very little by the application of pressure.

- Ultrasonic velocity could be used to control quality of castings poured at atmospheric pressure. Velocity could be used to control quality of pressurized castings provided a frequency higher than 2.25 MHz is used.

5.1.2 - Vacuum Assisted Filling of Aluminum Lost Foam Castings

The literature reports several efforts to improve mechanical properties of cast aluminum alloys by various innovative casting processes and metallurgical changes. The casting processes studied were resin bonded sand with chills and solidification under pressure using the Lost Foam Casting Process (LFC). Metallurgical studies include the effect of iron content, strontium additions (eutectic silicon modifier) and TiBor additions (grain refiner). A review of the pertinent literature has revealed several inconsistent results. For example, in 1996, Gerard and Osborne[10] reported a 50% increase in high cycle fatigue (HCF) of 319 alloy solidified under pressures of 200 – 500 psi using the Lost Foam process. In 2002, Wang, Jones and Osborne[8] reported little or no increase in HCF strength for A356 using pressure solidification and the gravity pour LFC process. In this study, fracture initiation sites were identified as folds. In 2003, Wang, Jones and Osborne[11] reported on the effect of iron on the microstructure and mechanical properties of A356 alloy. In this study, the fracture initiation sites were identified as pores. The % porosity and maximum pore size for the pressure solidified study was 0.3% and 371 microns respectively, compared to 0.07 % and 150 microns for the iron content study. This decrease in % porosity and pore size predicts an increase of fatigue according to other literature sources. The authors of the pressure solidification study

stated that “when porosity and pore size are minimized, oxide films are the dominant crack initiation sites”. The authors, and others, are correct in this assessment however; since the HCF and LCF strengths of A356 from the gravity poured, atmospheric pressure and pressure solidified processes are practically the same, there are some fracture mechanics issues in question. In fact, the answers to this issue lie in the % elongation from the tensile data. The tensile % elongation for the atmospheric castings was 3.5% and the % elongation for the pressure solidified castings was 1.5%. Percent elongation has always been a strong indicator of fatigue strength within a fixed alloy system; however the applied stress must be oriented such that crack initiation theories apply. The data suggest that oxide folds and pores act similarly in limiting the HCF strength of A356.
The addition of chills in resin bonded molds acts to increase the metal cooling rate and subsequently reducing the % porosity and pore size. This process is similar to the pressure solidification process which suppresses the growth of pores initiated by the release of hydrogen or trapped pyrolysis gases. This process is effective in producing castings with improved mechanical properties and is currently the process of choice for many casting suppliers and casting users.

Similar to other casting processes the mechanical properties of Lost Foam aluminum castings are degraded by the presence of folds and porosity. The root cause of folds has been traced to merging metal fronts contaminated with residual pyrolysis products and, of course, the ever present surfaces of aluminum oxides. The occurrence of folds in Lost Foam castings is usually associated with lower metal temperatures and chaotic filling. Lower metal temperatures are usually found in the last portions to fill in a casting. Chaotic filling can be caused by high momentum early in the filling process or fingering at the metal front later in filling due to varying permeability of the pattern. Since the presence of pyrolysis products on the metal front aggravates the fold formation process and can produce metal porosity, timely removal of the pyrolysis products is key to producing castings with a minimum of folds and porosity. Evidence of the residual pyrolysis products can be observed on casting surfaces as brown traces. Folds are almost always found within these traces. Typical foundry remedies for reducing fold occurrence are increased pouring temperature, patterns that include “no fold” beads, gating changes and pattern geometry changes. Increasing the pouring temperature has historically been the most common and least expensive remedy; however, this higher temperature increases the hydrogen solubility of aluminum and increases the likelihood of metal porosity.

Typical Lost Foam aluminum castings experience a pressure gradient during filling due to the changing metal head pressure. For example a 20 inch tall casting with a 24 inch tall sprue will experience a metal pressure of about 2.4 psig at the casting bottom and about 0.4 psig at the casting top. These pressures are a driving force that counters the gas pressure generated by the degrading pattern and controls metal filling rate and removal of the pattern pyrolysis products from the casting cavity. Typical Lost Foam castings suffer from increased defect severity near the casting top where

metal velocities and temperatures are lower.

Figure 5.1.2.1 illustrates the removal process for pattern pyrolysis products and probable defect formation. Based on this validated model it is clear that a vacuum applied on the sand side of the mold cavity could expedite the removal of pyrolysis products and minimize the effects of varying metallostatic head pressure.

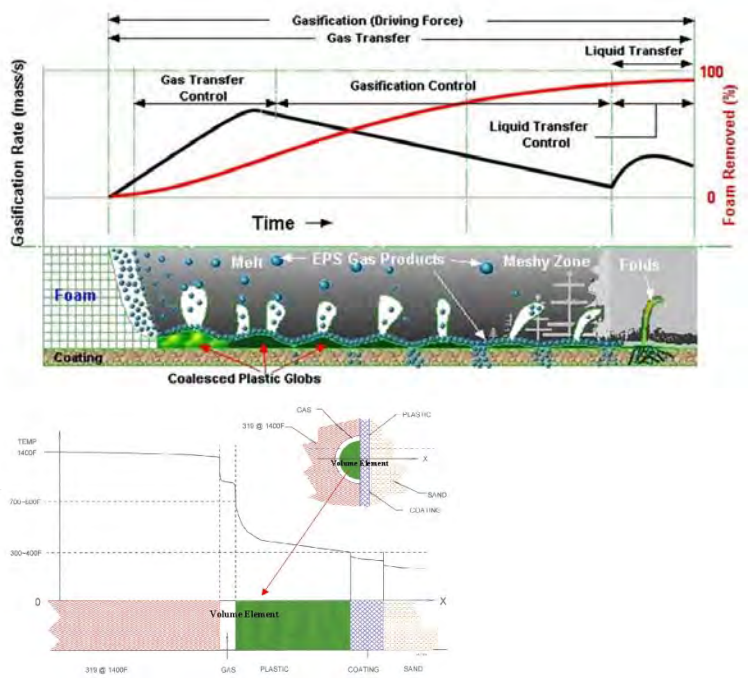

Figure 5.1.2.1 – Pattern Removal Process and Defect Formation

High silicon aluminum alloys (9% - 20% Si) increase the severity of folds. Conventional wisdom would lead us to believe that the higher energy content of these alloys would reduce the severity of folds by providing more time and energy for the removal of the pyrolysis products; however, the opposite is true. Castings poured with these alloys have severe surface pyrolysis defects, commonly known as ‘alligator skin’. A similar defect occurs in iron castings and is known as ‘lustrous carbon’. Yet to be proven, this defect is believed to be a result of high metal velocity which increases the liquid/gas ratio of degraded polystyrene patterns[7]. A study at UAB revealed that the ‘alligator skin’ could be eliminated in cylinder head castings with a 9% silicon alloy by 1.) increasing the pouring temperature to 1500^{o}F (816^{o}C) and 2.) vacuum assisted filling. Since this elevated temperature is not practical due to increased hydrogen solubility and reduced furnace life, the latter procedure was selected as worthy of further research.

The goals in this study are:

1) Minimize the effect of the changing metal head pressure by applying a vacuum to the sand/coating to control the metal filling rate from the sand side of the casting cavity.
2) Lower the pouring temperature to take advantage of the lower hydrogen solubility at lower temperatures.

As mentioned previously, elevated pouring temperatures can reduce the incidence of folds at the expense of increased hydrogen solubility and casting porosity. Vacuum assisted filling allows lower pouring temperatures with reduced hydrogen solubility. Hydrogen solubility as a function of temperature for various aluminum alloys is shown in Figure 5.1.2.2.

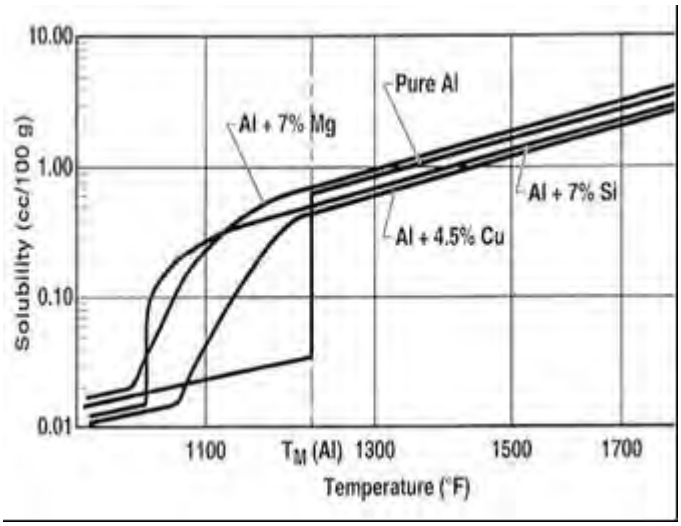

Figure 5.1.2.2 – Hydrogen Solubility in Various Aluminum Alloys as a Function of Temperature

Experimental equipment - Figure 5.1.2.3 illustrates a schematic of a vacuum assisted pouring apparatus. The flask has a screened chamber in the bottom where the vacuum is applied. Figure 5.1.2.4 shows the actual flask and instrumentation after pouring.

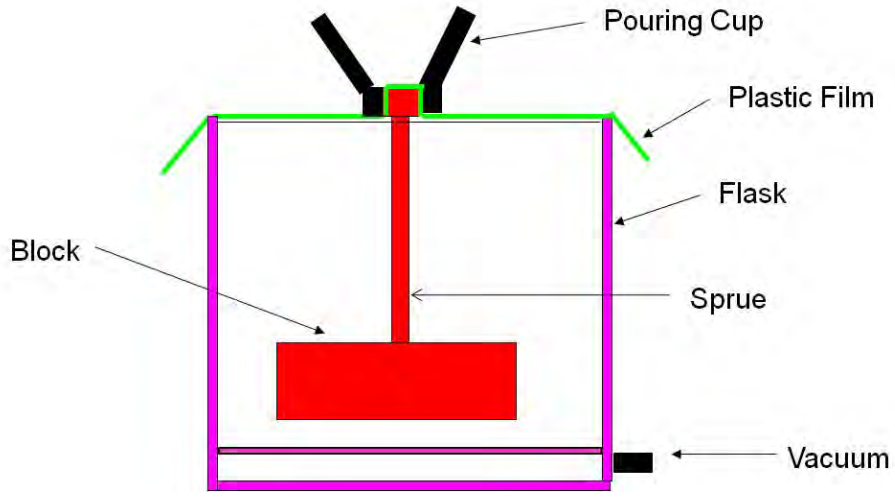

Figure 5.1.2.3 – Vacuum Assisted Pouring Schematic

Figure 5.1.2.4 – Flask and Instrumentation after Pouring

Experimental Methods and Procedures - A four cylinder engine block, poured with A319 aluminum, was selected for this study. Thermocouples were placed in the three central main bearing supports. Pressure probes were placed in strategic locations as illustrated in Figure 5.1.2.5. Porosity and tensile blanks were extracted from the locations shown.

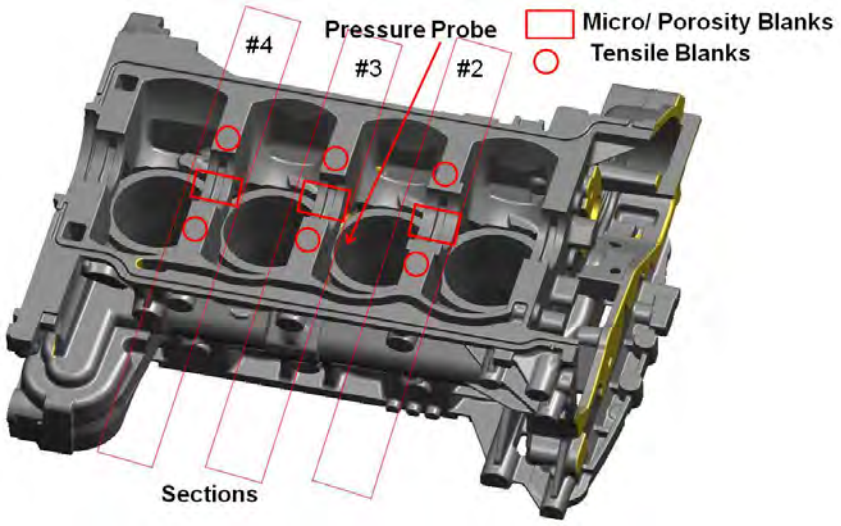

Figure 5.1.2.5 – Thermocouple, Tensile and Porosity Blanks and Pressure Probe Locations

The following variables were studied:

- Pouring temperatures: 1450°F (788°C), 1350°F (732°C), 1250°F (677°C)
- Pressure: -4.5 psig (233 mm Hg) – Based on previous studies.
- Recorded data: Pour temperature, pour times, thermocouple responses and pressure probe response.

After compacting sand around the cluster, a plastic film is placed over the top of the sand and sprue. A pouring cup is then installed, sealing the upper surfaces of the flask and sand (See Figure 5.1.2.3). Vacuum is applied and metal pouring is accomplished in the normal manner. Degassing of the melt was performed using Argon distributed through a rotating graphite tube for six minutes.

Casting Quality:

- Inspect for surface cleanliness (pyrolysis products and folds).
- Inspect for metal penetration.
- Section blocks main bearing journals #2, #3 and #4, Heat treat to T6 (Figure 6).
- Inspect main bearing blanks for microstructure and porosity.
- Machine tensile specimens and determine tensile properties using ASTM B557 procedures.
- Measure fracture face and below fracture face porosity of tensile specimens.

Results - Typical temperature and pressure responses are shown in Figure 5.1.2.6. Vacuum was maintained until all thermocouples in the block were at or below A319 solidus temperature (~500°C). Vacuum decreased approximately 0.5 psig after pouring due to gas generation from the foam

pattern. Only small differences in the temperature responses of the blocks poured at three different temperatures were noted.

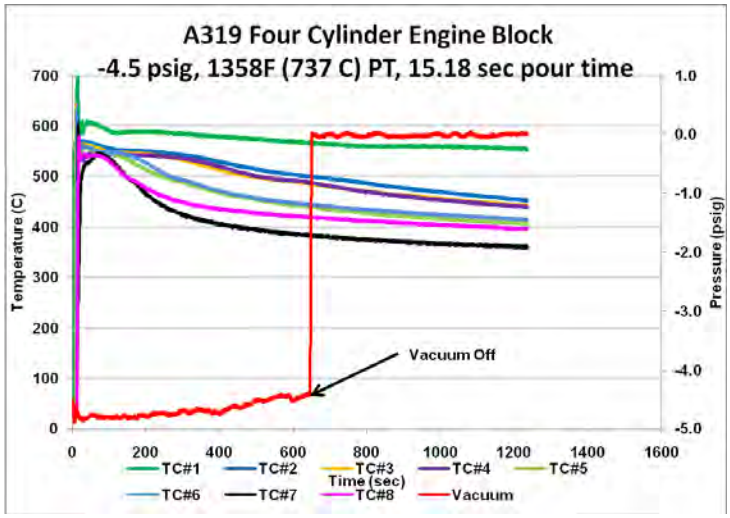

Figure 5.1.2.6 – Temperature and Pressure Responses for a 1350^0 F (737^0 C) Pour

Pour times for the blocks poured at 1450^{o}F, 1350^{o}F and 1250^{o}F are shown in Figure 5.1.2.7. Compared to typical production pour times, significant decreases in pour times were recorded. In addition pyrolysis traces on the casting surfaces were dramatically reduced. This indicated that the vacuum on the sand side of these castings was influencing the metal filling and pyrolysis product removal as predicted in the Introduction.

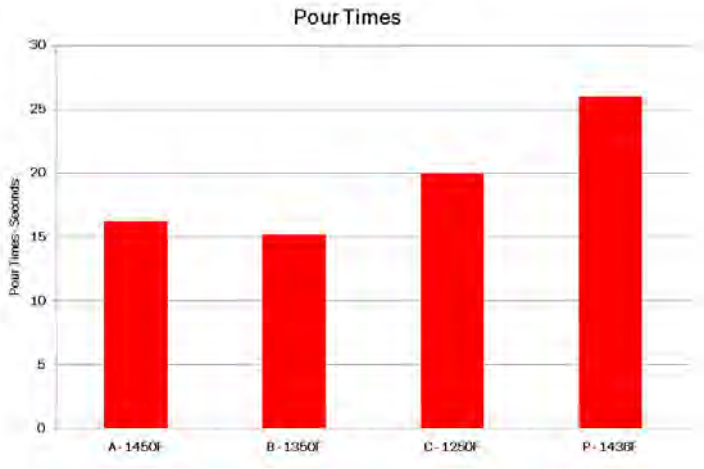

Figure 5.1.2.7 – Pour Times for Blocks Poured at Noted Temperatures

Porosity – Figure 5.1.2.8 illustrates the per cent porosity (measured on the main bearing blanks), decreased as the pouring temperature decreased. Figure 5.1.2.9 shows the average maximum pore size also decreased with decreasing pouring temperatures. The trends in these two figures indicated that the hypothesis of lower per cent porosity and smaller pore sizes for lower hydrogen solubility at lower pouring temperatures and/or the timely removal of pyrolysis products was confirmed.

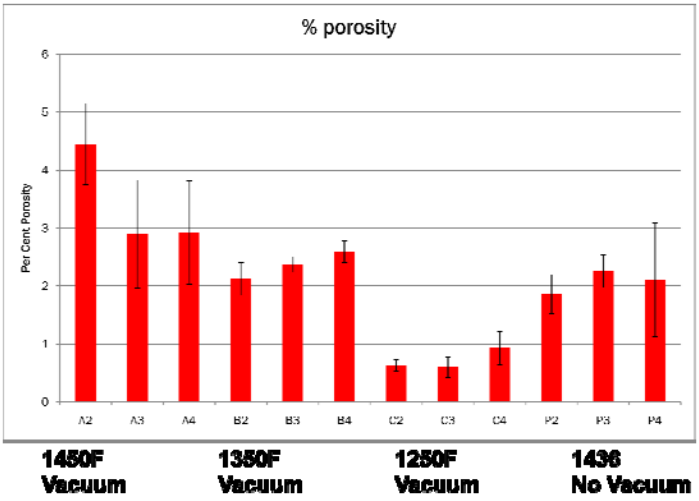

Figure 5.1.2.8 – Percent porosity of Main Bearing Blanks at Various Temperatures

Figure Figure 5.1.2.9 - Typical Porosity from Main Bearing Blanks

Tensile Properties - Tensile specimens were machined from sectioned blocks and stress-strain curves were recorded using a MTS 810 Materials Test System and ASTM B557 procedures. Ultimate tensile strength and per cent elongation were determined from the stress – strain curves. A total of 6 specimens were evaluated from each of the blocks poured at 1250°F, 1350°F, 1450°F. Eight specimens were evaluated from the production block. Average tensile properties are shown in Table 5.1.2.1 and Figures 5.1.2.10 and 5.1.2.11. These data suggest an increase in tensile ultimate strength and per cent elongation can be achieved using vacuum assisted pouring and reduced pouring temperatures. It is worthy to note that two of the 1250°F specimens failed at folds that extended to the specimen surface, hence the larger standard deviation for the per cent elongation data for the blocks poured at1250°F. This behavior is consistent with foundry experience; folds are usually located in the last portions to fill in a casting. Lower metal temperatures are present in these locations. An additional block was poured at 1250°F without vacuum assist to confirm that folds are associated with colder metal. Although the block filled completely, numerous folds extending to the casting surface were observed.

Table 5.1.2.1 – Average Tensile and Porosity Values for A319 - T6 blocks – Porosity properties from block sections

Number of Specimens	Approx. Pour Temperature - F	Avg. Ultimate Tensile Strength - PSI	Std. Dev.	Average % Elongation	Std. Dev.	% Porosity	Maximum Pore Size - Microns	Pour Time Seconds
6	1250	32,180	1607	1.06	0.20	0.72	206	16.3
6	1350	30,405	2236	0.89	0.16	2.36	306	15.2
6	1450	28,785	1758	0.77	0.10	3.42	479	19.9
8	1436 Production No Vacuum	31,166	1620	0.84	0.14	2.07	341	26.0

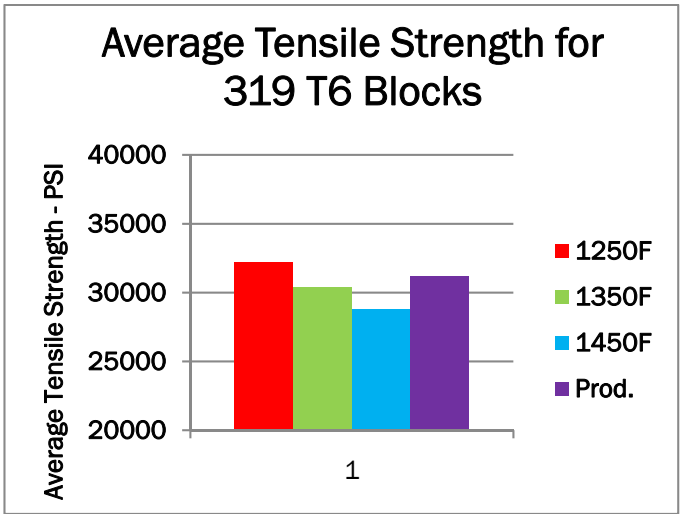

Figure 5.1.2.10 – Average Ultimate Tensile Strength for 319 T6 Blocks

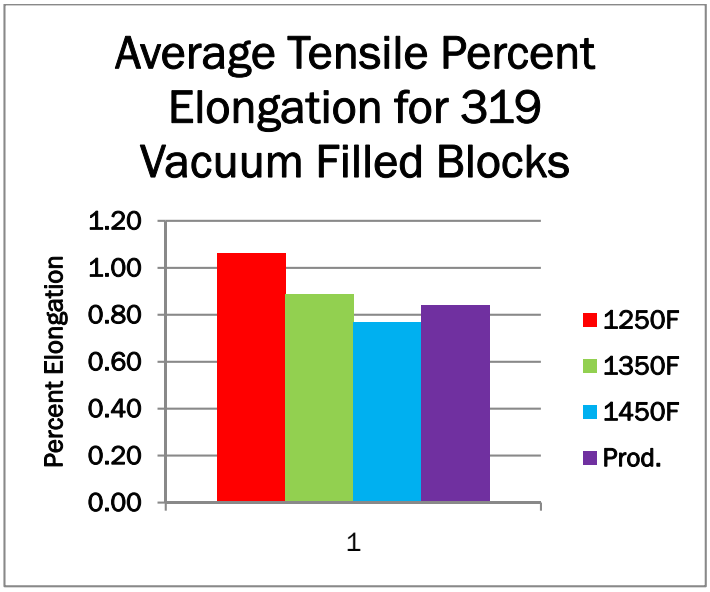

Figure 5.1.2.11 - Average Percent Elongation for 319 T6 Blocks

Since the improvements in tensile elongations were small a statistical analysis was performed to assure the improvements were valid. Table 5.1.2.2 illustrates the results and indicated that there was a 98% probability that the elongation values for the 1250^0 F casting were different than the production casting.

Table 5.1.2.2 - T-Test Probability Values Comparing Tensile Elongation at Different Pouring Temperatures To Production for 319T6.

Pouring Temperature	Average % Elongation	T-Test Probability of Difference Compared to Production
1250 F - Vacuum	1.06	96.9
1350 F - Vacuum	0.89	45.0
1450 F - Vacuum	0.77	72.4
Production – No Vacuum	0.86	0.0

The results of this study clearly indicated that mechanical properties of A319 castings can be improved using the LFC process with vacuum assist. Consistent with the literature, the mechanical property improvements were a result of decreased per cent porosity and pore size. The choice of A319 alloy was probably poor due to the limited achievable properties dictated by the microstructure of this alloy.

A follow on study, using a more ductile alloy (A356) was performed with

similar results. The trend of increasing % elongation with decreasing pouring temperature agreed with the 319 study at temperatures below 1350F. Fracture face porosity increased with increasing pouring temperature; however, the porosity values were significantly higher than expected. The nature of the fracture face porosity for the A356 samples appears to be both gas and shrinkage, with the shrinkage porosity increasing with increasing pouring temperatures.

5.1.3 – Pouring Compacted Graphite Iron using Lost Foam

Introduction - An investigation into the production of compacted graphite iron cylinder blocks using the lost foam casting process and the commercially accepted SinterCast technology was performed in a production foundry with excellent results. This breakthrough could provide an entirely new production market for the casting industry. Current automotive compacted graphite iron production is approximately 950,000 engine equivalents per year and is currently used for more than nineteen diesel engine blocks in vehicles produced by over eleven car and truck manufacturers and is the material of choice for NASCAR, NHRA and Pro Truck race engines due to higher strength, higher stiffness and reduced cylinder bore distortion compared to both gray cast iron and cast aluminum. However, none of these production cylinder blocks are produced using the lost foam casting process. A gray iron skin, which can significantly reduce strength and ductility, may form when compacted graphite iron is cast in green sand molds due to the reaction of the molten metal with the water and sulfur in the molding material. A "skin" has also been reported to form on castings produced in bonded sand molds[12]. The lost foam casting process uses a thin refractory coating that prevents the molten metal from contacting the supporting media, typically sand or synthetic mullite. Since the metal does not contact the molding media, the detrimental "skin" is minimized.

The lost foam casting process (LFC) is an established method of cost savings because many assemblies that are made by separate processes can be consolidated into a single casting. There are many examples of part consolidation that are possible by LFC, and the total cost and weight savings continue to make LFC an attractive choice for today's castings.

Compacted graphite iron (CGI) is being used in increasingly varied applications, in particular, where there is a need for higher elastic modulus (stiffness) and higher tensile strength than gray iron or aluminum and better thermal conductivity and better damping than ductile iron, such as cylinder blocks, cylinder heads and exhaust manifolds. CG iron achieves these superior properties by modifying the morphology of the graphite. In CG iron, the graphite forms an interconnected network of short, blunt-tip "vermiculi" along the edges of the eutectic cells. The blunt tips of this form of graphite eliminates the inherent stress concentration effect of the long, sharp tipped, graphite flakes present in gray iron and, the interconnected graphite network provides higher thermal conductivity and higher vibration dampening properties compared to the isolated, graphite

nodules present in ductile iron.

The SinterCast process is the most widely used production process for CGI. The SinterCast process uses thermal analysis to determine the degree of nodularization and the degree of inoculation in a melt and then calculates the appropriate amount of magnesium and inoculant that needs to be added in order to obtain the desired microstructure in the casting. The production of CGI requires more precise control of chemistry and inoculation than any other type of cast iron. Achieving microstructural uniformity throughout the casting, particularly in areas with significantly different cooling rate, however, is still a challenge.

In addition to molten metal processing, reactions of the molten metal with the mold and during solidification must be controlled in order to produce CGI castings with maximum mechanical properties. It has been reported that reactions between the molten metal with moisture or sulfur in the mold can cause the graphite to revert to the flake morphology and thus form a deleterious skin with low strength and low ductility[12]. Also, the unique solidification behavior of CG iron can produce a skin with lower strength and lower ductility than the bulk material.

LFC has been used to make complex assemblies in large numbers for many years, with current LFC producers regularly experiencing scrap levels of 2% or lower. LFC of iron parts has been limited to gray cast iron or ductile iron castings. A common problem is lustrous carbon defects, which may necessitate the use of more expensive co-polymer blends rather than expanded polystyrene (EPS) as the pattern foam. In the current study, sponsored by the AFS/DOE Lost Foam Casting Consortium, the production SinterCast process was used to produce CG iron cylinder blocks at the Grede-Columbiana lost foam iron foundry. The microstructures at the casting surfaces and in the bulk were examined and the tensile properties from sections of the cylinder blocks determined.

CGI is produced by precise control of metal chemistry and inoculation. Oxygen and sulfur concentrations in the iron melt must be considered so that the correct amount of magnesium and inoculant can be added to cause graphite nucleation and growth in a controlled fashion. There are a variety of molten metal treatment options; the SinterCast process, the NovaCast process, the use of special treatment alloys containing various amounts of magnesium and rare earth elements, and the use of titanium. When using magnesium, the process window for CGI production is very narrow, as shown in Figure 5.1.3.1. Titanium opens the process window, as is shown in Figure 5.1.3.2, but may reduce machinability due the formation of hard titanium carbide particles.

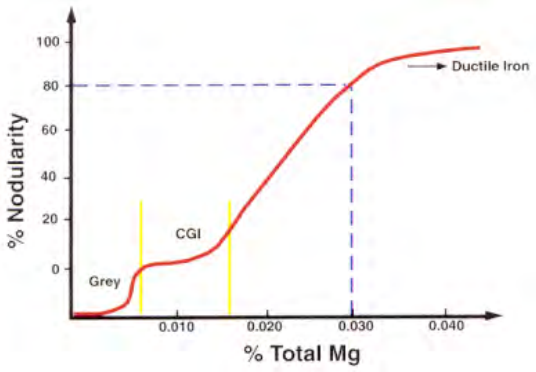

Figure 5.1.3.1 - Plot of nodularity vs. magnesium content showing the narrow range of magnesium content required to produce CGI.

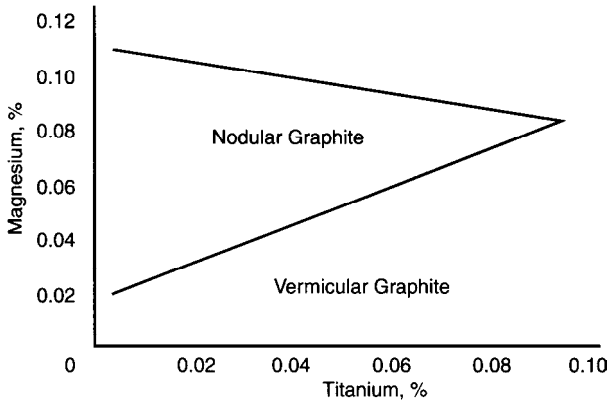

Figure 5.1.3.2 - Plot of magnesium content vs. titanium content showing the process windows that will produce nodular or vermicular graphite (CGI).

The CGI microstructure offers tremendous benefit to designers because of its improved mechanical properties compared to gray cast iron and aluminum, but this benefit can be lost if the graphite reverts back to the flake form at the surface of the casting. Further, the LFC process can produce thinner wall thicknesses, on the order of 3 mm or less, than the green sand process but the graphite morphology formed is a function of cooling rate and higher than desired nodularity may result in thin sections. Therefore, it is important to determine the microstructure in both thick and thin sections of CGI castings and to examine the microstructure at the surface of the casting.

Experimental Methods - In a previous study, CGI was produced using the lost foam process in the laboratory and a production foundry using the sandwich treatment process and titanium to control nodularity. In this study, the SinterCast process was used to produce the compact graphite iron without the use of titanium. A four-cylinder engine block was poured to provide an example of producing a difficult casting. The foam patterns for the

cylinder block were produced in EPS since they were readily available from a production aluminum foundry. The iron foundry changed the casting gating system from top-fill to bottom-fill, Figure 5.1.3.3, and applied their normal coating. SinterCast brought a Mini-system 3000 to the production foundry to produce the CG iron, Figure 5.1.3.4. At the production foundry, a heat of CG iron was "under-treated", evaluated by the SinterCast system and then adjusted to produce high-quality CG iron.

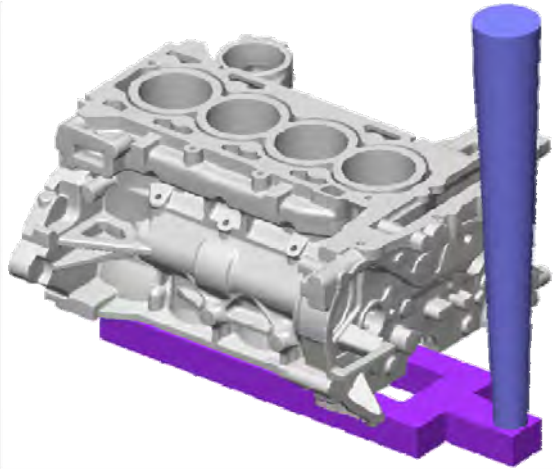

Figure 5.1.3.3 – Four Cylinder Block with Bottom Gating

Figure 5.1.3.4 - SinterCast System in the Foundry with Wire Feeder.

The bulk and surface microstructures of thick and thin casting sections were examined. Nodularity was calculated in accordance with ISO 16112:2006(E). Data was gathered from thirty (30) fields of view at 200x and the calculated nodularities reported as area percent. A typical casting cross section showing the locations of the micro samples is shown in Figure 5.1.3.5.

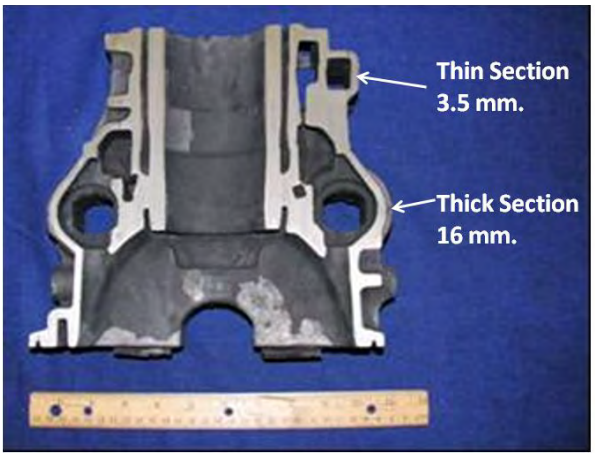

Figure 5.1.3.5 - Typical casting cross section showing the locations of the micro samples.

Tensile testing was performed in accordance with ASTM E8-04. Small-size tensile specimens proportional to the standard (nominal diameter = 0.350”/9 mm, gage length = 1.40”/36 mm) were machined from blanks sectioned from the cylinder block bolt bosses.

Four CG iron heats were made at the production foundry to give the SinterCast system time to "learn" the foundry process. The first casting was poured at a lower than desired temperature and was scrapped. The chemistries and pouring temperatures are listed in Table 5.1.3.1. The measured Mg contents appeared low; this may be due to being outside of the spectrometer calibration range for Mg.

Table 5.1.3.1. Chemistries and pouring temperatures of CG iron cylinder blocks.

		Composition, wt%						
Heat	Pouring Temp., °C	C	Si	Mn	Cu	Mg	Ce	S
1	1336	3.48	2.10	0.27	0.31	0.002	0.011	0.008
2	1378	3.45	2.13	0.27	0.32	0.002	0.011	0.009
3	1413	3.42	2.13	0.26	0.31	0.001	0.009	0.007
4	1454	3.63	2.16	0.27	0.32	0.001	0.010	0.008

Results - The microstructures of the CG iron produced were excellent. No flake graphite was noted at any of the surfaces examined and the nodularity in the thick sections was excellent (10-15%). As expected, the nodularity of the thin sections was higher (48-64%) due to the higher cooling rate. There was a thin "skin" at the surfaces but this skin did not contain flake graphite but instead was characterized by a higher than normal graphite content and probably resulted from a high cooling rate and perhaps segregation of magnesium during solidification. Typical bulk microstructures are shown in Figure 5.1.3.6, the surface microstructures

of the thin sections are shown in Figure 5.1.3.7 and the surface microstructures of the thick sections are shown in Figure 5.1.3.8.

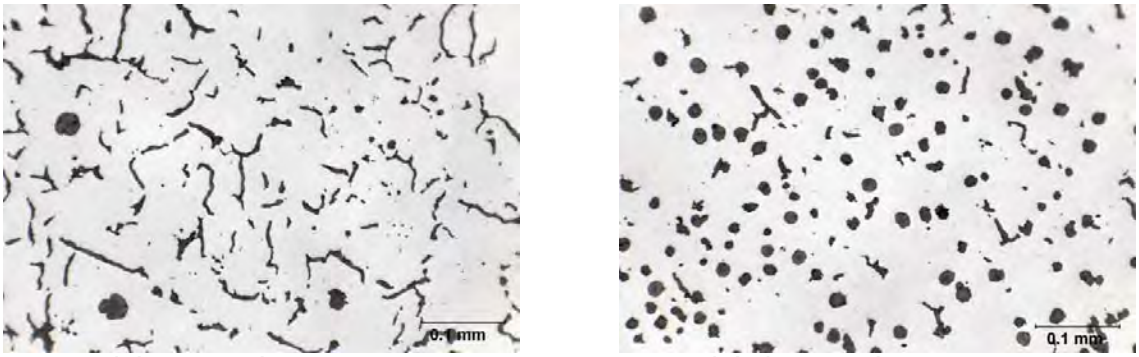

Thin Section Thick Section

Figure 5.1.3.6 - Typical unetched microstructures of thick and thin sections from the cast CG iron cylinder blocks showing excellent nodularity (10-15%) in the thick sections and higher nodularity in the thin sections.

(a) 1378°C pour temperature (b) 1413°C pour temperature (c) 1454°C pour temperature

Figure 5.1.3.7 - Typical unetched microstructures of the surfaces of the thin sections from the cast CG iron cylinder blocks poured by different temperatures showing a very thin "skin" that increased in thickness with increasing pouring temperature. The "skin" did not contain flake graphite but was characterized by higher than normal graphite volume fraction.

(a) 1378°C pour temperature (b) 1413°C pour temperature (c) 1454°C pour temperature

Figure 5.1.3.8 - Typical unetched microstructures of the surfaces of the thick sections from the cast CG iron cylinder blocks poured by different temperatures showing a very thin "skin" that increased in thickness with increasing pouring temperature.

The "skin" did not contain flake graphite but was characterized by higher than normal graphite volume fraction.

The nodularity of the thin sections decreased with increasing pouring temperature, the nodularity of the thick sections varied only slightly with increasing pouring temperature and the skin thickness increased with increasing pouring temperature. Table 5.1.3.2 lists the nodularities and skin thicknesses as a function of pouring temperature for CG iron produced using the lost foam casting process and SinterCast CG iron process controls. Due to the uneven nature of the skin thickness, the results reported are the average of about 25 individual measurements.

Table 5.1.3.2 - Nodularity and skin thickness as a function of pouring temperature for CG iron produced using the lost foam casting process and SinterCast CG iron process controls.

Section Size	Pouring Temperature	Nodularity	Average Skin Thickness
3.5 mm	1378°C	64%	0.014 mm
3.5 mm	1413°C	52%	0.054 mm
3.5 mm	1454°C	48%	0.100 mm
16 mm	1378°C	10%	0.098 mm
16 mm	1413°C	12%	0.128 mm
16 mm	1454°C	15%	0.171 mm

The "skin" produced on CG iron castings using the lost foam casting process were thinner than those produced by other casting processes. Since skin thickness is a function of pouring temperature, comparison of the skin thickness for CG iron castings produced by various processes is difficult. However, Table 5.1.3.3 lists the CG iron skin thicknesses reported in the literature produced by various casting processes at approximately 1400°C.

Table 5.1.3.3 - CG iron skin thicknesses for section sizes of approximately 3-16 mm produced by various casting processes at approximately 1400°C.

Process	Range of Skin Thicknesses
lost foam	0.01 - 0.13 mm
phenolic-urethane	0.12 - 0.25 mm
sodium silicate	0.13 - 0.39 mm
green sand	0.25 - 0.40 mm

The microstructures of the thick sections were compacted graphite in a matrix of ferrite plus pearlite. The matrix was predominantly ferrite due to the low levels of manganese and copper, 0.27 wt% and 0.32 wt% respectively. A typical thick section microstructure is shown in Figure 5.1.3.9.

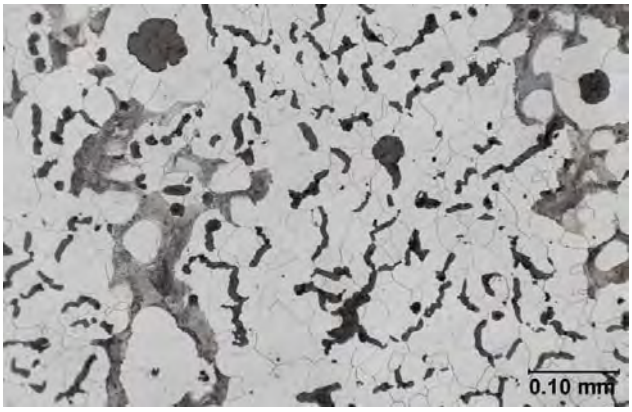

Figure 5.1.3.9 - Typical thick section microstructure showing compacted graphite in a matrix of ferrite plus pearlite.

The measured tensile properties of samples sectioned from the cylinder block castings indicated that the quality of the CG iron produced by the lost foam process were good. The tensile properties of specimens sectioned from the cylinder blocks were very consistent and close to meeting the ASTM Grade 300 specification for compacted graphite iron castings. Due to the low alloy content, which produced a largely ferritic matrix, the average yield strength was relatively low (211 MPa) but the average elongation (strain at fracture) was high (4.7%). A pearlitic matrix (harder and more wear resistant than a ferritic matrix) is desirable for a cylinder block. The properties were fairly consistent even though the samples were sectioned from different locations within the castings. The tensile properties of the specimens sectioned from the cylinder blocks are listed in Table 5.1.3.4.

Table 5.1.3.4 - Tensile properties of specimens sectioned from the CG iron cylinder block castings.

Pour Temp	**Ultimate Tensile Strength (MPa)**	**Yield Strength (MPa)**	**Elongation(%)**	**Elastic Modulus(GPa)**
1378°C	291	212	5.1	142
	286	214	5.5	143
1413°C	294	213	6.1	140
	288	216	5.4	142
1454°C	291	207	4.9	140
	288	204	3.6	144
average	290 +/- 3	211 +/- 5	5.1 +/- 0.8	142 +/- 2
Grade 250[25]	250	175	3	
Grade 300[25]	300	210	1.5	

There was no attempt made to determine if the cylinder blocks produced in this study were suitable for engine build since the producing foundry did not have the required quality standards for this component. However, a visual examination for fill defects and lustrous carbon was performed. No obvious fill defects and no lustrous carbon defects were noted on the castings.

This exploratory research was significant because it demonstrated that complex castings can be poured in CG iron using the lost foam casting process, these casting had only a thin "skin" and the "skin" was free of the deleterious flake graphite. Also, it demonstrated that it may be possible to produce quality CG iron castings using low cost EPS foam rather than more expensive PMMA or co-polymer foams.

Subtask 5.2 – Design Package

A committee was formed to develop an ASTM standard for tensile and fatigue testing for the Lost Foam process. This idea originated in AFS Division 11. The purpose of this standard was to enable designers to use mechanical properties achieved by using castings in lost foam process. The UAB data was combined with data evaluated at Mercury Marine and GM. This design package would provide designers with the range of tensile properties expected from Lost Foam castings with the effects of cooling rates and solidification under pressure. This data is not intended for inputs to stress predictions since insufficient replications were generated to

provide statistical variability.

An all inclusive ASTM standard was impossible to assemble due to the many variables that dictate properties. For example tensile properties vary with porosity, dendrite arm spacing, silicon particle morphology, melt quality (oxide films) and metal composition. The idea of an ASTM standard was abandoned for these reasons and a decision was made to assemble a limited design package of tensile properties based on the data generated in the pressure solidification study (Subtask 5.1.1). The tensile properties from this study are listed in Table 5.2.1. Significant scatter in the data exists due to the variations in the controlling factors discussed above. The tensile data shown should be used as guidelines for designers to choose not only the choice of aluminum alloys but also the casting process.

Table 5.2.1 – Tensile Properties for Various Aluminum Alloys, Heat Treatment Conditions and Casting Processes.

Alloy	Heat Treat	Ultimate Tensile Strength Range (ksi/MPa)		Yield Strength Range (ksi/MPa)		Percent Elongation %	
		1 atm	10 atm	1 atm	10 atm	1 atm	10 atm
A356	T6	28.3-37.7/ 195-260	31.3-38.3/ 216-264	24.2-25.6/ 167-177	23.4-25.3/ 161-174	1.35 - 8.6	3.1-12.8
A319	T7	30.7-39.3/ 212-271	30.1-41.0/ 208-283	30.2-33.7/ 208-232	29.5-35.0/ 203-241	0.5-1.1	0.5-1.6
A206	T4	34.2-54.3/ 236-374	44.3-54.9/ 306-379	24.0 - 32.5/ 166-224	25.2-31.8/ 174-219	2.0-18.0	11.0-17.0

Subtask 5.3 – Marketing Plan

The objective of this subtask was to showcase the advantages of the Lost Foam Casting Process and present technical improvements achieved through the Lost Foam Consortium to existing and prospective Lost Foam suppliers and Designers. This was achieved through presentations by existing buyers and suppliers where expectations and achievement of the expectations of the process were presented at sponsors meetings and AFS Conferences. For

example a presentation by a sponsor (Emerson Climate Technology) outlined their expectations for Lost Foam castings. This was followed by a presentation by the casting supplier (Fundilag) servicing Emerson where the actions required to achieve the expectations were presented. In addition two designer workshops were held.

Several additional sponsors discussed their customer expectations and the methods used to achieve these expectations. This process of general approaches to achieving casting expectations has been repeated through this program, resulting in improvements in marketing Lost Foam Castings. Participating sponsors were Casti, PSA Peugeot Citroen, Arena Flow, Bombardier, Flow Science, Foseco Morval, GM Powertrain, Lovink Terborg, Mercury Marine and Styrochem International.

A panel discussion organized by UAB personnel was given in 2005 AFS Casting Congress and Cast Expo on April 16, 2005 in St. Louis, MO. The topic of this panel was “Showcasing the capability of the lost foam casting process”. Dr. Wanliang Sun from UAB hosted the panel discussion, and Dr. Charles Bates gave an outlook for the lost foam casting process at the end of the panel discussion. The panel discussion provided metal casters with practical information on the production of lost foam patterns and castings and highlighted the capability of the lost foam casting process. This session was highlighted in the Modern Casting magazine.

The first AFS - UAB designers’ workshop for lost foam castings was successfully held on November 15-16, 2005 in Fond Du Lac, Wisconsin. There were totally 119 participants representing about 80 companies from 7 countries. The attendees covered a big varieties including designers, product engineers, product managers, buyers, lost foam casting manufactures and suppliers. The workshop featured 16 tabletop shows, 16 presentations, and a tour of the Mercury Marine lost foam aluminum casting Facility. Presenters of the tabletop and presentations are product design engineers, product release engineers, lost foam casting manufacturers and suppliers. Figure 5.3.1 is photo of the attendees taken at the workshop.

Figure 5.3.1 – Attendees at the First UAB Designers Workshop

Through this workshop, the lost foam casting process was exposed to the designers as a whole. Every aspects of the process including historic review, process steps, process advantages, design criteria, case studies and future vision of the process were discussed in the workshop. The workshop brought lost foam castings on the designers' table as one of their choices toward a competitive design. Lost foam castings provide them design from freedom to consolidate multiple castings into one to save cost in machining, assembling and reduce product weight. Smooth as-cast internal passage surfaces improve component performance. With "hands on" analysis of lost foam castings during presentations and tabletop shows, the design engineers were looking for another niche for their designs. Figure 5.3.2 illustrates the "hands on" analysis approach.

Figure 5.3.2 – "Hands On" Approach

A Tool Engineer from an electrical tool company was also thinking about lost foam casting very hard, "I hope our tools are as light as possible,

so our customer can grab it easily in work. Lost foam castings could help to save some pounds. ”

Surprisingly, the workshop generated unbelievable interests in lost foam castings. After closing of registration, many requests still flew in. Some even came without registration.

The workshop also brought the lost foam industry closer to the designers. With suggestions, concerns and questions raised by the workshop participants, researchers, suppliers and manufacturers of lost foam castings are working as one to meet the demands of the designers and bring more castings to the community. This could be the kick off of the revival and prosperity of the lost foam industry.

A survey on the workshop taken in November was sent out to attendees. The following are questions and responses in the survey with a value of 1indicating poor and a value of 5 indicating good.

1. How knowledgeable do you consider yourself about the Lost Foam process? (3.7)
2. What category best fits your interests in the Lost Foam Process?
3. Were the format and organization satisfactory? (3.6)
4. Did the presentations meet your needs? (3.6)
5. Were the table top exhibits interesting and informative? (4.2)
6. Was the plant tour informative? (3.2)
7. Do you consider the presentations too commercial? (2.2 - No)
8. Please give your suggestions for specific topics or information you would like to see presented at the next workshop.

A second “Lost Foam Workshop” was held on March 13 – 15, 2007 in Birmingham. This workshop was directed toward designers in an effort to expand the use of Lost Foam Castings. This workshop showcased Lost Foam suppliers and the lessons learned from their mistakes along with casting design criteria and case studies. Table top displays represented the current state-of-the-art castings, computational modeling and foundry supplies such as coatings, sand (casting media) and processing equipment. A tour of the UAB laboratories, an iron Lost Foam foundry and an aluminum Lost Foam Foundry were available. This workshop was a success in bringing designers closer to the production issues of the foundry.

A significant accomplishment of this program was the publication of a book titled “Lost Foam Casting Made Simple”. This book was written over a two year period by knowledgeable personnel in the industry. The book was intended to include the most recent advancements in Lost Foam Casting technology and practices and to update the first book on Lost Foam written by Raymond Monroe in 1992. The author of each chapter was selected on the basis of knowledge and experience in the subject of the chapter. Final editing of the chapters was accomplished by personnel with the most experience in research, application and materials selection for the process.

This book focuses on technical advances and the practical application of these advancements. It is intended to be a valuable reference for potential users of Lost Foam Castings. Figure 5.3.3 is photo of the book cover as it was published by AFS Division 11 in 2008.

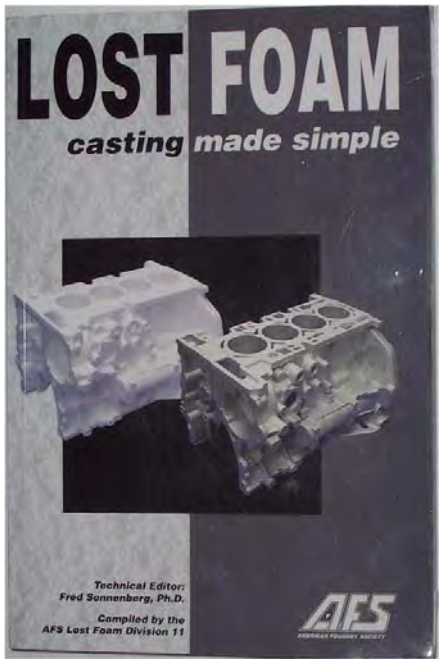

Figure 5.3.3 – Lost Foam Casting Made Simple Book

Task 6 – Technology Transfer

The objective of this task was to transfer the developed technology to the production floor of the sponsoring companies. This was accomplished through sponsors' meetings held at four month intervals. Technical presentations were made by UAB personnel followed by discussions where sponsors indicated their direction for further research and requests for assistance to apply the research to their facilities. This has led to numerous plant trials and tutorials where the research was applied to the production floor. This process has worked well for previous Lost Foam research programs.

Another method of transferring technology was presentations at AFS sponsored Lost Foam Conferences and Casting Conferences.

BENEFITS ASSESSMENT

Casting scrap has continued to decrease in both aluminum and iron Lost Foam foundries. This reduction is due to the continued effort by the sponsors and researchers to develop innovative equipment and procedures to address specific casting quality issues. Typical casting scrap rates for both aluminum and iron castings have been reduced to less than 2% for simple shapes and less than 6% for complex castings with intricate passages. This is a significant improvement from the 25% - 30% scrap rates that were common fifteen years ago.

The Pattern Permeability Apparatus has been instrumental in reducing pattern and casting scrap by providing a tool to measure the pattern properties that affect casting scrap. Using the Pattern Permeability Apparatus, pattern blowing equipment and procedures have been modified to achieve the best quality patterns. This has been a learning experience for pattern blowing companies. Perfect patterns are not yet achievable; however, with additional study the bead packing issues can be resolved.

Improved gating, achieved through modeling and casting validation, with accurate input properties of the metal, has been a significant advancement in reducing unfed metal shrinkage and scrap castings.

Optimization of the bromide additive to pattern materials has made a significant improvement in casting quality through the reduction of fold defects in aluminum castings and lustrous carbon defects in iron castings.

With the downturn of the economy that affected the casting industry, it is difficult to assess the energy savings accurately. This new technology was predicted to result in an average energy savings of 7.77 trillion BTU’s/year over a 10 year period. Current (2011) annual energy saving estimates based on commercial introduction in 2011 and a market penetration of 97% by 2020 is 5.02 trillion BTU’s/year and 6.46 trillion BTU’s/year with 100% market penetration by 2023.

Along with these energy savings, reduction of scrap and improvement in casting yield will result in a reduction of the environmental emissions associated with the melting and pouring of the metal which will be saved as a result of this technology. The average annual estimate of CO_2 reduction per year through 2020 is 0.03 Million Metric Tons of Carbon Equivalent (MM TCE).

See Appendix A for additional discussion.

COMMERCIALIZATION

The new Lost Foam book, “Lost Foam Made Simple” is available through AFS and should reap long term rewards in promoting the Lost Foam industry. This book is a summary of twenty years of applied research, reduced to practical applications and instructions. All quality control equipment and procedures for sands, coatings, patterns, metal and modeling are practically presented.

The Pattern Permeability Apparatus is available through UAB along with servicing and recalibration. Instructions for using this apparatus are included in the Lost Foam book.

Accomplishments

- A book titled “Lost Foam Made Simple” was written and published by AFS.
- A Pattern Permeability Apparatus was developed and commercialized.
- Computational modeling accuracy was improved to predict temperatures in relatively slow filling Lost Foam Castings by using accurate enthalpy data.
- Computational modeling was used to predict areas of unfed metal shrinkage using accurate temperature predictions and improved density data.
- The amount of bromide additive to pattern materials has been optimized through a comprehensive study using the Pattern Pyrolysis Apparatus.
- The root cause of variable pattern permeability was traced to inconsistent bead packing.
- Mechanical vibration of the tool provided uniform bead packing.
- Gating of Lost Foam castings has been improved to prevent unfed metal shrinkage by positioning gates to provide the shortest possible metal feed path.
- Mechanical properties of A319, A356 and A206 can be significantly improved using pressure solidification.
- Mechanical properties of A319 and A356 can be significantly improved using vacuum assisted pouring.
- Compacted graphite iron engine blocks have been successfully poured in Lost Foam with little skin effect.
- A design package of tensile properties of A319, A356 and A206 was developed that includes the effects of solidification with pressure and without pressure, with and without a chill and using Lost Foam and sand molds.
- Two design conferences were held to familiarize designers, casting producers and users with the Lost Foam process.

CONCLUSIONS AND RECOMMENDATIONS

Although many technical achievements have led to significant improvements in the quality of Lost Foam Castings during this program, the most commercial benefit can be achieved through two additional research efforts. First, the production of Compacted Graphite engine blocks without the gray iron skin could transform the diesel engine market in the US. This breakthrough provides the opportunity to design the next generation of diesel engines to include the benefits of the Lost Foam Process such as part consolidation, weight savings due to the improved mechanical properties of CGI and stiffer cylinder bores resulting in reduced emissions. Second, the next step in maturing the Lost Foam Casting Process could be the implementation of techniques to eliminate variable pattern permeability. This would significantly reduce casting and pattern scrap, saving energy at both steps in the process.

Presentations and Publications

- Wanliang Sun, “Researchers Help Unveil the Art of Lost Foam Casting”, Foundry Management & Technology, September 2004, P30
- Wanliang Sun, Harry Littleton, “Real Time X-Ray Visualization of Effects of Glue Joints on Metal Filling and Defect Formation of Lost Foam Castings”, AFS Transactions, 2005
- Wanliang Sun, Harry Littleton, Charles Bates, “Characterization of Metal Filling Behavior of Lost Foam Castings Using Real Time X-Ray Technology”, 2005 TMS Annual Meeting, 2005
- Sun, W., Littleton, H. E., “Real Time X-Ray Investigation On Formation Of Lustrous Carbon Defect In Lost Foam Iron Castings”, AFS Trans., 2006
- Barendreght, J. A., Littleton H. E., “Development and Validation of a Lost Foam Pattern Quality Measurement System”, 111 th Metalcasting Congress, May 15 – 18, 2007, Houston, Texas
- Littleton H. E., Griffin J. A., “Understanding and Improving Bead Filling Parameters that Affect Lost Foam Pattern Quality”, 112th Metalcasting Congress, May 17 – 20, 2008, Atlanta, Georgia
- Scarber Preston, Littleton H. E., Druschitz Alan, “Preliminary Study of Compacted Graphite Iron Engine Blocks Produced by Lost Foam Casting”, 113th Metalcasting Congress, April 7 – 10, 2009, Las Vegas, Nevada
- P. Scarber, Jr., H. Littleton, and A. Druschitz, “Reducing Porosity in Aluminum Lost Foam Castings through Computer Simulation”, SAE International World Congress, 2009
- Alan P. Druschitz & Harry Littleton, “Advanced Lost Foam Casting Processes and Materials” ”, SAE International World Congress, Warrendale, PA (2009).
- Littleton, H. E., Druschitz, A. P., “Vacuum Assisted Filling of A356 Aluminum Engine Blocks Using the Lost Foam Casting Process, 115th Metalcasting Congress, April 5-8, 2011
- Littleton, H. E., Druschitz, A. P., “Vacuum Assisted Filling of Lost Foam Castings”, AFS Transactions, Paper #10-062(2010)
- Littleton, H. E., Druschitz, A. P., “Advantages of Pouring Compacted Graphite Iron Using the Lost Foam Casting Process, 115th Metalcasting Congress, April 5-8, 2011
- Scarber, P., Littleton, H. E., “Simulating Macro Porosity in Aluminum Lost Foam Castings”, AFS Transactions, Paper #08-145(2008)
- Chintalapati, Pavan, “Solidification Under Pressure of Aluminum Castings”,Phd thesis, UAB,2011.

REFERENCES

1. Qi. Zhao, John T. Burke and Thomas W. Gustafson, “Foam Removal Mechanism in Aluminum Lost Foam Casting”, AFS Transactions, Paper #02-083(2002).
2. D. A. Caulk, General Motors Research and Development Center, “A Pattern Decomposition Model for Lost Foam Aluminum” AFS Transactions, Paper 07-039(2007).
3. D. A. Caulk, General Motors Research and Development Center, “A Pattern Decomposition Model for Lost Foam Aluminum” AFS Transactions, Paper 07-040(2007).
4.Scarber, P., Littleton, H. E., “Simulating Macro Porosity in Aluminum Lost Foam Castings”, AFS Transactions, Paper #08-145(2008).
5. •Wanliang Sun, Harry Littleton, Charles Bates, “Characterization of Metal Filling Behavior of Lost Foam Castings Using Real Time X-Ray Technology”, 2005 TMS Annual Meeting, 2005.
6. Biederman, S. W., Zhao, Q., Metal Casting Technology, “High-Speed Video Analysis of Pattern Filing and Fusion in the Molding Operation of the Lost Foam Casting Process”, AFS Transactions, Paper #06-034(2006).
7. Littleton, H. E., Molibog, T., Sun, W., “The Role of Pattern Permeability in Metal Filling and Defect Formation for Lost Foam Castings”, AFS Transactions, Paper #03-090(2003).
8. Wang, Q. G., Jones, P. E., Osborne, M., “The Effects of Applied Pressure during Solidification on the Microstructure and Mechanical Properties of Lost Foam A356 Castings”, Proceedings from the 2nd International Aluminum Casting Technology Symposium, October 7 – 9, 2002, Columbus, Ohio.
9. Boileau, J. M., Zindel, J. W., Allison, J. E., “The Effect of Solidification Time on the Mechanical Properties in a A356-T6 Aluminum Alloy”, SAE International Congress & Exposition, Detroit, Michigan, February 24 – 27, 1997, Paper #970019.
10. Gerard, D. A., Osborne, R., unpublished research (1996).
11. Wang, Q. G., Jones, P. E., Osborne, M., “Effect of Iron on the Microstructure and Mechanical Properties of an Al-7%Si-0.4%Mg Casting Alloy”, Society of Automotive Engineers, Paper #2003-01-0823.
12. Boonmee, S., Moran, M. K., Stefanescu, D. M., “On the Effect of the Casting Skin on the Fatigue Properties of CG Iron”, AFS Transactions, Paper #11-020(2011).

Appendix A – Benefits Assessment Analysis

Lost foam research has increased the understanding and control of this complex casting process, making it an increasingly attractive alternative to green sand and similar processes. Lost foam considerably reduces scrap, improves yield, and reduces melting requirements.

An analysis of the entire process indicates that total energy savings of about 27% coupled with a 46% improvement in labor productivity and the use of 7% by weight fewer materials in lost foam casting compared to green sand or resin bonded sand molding. Productions cost reductions of 20% to 25% are possible on simple cored items. Productions cost reductions of 44 - 50% are possible on complex castings.

Based on total 1991 tonnage, total energy consumption for all iron, steel and aluminum castings produced (1991 tonnage; and adjusted for scrap and yield) is 24e+12 Btu using sand casting process. Under lost foam process energy consumption would be 17e+12 Btu. Converted to kWh, energy estimates are 7.02 B kWh using sand casting versus 4.98 Bill kWh using lost foam.

The U.S. foundry industry disposes of 8 million tons of sand each year. Over 93% of the industry utilizes the green sand process. Minimal sand disposal is required when using lost foam casting. Solid waste reductions of 700,000 tons of sand per year are projected. The estimate is based on 10% of the presently produced sand castings being converted to lost foam castings.